January 2012

# Reconfigurable Antenna and RF Circuits Using Multi-Layer Stretchable Conductors

Riaz Ahmed -. Liyakath
*University of South Florida*, riaznumerouno@gmail.com

# Reconfigurable Antenna and RF Circuits Using Multi-Layer Stretchable Conductors

by

Riaz Ahmed Liyakath

A thesis submitted in partial fulfillment
of the requirements for the degree of
Master of Science in Electrical Engineering
Department of Electrical Engineering
College of Engineering
University of South Florida

Co-Major Professor: Arash Takshi, Ph.D.
Co-Major Professor: Gokhan Mumcu, Ph.D.
Jing Wang, Ph.D.

Date of Approval:
June 28, 2012

Keywords: Zoflex-Conductive rubber, PDMS, Micro-Stripline Loss Mechanism,
Aperture-Coupled Feed, Stretchable Antenna

## DEDICATION

*Dedicated to my mother and father for being the reason for who I am today*

I would like to thank my parents and my sister for their love, affection and kindness. My parents made me realize the importance of education at a very young age and have provided me everything that I wanted. I thank my sister for her belief in me and wanting to see me as a very successful person. I also thank Kani for her constant encouragement and support, which has helped me to overcome difficult situations and realize my true potential.

## ACKNOWLEDGMENTS

I would thank everyone who has helped me in life to reach this level. At this moment, I would like to thank Dr. Arash Takshi for being a wonderful human being and my adviser. I am also grateful for being given the opportunity to work as research assistant in the Bio/Organic-Electronics group and for being given financial support throughout my graduate education.

Dr. Arash has been kind, patient and has given me the freedom to express myself. He has supported me through the hardships and his appreciation has been a real boost for me. I would like to mention his whole-hearted support during the last few months of my research and his guidance to write and defend my thesis. Under his supervision, I understood that it is important to like what you do and also learnt that an engineer finds a solution for every problem however simple or complex it may be.

I am also grateful for being advised by Dr. Gokhan Mumcu. I have always been amazed by his knowledge, hard work and passion. I would like to thank him for guiding through my difficulties and motivating me to study the subject in depth. The discussions I have had with him have been very fruitful and helped me to grow and expand my knowledge in the field of RF circuits and antennas. Also from him, I also understood importance of learning the fundamentals which is the key to success. I also would like to thank Dr. Jing Wang for accepting to be a part of my committee and for the inputs he has

provided to improve the quality of the work presented here. I have enjoyed discussions I had with him for my courses as well as related to my research.

My days in graduate school will not be complete without mentioning about my friends in ENB 351 and ENB 412. I have enjoyed every moment of the conversation with my dear friends Joel, Houman and Anand. The talks on various topics remain fresh in my mind. I would like to thank you guys for making my stay memorable. I also would thank my friends in the WAMI group Mike, Saurabh, Ibrahim, Maria, David, Abhishek and finally Ahmad for his support throughout my masters. I would also like to thank my senior, Sivalingam for guiding me from the beginning and also Jagan and Ashok for their support. Also, I would like to thank Sai, Shobana, Divakar and my under-graduate school friends for the wonderful times I have shared with them.

Finally, all these experiences would not have been possible without God. I feel blessed and thank the almighty for giving me the opportunity. The past two years have been a steep learning curve for me and I only wish to continue this wonderful journey into the world of science and technology.

**TABLE OF CONTENTS**

## LIST OF TABLES

## LIST OF FIGURES

## ABSTRACT

The growth of flexible electronics industry has given rise to light-weight, flexible devices which have a wide range of applications such as wearable electronics, flexible sensors, conformal antennas, bio-medical applications, solar cells etc. Though several techniques exist to fabricate flexible devices, the limiting factors have been durability, cost and complexity of the approach. In this research, the focus has been on developing stretchable (flexible) conductors using a multi-layer structure of metal and conductive rubber. The stretchable conductors developed using this approach do not lose electrical connection when subjected to large strains up to 25%. Also, the conductivity of the conductive rubber has been improved by ~20 times using the multi-layer approach. Furthermore, the multi-layer approach was used to fabricate devices for RF and antenna applications. A flexible micro-stripline was fabricated using the multi-layer approach to study the performance at microwave frequencies up to 5 GHz. It was observed that using an optimal metal and conductive rubber layer structure can help to reduce the loss of the device by 58% and also the device does not get damaged due to bending. In addition to this, an aperture-coupled patch antenna at 3.1 GHz was fabricated using the multi-layer approach to demonstrate reconfigurability. Ideally, the multi-layer patch antennas can be stretched up to 25% which helps to tune the resonance frequency from 3.1 GHz to 2.5 GHz. The multi-layer patch antennas were tested up to ~10% strains to study their

radiation properties. It was demonstrated that using an ideal multi-layer structure of metal and conductive rubber layer can help to improve the antenna's peak gain by 3.3 dBi compared to a conductive rubber based antenna.

# CHAPTER 1

# INTRODUCTION

## 1.1 Background

The field of electronics and communications has seen tremendous growth in the past decade. The focus has been on making devices smaller, faster and providing more features to the user. The current silicon-based technologies enable to produce chips in the range of a few nanometers [1]. While the focus has been on small area applications, it must be realized that there are many applications where large area electronics would be preferred. Some of the examples include large area antennas for beam scanning, solar cells [2], and sensitive skins [3]. Also, some of the large area applications also need the devices to be conformal and light-weight. For instance, the current antennas used in Un-manned Air Vehicles (UAV) are stand-alone structures which add to weight of the air-crafts. The protruding structures are also create system degradation and maintenance issues [2]. Similarly, the radar systems carried by space vehicles generally includes bulky phased array antennas which take up a lot of space. If these antennas can be designed using flexible, light-weight materials then they can conform to the surface of air-crafts or space vehicles and offer better performance. Moreover, using soft materials for the fabrication of these antennas can help to save space as they can be rolled as sheets and

deployed when needed. Wearable electronics for body-worn devices is another application where the conformal property of flexible electronics will be useful.

There has been active research in the field of flexible electronics to improve the conductivity of the devices without compromising on the flexibility. Many methods have been proposed to improve the electro-mechanical properties, but they are limited by durability as well as complexity of fabrication. The aim of this research has been to develop a technology to produce durable flexible/stretchable conductors using simple and inexpensive fabrication techniques. Various materials and approaches have been investigated to find out the best methodology to achieve repeatable performance over several cycles of strain. The applications of multi-layer stretchable conductors to RF and antenna devices have been tried out. A flexible transmission line and a reconfigurable antenna have also been demonstrated using the multi-layer approach.

### 1.2 Contribution of the Work

The outcomes of the work have been the development of stretchable conductors using a multi-layer approach. These stretchable conductors have wide range applications in wireless sensors, wearable electronics, high frequency electronics etc. As discussed in the previous section, one of the challenges in the field of flexible electronics has been to use this technology for RF and antenna applications. The stretchable conductors fabricated in this research have been used to develop flexible micro-striplines and a reconfigurable patch antenna at 3.1 GHz. The results are promising and this technology can be used to make planar RF circuits like filter, switches, matching circuits for active

devices, multi-band antennas, beam-forming antennas, antennas for bio-medical applications etc.

### 1.3 Thesis Organization

In this thesis, in chapter 1, a brief introduction about the background of the research work performed, results achieved and the various applications that this technology can be used for is listed. In chapter 2, a background review on flexible electronics is performed. The previous work on flexible electronics, as well as, various applications to highlight its scope is discussed. The different approaches for the fabrication of flexible electronics, as well as, the merits/demerits of each approach are discussed. Also, the multi-layer approach for making stretchable conductors in this research is explained.

In chapter 3, the theory of a stretchable conductor is explained. Equivalent circuit models of the stretchable conductor with single metal layer, two layers and multi-layers of metal and conductive rubber layer are proposed. The change of resistance of the various structures due to stretching is discussed. Finally, the technique for conductivity measurement is elaborated and the theoretical formulas are listed out.

In chapter 4, various materials for the fabrication of multi-layer stretchable conductors are studied. The important properties of the materials for different layers of the stretchable conductor are discussed. The best candidates are chosen and various multi-layer structures are fabricated and studied. The conductivity measurement results for various samples stretched up to 25% are presented. In addition to this, the repeatability in the electro-mechanical property of the samples is investigated.

In chapter 5, the geometry of micro-strip transmission lines is discussed. The loss mechanism of the structure is explained. The theoretical equations for the design of 50-ohms micro-strip lines are listed. The dielectric characterization of PDMS for microwave frequencies is performed. The dimensions of the 50-ohms micro-strip lines are calculated and the multi-layer approach is used for the fabrication of flexible transmission lines. The 2-port measurements of the fabricated transmissions are performed to study its reflection and transmission properties. The micro-striplines are also bent and the effect of bending on the performance is investigated.

In chapter 6, the design and fabrication of a reconfigurable antenna are discussed. Based on the design considerations, a suitable method for feeding technique for the antenna is chosen. The theory and working of the patch antenna is discussed. The antenna dimensions calculated theoretically are used as the starting point for the design in the 3D EM Simulation software Ansoft HFSS. The performance of the multi-layer approach based antennas as well as the effect on stretching on the antenna performance are studied using the HFSS model. The multi-layer patch antennas are fabricated and their performance is studied.

In chapter 7, a complete summary of the work performed as well as the results achieved are discussed. The current research as well as recommendations for future work is also provided.

# CHAPTER 2

# FLEXIBLE ELECTRONICS

## 2.1 Introduction

The need to produce light weight and inexpensive devices has been the driving force for macro-electronics. The term macro-electronics generally refers to devices which need the electronics to be wide-spread and distributed [2]. With the current Si-based technologies, the cost for production of large circuits would outweigh its efficiency.[2] In this regard, a special breed of materials known flexible conductors/devices has gained a lot attention. The branch of science which details in developing and imparting electrical properties to mechanically flexible structures is known as flexible electronics. In chapter, an over-view of flexible electronics as well as the previous work done is discussed. The commonly used technologies to develop flexible conductors include: thin-film-depositions, microfluidics, electronic-textiles, conductive rubbers, and ion-implantation on flexible substrates. These techniques are discussed briefly and their merits and demerits are listed. The multi-layer stretchable conductors approach used in this research has also been discussed.

## 2.2 Applications and Previous Work in the Field of Flexible Electronics

Flexible devices have significant advantages like low-weight, low cost, corrosion resistant [4], good electro-mechanical properties and ability to conform to curvilinear surfaces. These properties have given the potential to create devices for applications which has not been possible with the current planar, rigid structures. These applications include sensors, artificial skin, flexible displays, RFID's (Radio-Frequency-Identification) tags, antennas, bio-medical devices, solar cells/photo-voltaics etc. The various applications as well the previous work in flexible electronics are discussed below:

### 2.2.1 Sensors

One of the promising applications of flexible electronics has been the development of sensors for changes in the environment. Some of these include, pressure sensors [5, 6], temperature sensors [7-10], tactile sensors[11, 12], bio-sensors [13], strain sensors [14] and chemical sensors for detecting hazardous gases, environmental gas monitoring in storage and space vehicles applications [15-17]. Since flexible electronics technology can be used to fabricate large area devices, it can be used for creating sensitive skins/E-skins [3, 8, 18]. Sensitive skins are large area flexible network with data collection capability. Sensitive skins can monitor temperature, pressure, force, biological changes in the body or remote, inaccessible areas.[3]. They can also be used to make the human prosthetics sensitive to touch. Moreover, they can be used as skin's for robots and humanoids.[18, 19]. The conformal nature of flexible sensors can also be used for built-in sensors for structural health monitoring[2]. In addition to this, fabrication of sensors which detection human motion are also possible [20]. These sensors can be used for motion capturing for gaming applications.

### 2.2.2 Flexible Displays

The advent of portable electronics has given the need to develop flexible, light–weight and durable displays. The cathode ray tubes were replaced by liquid crystal display and flexible displays are touted as the next generation of display [21]. The significant advantages of using flexible displays are that they are conformal- they can be rolled-up, bent or folded, light-weight and can be produced as large sheets if needed. Also, there has been an active research to develop flexible active-matrix-organic-light-emitting-diodes (AMOLED) displays using polysilicon TFTs [22, 23] and a few devices have already been demonstrated [24, 25]. The flexible displays have many application such as smart cards, thin sheet displays in automobiles, electronic newspapers, portable and wearable electronics devices such as mobile phones, music players and flat panel displays for laptops and computers [26].

### 2.2.3 RF and Antenna Applications

The flexible and conformal nature of flexible electronics is promising for RF devices and antennas. RFID antennas have been made on flexible substrates such papers and polymers [27-30]. Low cost, light-weight and ability to conform to curvilinear surfaces are the features needed for the flexible RFID's. The flexible RFID tags can be used for preventing theft, tracking good in logistics services, food safety warranties, library services [31], prevent tampering with power meter's [32] and in general monitoring or locating of nearby objects.

Another promising application of flexible electronics has been to, fabricate conformal, wearable as well as load-bearing antennas [33]. The flexible antennas using conductive textiles/E-fiber have been demonstrated for body-worn/wearable applications

[34-37]. The antennas fabricated using conductive textiles are known as textile antennas. These antennas operate close to the surface of the human body and are used for wireless communication around the body surface and generally are classified as body area networks (BAN). They have many applications such as health-care monitoring systems for patients as well as implantable antennas for medical wireless communications [38]. These antennas can continuously monitor the health of a patient and transfer the data through the internet by communicating with WLAN (Wireless local area network).

The flexible antennas have also been manufactured using Electrically Conductive Composites (ECC) [4] and carbon nano-tubes [33, 39]. But these antennas suffer from poor radiation due to relatively low conductivity of the radiating patch.

The antennas using fabricated conductive textiles/E-fibers are only flexible. Reconfigurable/tunable antennas have been fabricated using micro-fluidics approach and pre-strained metal fabrication techniques [40-43]. These antennas have many applications as they can be used for beam-forming and beam-bending antennas. Some of the applications of these antennas include, antennas for automotive radars, military surveillance and also high-data rate wireless communication systems [44].

The flexible polymer substrates have also been used for making reconfigurable metamaterials.[45, 46] The metamaterials are negative refractive index materials which have been used for cloaking applications. Most of the metamaterials structures have been fabricated on rigid substrates which limit their use on curved surfaces. However, a flexible meta-material structure has been demonstrated which can wrapped around objects for cloaking purposes [47]. Also, re-configurable metamaterials offer possibilities

for the development of nano-photonic all-optical data processing circuits, smart surfaces, adaptable detection, imaging systems etc. [48].

### 2.2.4 Bio-Medical Applications

Flexible electronics can be used to make wearable devices which can be used for body-health monitoring. The light-weight, conformal nature of flexible electronics which provides comfort to the end user has been one of the main advantages for developing wearable devices using the flexible electronics technology. For example, flexible antennas can be used to detect tumor cells [49] . A flexible and wearable bio sensor for tear glucose measurement has been demonstrated in the work by Iguchi et. al. [50]. The bio-compatibility of the commonly used flexible substrate PDMS also offers potential to develop implantable devices. Bio-degradable polymers have been used for drug delivery [51] and implants bone and dentals parts [52, 53]. Another interesting work done by Dr. Rogers, has demonstrated an electronic eye camera based on silicon optoelectronics [54].

### 2.2.5 Solar Cells

Flexible electronics can also be used for large area applications like solar cells. Since the electronics can be easily spread over a large area it can help to absorb the solar radiation better. Organic solar cells using carbon nano tube electrodes on polymer substrates have been demonstrated [55]. Also, organic thin film polymers are considered to be good alternatives to the silicon solar cells.

## 2.3 Materials and Approaches Used for the Fabrication of Flexible Electronics

Over the years, many techniques have been demonstrated for fabricating flexible electronics. The challenge has been to maintain good electrical properties when the

device is bent or twisted. The different techniques for fabrication of flexible electronics are shown in Fig. 2.1.

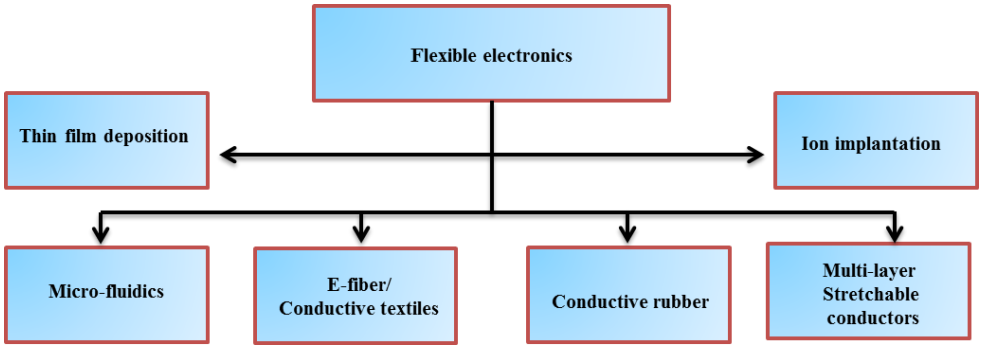


*Fig. 2.1 Classification of Techniques for Fabrication of Flexible Electronics*

### 2.3.1 Thin Film Deposition

In this technique, a thin layer of a metal is deposited on a flexible polymer. Due to the limited stretchability in metals, the metal layer cracks when the substrate is subjected to strains larger than1% [56]. But several techniques have been found to prevent damaging the metal film. One of the approaches is to use a horse-shoe shaped metal pattern [57]. The idea is that the stress is distributed over a wider area instead of being concentrated in a small portion [58]. This approach enhances the stretchability of the structure. But the disadvantage is that, the fabrication process involves making complicated masks to maintain the angle and radius of the horse-shoe which are important to have a uniform stress distribution. Also, the horse-shoe shape patterning could be complex for the fabrication of large area devices.

Another method is to use buckled metal strips on a soft substrate [59]. The buckles can be applied by applying pre-strain to the substrate before the metal deposition [60-62]. Removing the strain after fabrication, the metal layer buckles. The structure can

be stretched up to the pre-strain value without loss of electrical connection. But since it is pre-strained in a particular direction during fabrication, it can be stretched only in that direction. Also, the technique is applicable for pre-strains up to 20% [62]. Any strain beyond that could lead to the complete loss of electrical connectivity.

### 2.3.2 Microfluidics

Thin metal films deposited on flexible polymers develop micro-cracks [63]. The damage could be irreversible, if it is subjected to large strains. To overcome this problem, micro-channels are formed in a polymer substrate and filled with liquid metal alloys like Eutectic Gallium indium (EGaIn) and Galinstan [64]. These are low viscous materials with a high conductivity. The advantage of using a liquid metal is that it preserves the electrical conductivity when the device is stretched or deformed [44]. Despite the high conductivity and large flexibility in the microfluidic devices, the approach has several limitations. Indium metal is scarce and so it is expensive [65]. Also, the GaIn alloy is toxic and hence it is not advisable to be used for bio-implantable applications. The micro-cavities need to be sealed properly to prevent leakage of the liquid metal which makes the fabrication process complicated. Leakage of the liquid metal can completely damage the device. Also, the liquid metals also corrode the nearby metals by dissolving which poses difficulties to the connectors [39]. In addition, the microfluidic based devices have limited operational temperature range due to the large thermal expansion coefficient in liquids alloys at high temperatures. On the other hand, the silicone based substrates contract at high temperatures and this thermal expansion coefficient mismatch can lead to deformation of the structure with a change in temperature.

### 2.3.3 E-Fibers/Conducting Textiles

Wearable electronics has become popular over the years due to development of flexible electronics using conductive textiles or E-fibers. The conductive layer consists of usually thin metal films coated on textile fibers [34, 66, 67] . Since they can be attached to clothes, they offer many advantages such as flexibility and comfort to users. Research works in this field have focused on finding new materials to be used as the conductive layers as well as shielding the human body from electromagnetic radiation at high frequencies [35, 38]. The significant challenge is the fabrication process which has to done by sewing. This approach might not be feasible for very small and complex circuits. Also, they are only flexible and cannot be stretched.

### 2.3.4 Conductive Rubber/ Electrically Conductive Composites (ECCs)

Electrically conductive composites (ECC) consist of nano/micro-size conducting particles (fillers) in a polymeric host [65]. The most common materials used as the fillers are silver and various form of carbons (e.g. carbon black, charcoal, carbon nanotubes [39] etc.). Fabricating the conductive polymers may include several steps and may be complex.

The mechanism of conduction in conductive rubbers is shown in Fig. 2.2. Based on the concentration, size and the distribution of filler, the mechanism of conduction in a conductor rubber can be explained based on three types of arrangement of conductive particles – separate, adjacent and touching [68]. As seen in Fig. 2.2 (i), when the conducting particles are separated by a large distance the improvement in effective conductivity is negligible and the value is closer to the conductivity of the polymer. When the particles are present close to each other, separated by a small distance in the

range of few nanometers, as seen in Fig. 2.2(ii), then a high field strength is generated in the gap which leads to the flow of emission current [69]. A special case of this field emission is the tunneling effect. The tunneling effect takes place when the separation between two-conductive particles is very small and hence the field generated causes the electrons to jump through energy barrier in the polymer matrix. The third case is when the particles over-lap or touch each other. This is seen in Fig. 2.2(iii). In this case, physical contact of the conductive particles leads to conduction in the conductive rubber structure.

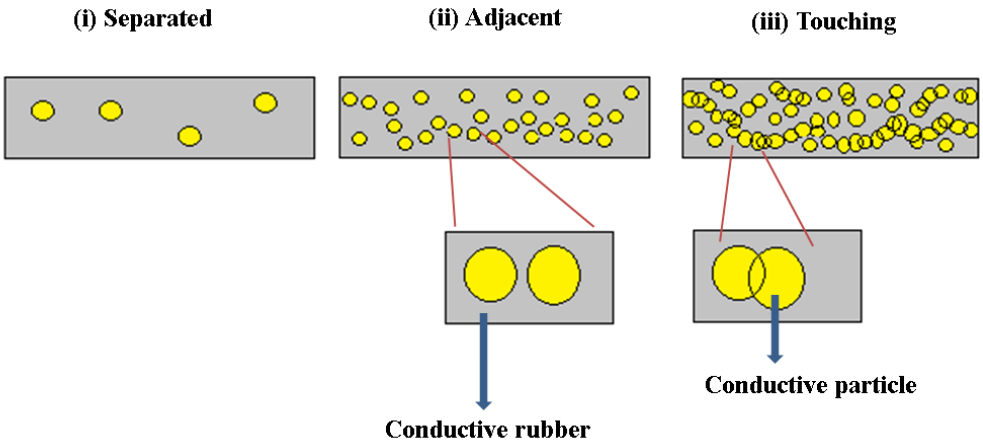


*Fig. 2.2 Mechanism of Conduction in Conductive Rubber. (i) Conductive particles are separated by a large distance (ii) Conducting particles are present adjacent to each other separated a few nanometers (iii) Conduction particles touch each other*

Generally, the conductivity of the composites with silver particles is higher than that in materials with carbon fillers. The conductivity can also be increased by increasing the concentration of the filler. However, the flexibility and stretchability of the composite reduces significantly for very high concentration of the filler. Typically conductive rubbers have conductivity $\sigma<10^4$ S/m. This level of conductivity is too low for use in RF

and antenna applications [4]. It should also be mentioned that the conductivity of an ECC material changes under strain.

### 2.2.5 Ion Implantation

Another interesting technique to create conductive patterns on flexile substrates is direct metal ion implantation. In this process, the metal to be formed on the substrate is ionized under a vacuum arc and penetrated into the substrate [70, 71]. The thickness of the layer as well as the conductivity depends on the accelerating energy of the ions as well as the ion dose [70]. This method is suitable for very thin films in the range of a few nanometers. Fabrication of thick films with this method is expensive and requires long exposure of high energy ions to the substrate which can damage the surface of the substrate.

Most of the discussed techniques are more suitable for flexible circuits with limited stretchability. The microfluidic approach provides excellent conductivity with high stretchability, but the structure has poor durability. In contrast, ECCs are very reliable. The problem in conducting rubbers is the low conductivity. As a solution to achieve high conductivity, combination of conducting rubbers and metal layers has been introduced as a multi-layer structure [72].

### 2.2.6 Multi-Layer Stretchable Conductors

In this approach, pre-strained thin metal films and conductive rubber layers are combined to fabricate stretchable conductors [72]. Theoretically, the conductivity of the multi-layer structure can be expected to be closer to metal at low strains and to the conductive rubber at high strains. The fabrication procedure is explained in Fig. 2.3. At large strains, the metal layer cracks, but the conductivity would be preserved by the

rubber layer. The theory of the approach is explained in the next chapter. This structure is durable with high conductivity and high stretchability.

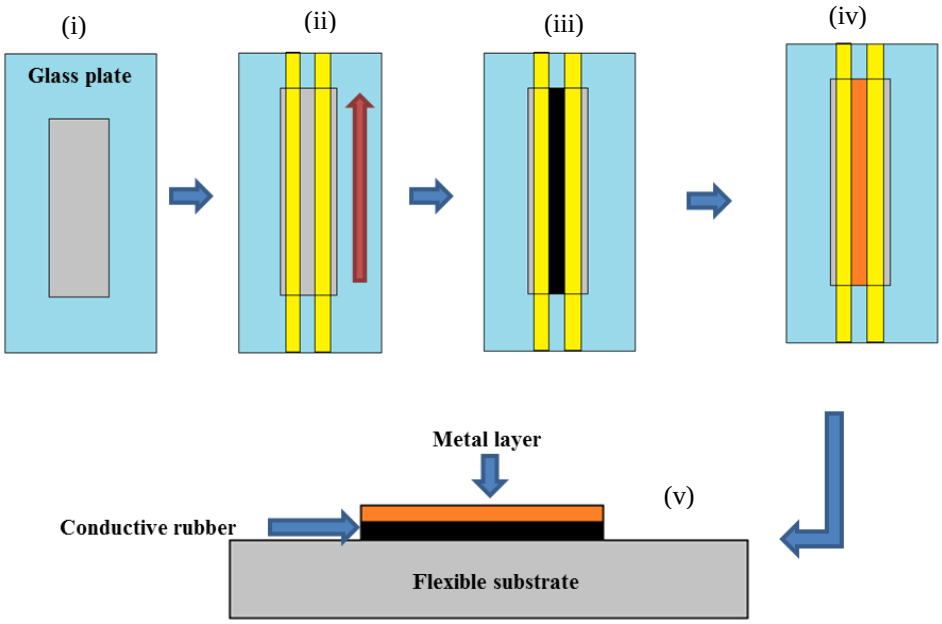


*Fig. 2.3 Fabrication of Multi-Layer Stretchable Conductors. i) Flexible substrate is cut to dimensions, ii) Substrate is pre-strained and taped , iii) Conductive rubber layer is cured, iv) Metal layer is deposited on top, v) Side view of multi-layer structure.*

## 2.4 Conclusion

In this chapter, an over-view of flexible electronics was given and the various applications were listed to show the potential and scope of flexible electronics. Various approaches for the fabrication of flexible electronics were discussed. It was observed that each technique had its own merits and de-merits. The main consideration in the fabrication techniques have been simplicity and durability. Taking this account, a multi-layer approach for the fabrication of flexible electronics was discussed.

# CHAPTER 3

# THEORY OF STRETCHABLE CONDUCTORS

## 3.1 Introduction

In chapter 2, the multi-layer approach using pre-strained metal and conductive rubber combination was discussed. Before explaining the fabrication process, it is important to understand the theory associated with the stretchable conductors. In this chapter, an equivalent model is proposed to explain the circuit behavior of the multi-layer stretchable conductor. Equivalent circuits of metal layer, metal-conductive rubber layer and multi-layer structure are proposed to analyze the performance under stretched and non-stretched conditions. In the last section, the technique for measurement of conductivity is explained.

## 3.2 Equivalent Circuit Model of a Single Metal Layer on a Flexible Substrate

A single, unstretched metal layer on top of a flexible substrate is shown in Fig. 3.1. This layer is assumed to be continuous and hence offers a total resistance $R_M$ to the passage of current. Since the metals have high conductivity the resistance $R_M$ is considered to be very low.

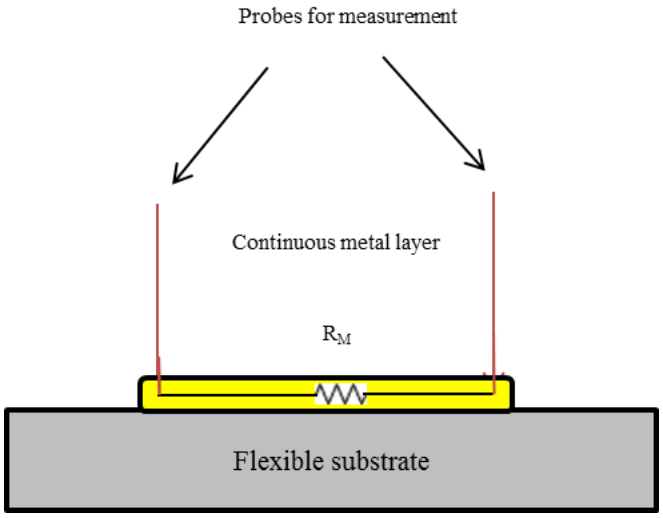


*Fig. 3.1 Unstretched Single Metal Layer on Flexible Substrate and its Equivalent Circuit*

When the substrate is stretched, the metal layer cracks and breaks into disconnected islands. Each island contributes a small resistance $R_{mi}$ to the total resistance value of $R_M$. The stretching results in loss of electrical connection. The stretching of metal layer on the flexible substrate is shown in Fig. 3.2.

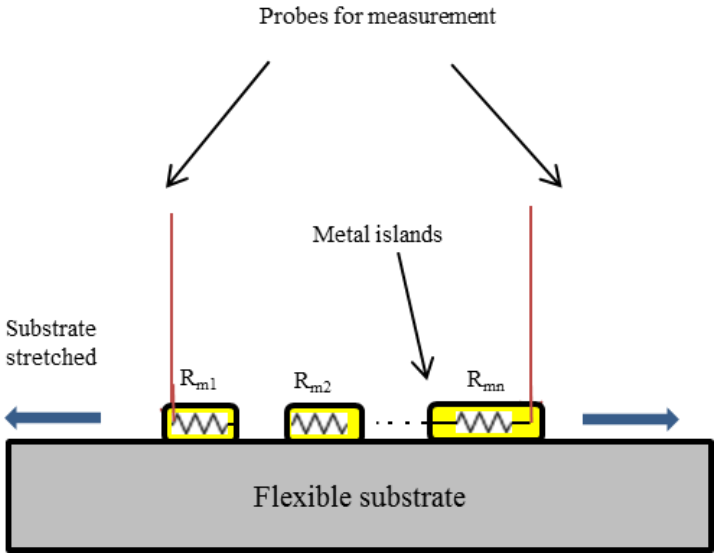


*Fig. 3.2 Metal Islands Formed Due to Stretching of the Substrate and its Equivalent Circuit*

$$R_M = R_{m1} + R_{m2} + \cdots + R_{mn} = \sum_{i=1}^{n} R_{mn} \quad (3.1)$$

where *n* is the number of the islands. Hence, from Fig 3.2, it can be understood that a single metal layer on top of a flexible substrate cannot be stretched.

### 3.3 Equivalent Circuit Model of a Two-Layer Structure

To maintain the electrical connection, a two-layer structure consisting of a metal layer on top of a conductor rubber, can be utilized. It is important to note that the resistance is measured at the ends of the top metal layer. The total resistance offered by the metal layer and the conductive rubber layer is assumed to be $R_M$ and $R_R$, respectively. Before stretching, the metal layer is continuous and hence the total resistance offered by the two-layer structure, $R_{TL}$, can be considered as a parallel combination of resistances $R_M$ and $R_R$. Considering that the resistance of the metal layer can be much smaller than the resistance in the rubber layer. Then,

$$R_{TL} = \frac{(R_M \times R_R)}{(R_M + R_R)} \cong R_M \quad (3.2)$$

When the substrate is stretched the metal layer on the top cracks into disconnected islands but the conductive rubber, due to its flexibility, helps to retain the electrical contact. The equivalent circuit of a stretched two-layer structure is shown in Fig. 3.3.

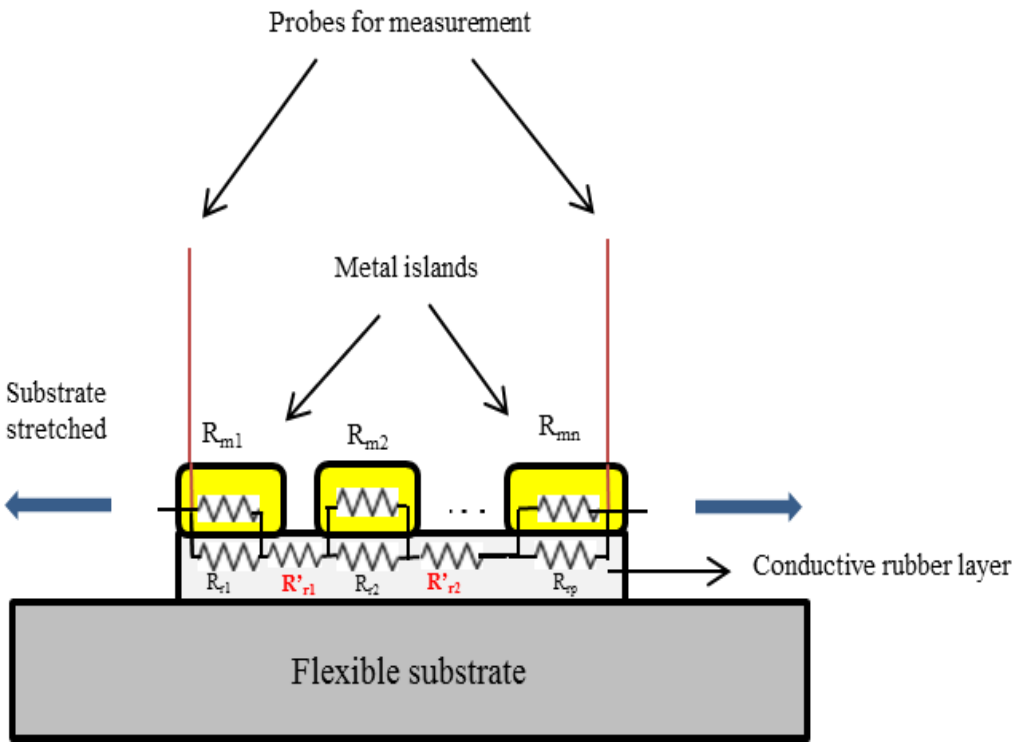


*Fig. 3.3 Stretched Two-Layer Structure and its Equivalent Circuit*

As shown in Fig. 3.3, the total resistance of a stretched two layer structure can be obtained by applying a resistive model. In this model, $R_{mi}$ is the resistance offered by individual islands of metals, $R_{rj}$ is the resistance offered by small area of the conductive rubber under the metal islands and $R'_{rk}$, is the resistance of the pieces of the rubber in the gap of the metal islands. From Fig. 3.3, it can be seen that, due to the presence of resistance $R'_{rk,,}$ the two-layer structure does not lose electrical connection when it is stretched. Moreover, the parallel combination of $R_{mi}$ and $R_{ri}$ in Fig. 3.3 is approximately equal to $R_{mi}$ we can simplify the model to the one shown in Fig. 3.4.

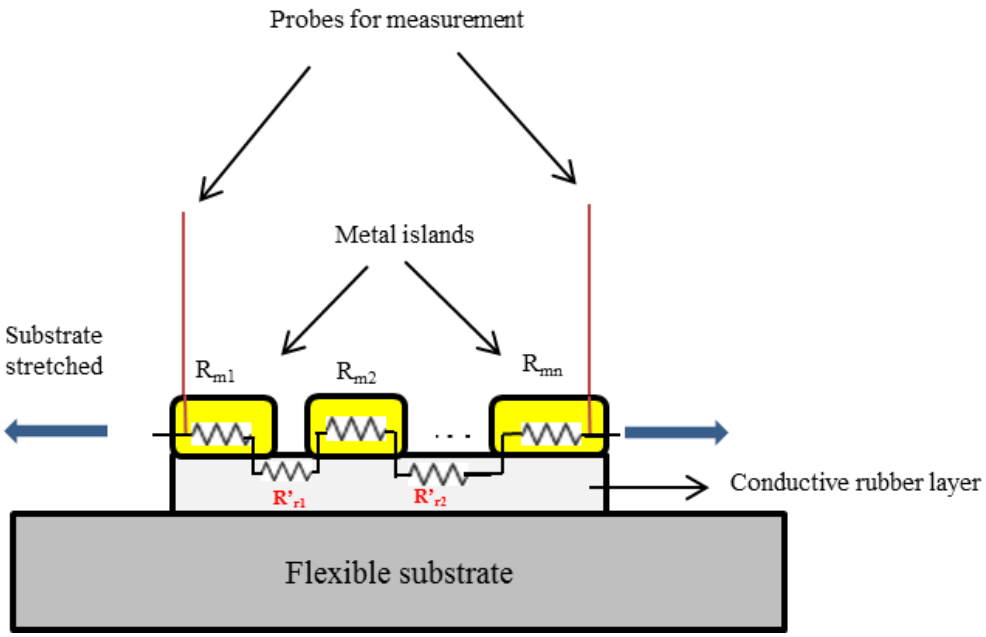


*Fig. 3.4 Simplified Model of a Stretched Two-Layer Structure*

The total resistance of the structure in Fig. 3.4 $R'_{TL}$ is given as,

$$R'_{TL} = \sum_{i=1}^{n} R_{mi} + \sum_{k=1}^{n-1} R'_{rk} \tag{3.3}$$

$$R'_{TL} = R_M + \sum_{k=1}^{n-1} R'_{rk} = R_M + R'_R \tag{3.4}$$

where $R'_R$ is the total resistance of the rubber material in the gap between the metal islands. Assuming that the original length of the conductive structure is $L$ and the length is increased by amount of $\Delta L$ when stretched, $R'_R$ would be expressed by:

$$R'_R = \frac{1}{\sigma_R} \frac{\Delta L}{A} \tag{3.5}$$

where $\sigma_R$ is the conductivity of the conductive rubber layer and A is the cross-section area of the conductive rubber layer. From equation (3.4), it is seen that high values of resistance $R'_R$ would lead to a high total resistance of the two-layer structure $R'_{TL}$. Also, equation (3.5) suggests using a high conductive rubber to achieve a low resistance in a

stretched two-layer structure. Nevertheless, the resistance of the rubber layer dominates the resistance and the value increases with strain.

### 3.4 Equivalent Circuit Model of a Three-Layer Structure

As shown in Fig 3.5, a multi-layer structure consists of a metal layer at the bottom followed by a conductive rubber on top of it and another layer of metal on the conductive rubber layer.

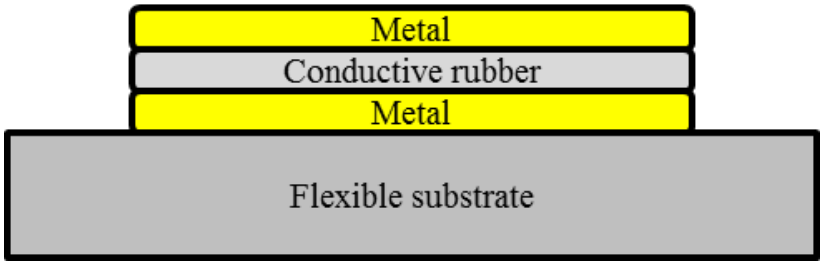


*Fig. 3.5 Side View of a Multi-Layer Structure (Not Shown in Scale)*

In the relaxed mode, the metal resistance $R_M$ dominates as discussed in 3.2 and the multi-layer structure has a high conductivity. When the structure is stretched, the metal layers at the top and bottom of the multi-layer structure cracks leading to the formation of disconnected islands. But it is important to note that, the formation of cracks is non-uniform and the metal islands likely overlap at some portions. The equivalent circuit model of the multi-layer structure is shown in Fig. 3.6.

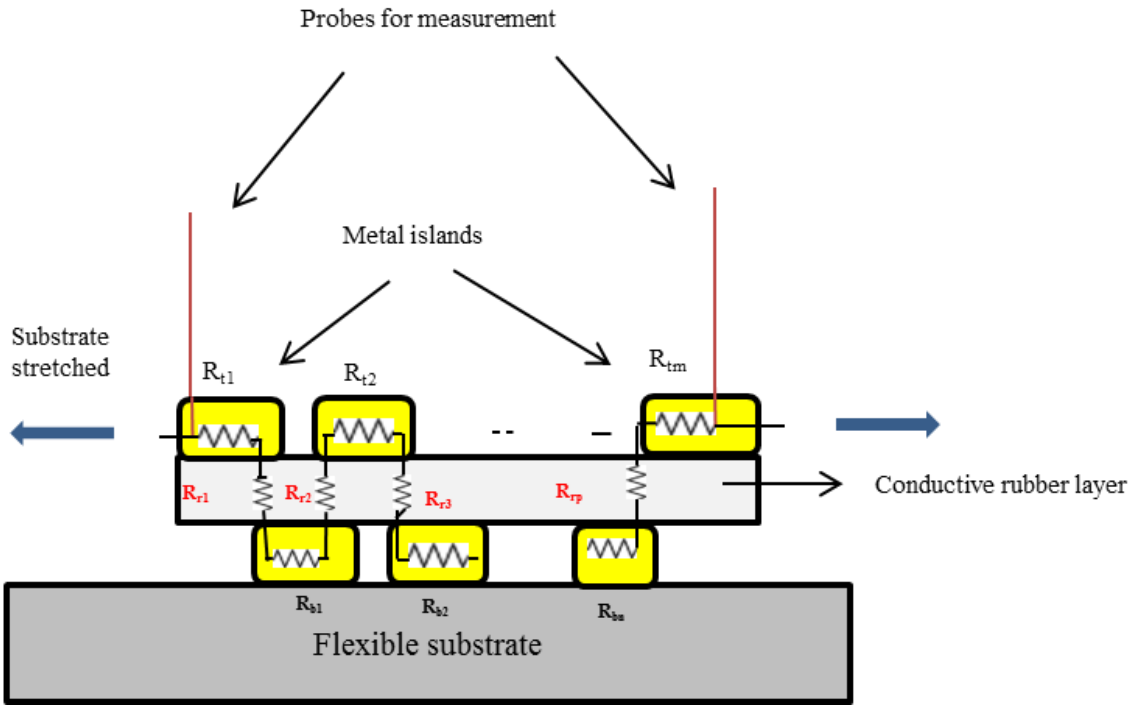


*Fig. 3.6 Stretched Three-Layer Structure*

In this model, $R_{ti}$ is the resistance of the $i_{th}$ island on the top metal surface, $R_{bj}$ is the resistance of the $j_{th}$ island on the bottom metal surface and $R_{rk}$ is the resistance between a top and a bottom island through the conductive rubber. The total resistance of the stretched multi-layer structure $R'_{ML}$ can be given as

$$R'_{ML} = \sum_{i=1}^{m} R_{ti} + \sum_{j=1}^{n} R_{bj} + \sum_{k=1}^{p} R_{rk} \tag{3.6}$$

where,

$$\sum_{i=1}^{m} R_{ti} = R_T \tag{3.7}$$

$$\sum_{j=1}^{n} R_{bj} = R_B \tag{3.8}$$

$$\sum_{k=1}^{p} R_{rk} = R_R \tag{3.9}$$

From equation 3.6, it can be seen that the resistance is combination of top and bottom metal surface as well as the conductive rubber layer in between them. Since $R_T$ and $R_B$ are very small, the overall resistance of the multi-layer structure at high strains is determined by the resistance of conductive rubber $R_R$ in the stretched mode. The overlap of top and bottom surface is shown in Fig. 3.7.

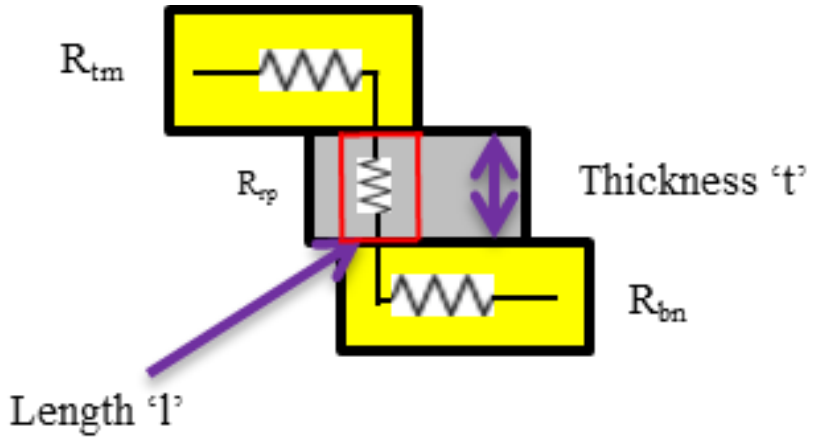


*Fig. 3.7 Overlap of Metal Layers on the Top and Bottom Surface of the Conductive Rubber*

Fig 3.7 can be further used to analyze the value of resistance $R_{rp}$ of the small area of conductive rubber between top and bottom metal islands which overlap. It is given by,

$$R_{rp} = \frac{t}{\sigma_R \times l \times w} \tag{3.10}$$

where l is the length of the overlapped section, t is the thickness of the conductive rubber layer and w is the width of the overlapped section. So by increasing the over-lap length 'l' between the metal islands, the resistance $R_{rp}$ can be reduced even at high strains. Hence by comparing equations (3.4), (3.5), (3.6), and (3.10), we can observe that the three-layer structure is less sensitive to strain compared to the two-layer structure. This discussion of multi-layer structure assumes the top and bottom metal surfaces are smooth. If the

conductive rubber has high surface roughness then the top metal layer will not be continuous. In this case, the top and bottom metal layers overlap is reduced due to surface roughness and hence the three-layer structure behaves more like the two–layer structure.

### 3.5 Conductivity Measurement Technique

The resistance of a conductor can be measured by passing a current through and measuring the voltage across it. The ratio of the voltage to the current is the resistance value. This can be done using an ohmmeter using two terminals at the ends of the connector. The main disadvantage with this technique is that the contact resistance offered by the terminals is also included in the measurement, which results in inaccurate measurement, particularly for low resistances conductors. To avoid this, 4-probe or 4-terminal measurement is recommended. The basic block diagram is shown in Fig. 3.8.

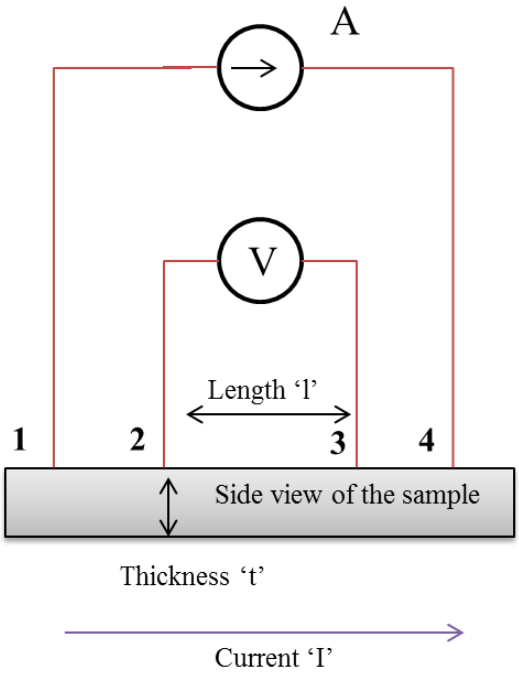


*Fig. 3.8 4-Probe Measurement*

It consists of 4 terminals, the outer terminals (1, 4) are used to apply the current across the sample and the inner terminals (2, 3) are used to measure the voltage across the small area of the sample. The resistance, *R*, between probes 2 and 3 is accurately calculated by measuring the voltage across it and dividing it by the total current I. For a strip-shaped conductor with a known width, *w*, and thickness, *t*, we can calculate the bulk conductivity, $\sigma$, using the resistance equation

$$R = \frac{1}{\sigma}\,\frac{l}{t \times w} \tag{3.11}$$

In this work, to measure the conductivity of a multi-layer sample, the resistance on the top surface is measured using 4 probe measurement (4PM). The total thickness of the multi-layer sample (includes metal layers and conductive rubber layer) and widths are measured. Assuming all the layers are continuous and uniform, we apply equation 3.11 to determine the effective value of bulk conductivity.

### 3.6 Conclusion

In this chapter, the theory of stretchable conductors was explained with equivalent circuit models. It was seen that using a multi-layer structure of metal and conductive rubber the electrical connection can be retained when the structure is stretched. Moreover, the multi-layer structure resistance can be kept low when it is stretched due to the overlap of top and bottom metal layers on the conductive rubber. Also, it is important to understand that to have high conductivity of the multi-layer structure the conductive rubber should have: i) high conductivity and ii) low surface roughness. Finally, the conductivity measurement technique to be used for study the multi-layer structures in this research was also discussed.

# CHAPTER 4

# FABRICATION AND DC MEASUREMENTS OF STRETCHABLE CONDUCTOR

## 4.1 Introduction

Stretchable/flexible conductors have been fabricated using different techniques such as thin film deposition, conductive ink printing, micro-fluidics, conductive rubber etc. as discussed in section 2.2. The approach used in this research was using a multi-layer combination of metal and conductive rubber. The critical factors which affect the performance of the multi-layer structure are conductivity and flexibility of the conductive rubbers and adhesion properties of metal layers.

In this chapter, a detailed investigation of various materials that can be used as the candidates for conductive rubber and metal layers are investigated based on conductivity and flexibility. The materials studied for the conductive rubber layer include Carbon paste, Silver paint, Silver paste, Silver grease, Elastosil® LR31262, LR3163, and Zoflex® FL45. The best candidate from those was chosen as the material for the formation of conductive rubber layer in the multilayer structure. The next step was to choose a metal with good adhesion properties. The popular metals for thin film deposition – copper and gold were deposited on top of the conductive rubber and studied to verify their adhesion properties. The third part of the chapter is about the study of

different multi-layer combinations to see which has the best conductivity. The samples were tested using a custom made stretch setup and were subjected to strains up to 25% to study their electrical properties. The samples were also subjected to several cycles of strain to verify the repeatability.

## 4.2 Investigation and Characterization of Materials

### 4.2.1 Introduction

The multi-layer approach which consists of metal layers in combination with conductive rubbers on a flexible substrate was discussed in section 2.2.6. As discussed in chapter 3, the conductive rubbers with high conductivity can help to reduce the resistance of the multi-layer structure at high strains. Also, the metals need to have good adhesion properties. Hence, to achieve good electro-mechanical properties it is important to investigate various materials and find the ideal candidates.

In this section, different materials are investigated for the substrate, conductive rubber and the metal layer. The list of materials that were available for the fabrication of stretchable conductor is shown in Fig. 4.1. For the substrate layer, popularly used flexible substrates such as Silicone and PDMS were considered. For the conductive rubber layer, materials listed in Fig. 4.1 were studied based on their flexibility and conductivity. For the metal layer, widely used metals – gold and copper were studied for their adhesion properties. To fabricate the conductive rubber and metal layers, a mask using Kapton tapes was used. The masking technique has been discussed in appendix A.

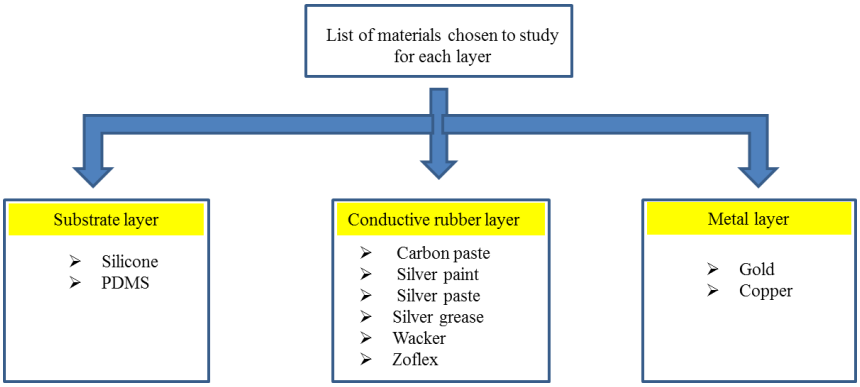


*Fig. 4.1 List of Materials Chosen to Study for Fabrication of Each Layer of Stretchable Conductor*

### 4.2.2 Substrate

Silicon based materials have been widely used in the field of flexible electronics. The commonly used polymer substrates have been: Silicone and PDMS (Polydimethylsiloxane). In general, Silicone has higher stretchability than PDMS [42]. It can be used for techniques using microfluidics approach where there is no metal deposition on the surface of the polymer.

In the work performed by Takshi and Madden [72], it has been shown that in the case of metal deposition on a polymer substrate, the strain is distributed evenly on a PDMS substrate compared to Silicone. This helps in getting a repeatable resistance over several cycles. Therefore, PDMS was chosen as the substrate material for developing stretchable conductor in this research. PDMS is also the widely used substrate for flexible electronics. PDMS has a number of useful properties such as bio-compatibility [73], thermo-mechanical stability [74], low Young's modulus (<2MPa) [75] and is relatively simple to fabricate.

The Dow corning Sylgard®184 polymer kit was used for PDMS film fabrication. The fabrication process was done in a step-wise manner. The PDMS kit had two parts –

base and a curing agent. First, the base and the curing agent were mixed in the ratio 10:1 and spread over a glass plate. The glass plate had a rectangular frame which was built using glass slides of 1mm thickness. Since the mixture contained air bubbles, it was placed in a vacuum chamber for 30 minutes. Finally, it was cured on a hot plate by heating at 100℃ for 1 hour. Using this method, thin sheets of PDMS of dimensions 75mm×75mm×1mm were fabricated. The process of PDMS fabrication is shown in Fig.4.2.

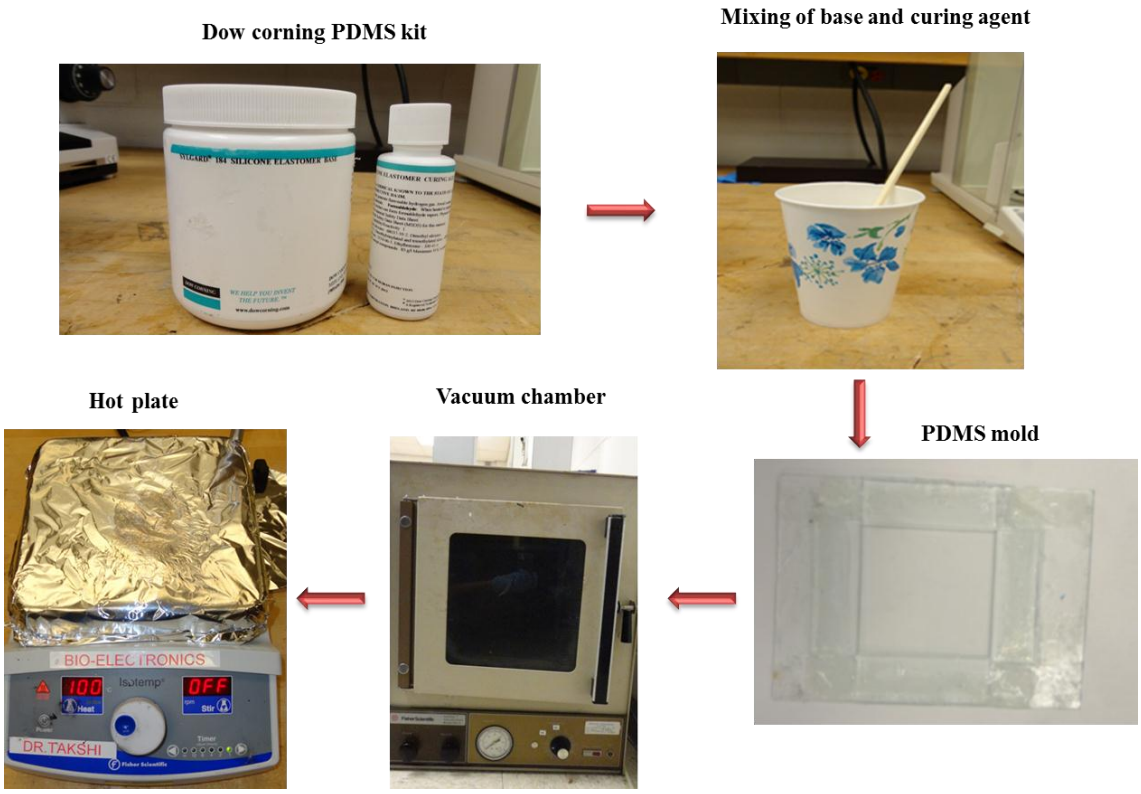


*Fig. 4.2 Fabrication Process of PDMS*

The smoothness of the PDMS layer is important as it helps to form, continuous films deposited over it. While de-gassing in the vacuum chamber, the air-bubbles escape. If the bubbles are too big, then it leaves small cavities which results in non-uniform

PDMS layer formation. So it is important to mix the base and the curing agent well to avoid the problems. A PDMS film made using this procedure can be seen in Fig. 4.3 (i). The surface roughness was found to be about 2 nm after studying with atomic force microscopy (AFM). The AFM image of the surface of PDMS can be seen in Fig 4.3 (ii).

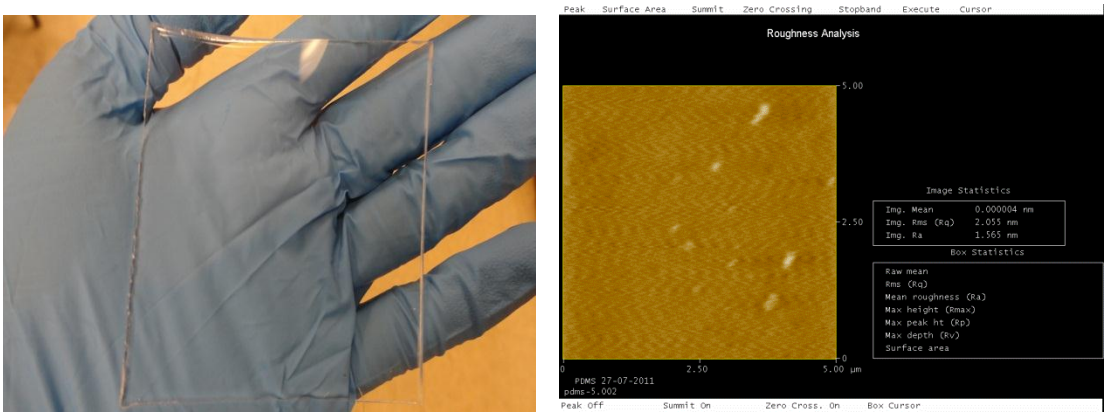


(i) (ii)

*Fig. 4.3 i) Fabricated PDMS Sheet, ii) AFM Image of PDMS. It can be seen that PDMS is smooth and has a low surface roughness of 2nm.*

### 4.2.3 Conductive Rubber Layer

#### 4.2.3.1 Introduction

Conductive rubbers/electrically conductive composites are materials having a good flexibility and conductivity. The conductive rubbers were discussed in section 2.2.6. Flexibility and conductivity are the important trade-offs while choosing a material as a conductive rubber. Since, it was discussed in chapter 3 that a conductive rubber helps to improve the overall conductivity of the multi-layer structure when it is stretched, the main focus while choosing the conductive rubber was to find an optimum material with high conductivity and flexibility. In this section, a few candidate materials for the

conductive rubber layer in the multi-layer structure are investigated to study their electro-mechanical properties.

#### 4.2.3.2 Carbon Paste

A carbon paste, which consists of small graphite particles in a liquid carrier, was purchased from SPI Supplies to be tested as the elastic conductor [76]. The product was in the form of a black paste and was easy to spread. A film of the material was made by spreading it on a masked PDMS and was cured by leaving in the room temperature for 48 hours. The 4 probe measurement (4PM) gave a conductivity of about ~2 S/m. It was also observed that the carbon paint had poor adhesion to PDMS.

#### 4.2.3.3 Silver Paint

Silver paint (from SPI Supplies) was also tested. The paint was in liquid form containing pure silver particles. Due to its liquid state, it can be painted on any surface and cured in room temperature. The conductivity of the paint was measured to be ~3 S/m. Also, it was found that the film cracks very easily when subjected to small amount of strains. The poor conductivity measured may be because of the destructive effect of the probes during the measurement.

#### 4.2.3.4 Silver Paste

Silver paste from SPI Supplies which consists of pure silver particles in a liquid carrier was tested. Although it had a relatively high conductivity of $2.86 \times 10^3$ S/m and better adhesion to the surface compared to carbon paste and silver paint, it was not possible to use it as the conductive rubber layer because of its low flexibility.

#### 4.2.3.5 Silver Grease

The silver grease purchased from SPI supplies consisted of an oily, grease material filled with silver particles. Due to the oily nature of the product, the material did not dry when spread on PDMS and hence it was not possible to use it as a as the conductive rubber layer.

#### 4.2.3.6 Wacker Conductive Rubbers

Two different products from Wacker were tested: ELASTOSIL® LR3162 A/B and LR 3163 A/B [77]. Both products were two-part electrically conductive liquid Silicone-based rubbers [77]. The preparation procedure for the products was almost the same. Part A and part B were mixed in the ratio 1:1 (2.5 g: 2.5 g). Since the materials were very viscous, they were diluted by adding a solution of acetone and toluene in the ratio 1:1 (7.5 m: 7.5 ml) and mixing for 10 minutes till a paste form was achieved. The diluted materials were then spread on Kapton-masked PDMS substrates and heated at 60℃ for 5 hours. In comparison, LR3162 had a higher conductivity (~6.25 S/m) than LR3163 (~0.444 S/m).

#### 4.2.3.7 ZOFLEX® FL45

ZOFLEX® FL45 is a two-part conductive rubber with high conductivity and flexibility [78]. The part A and B were mixed in the ratio 6.63:1 for about 2 minutes and spread over the masked substrate with the help of a glass slide. It is then cured by heating on a hot plate at 50℃ for 8 hours.  A fabricated Zoflex sample is shown in Fig.4.4.

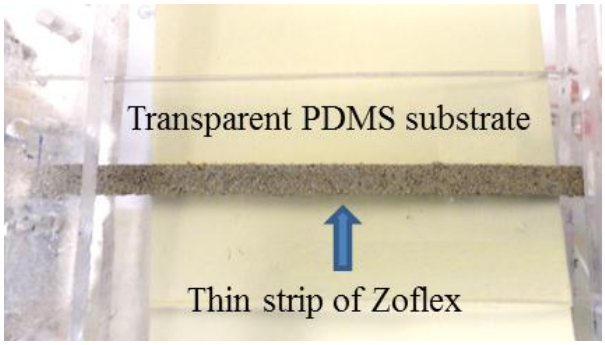


*Fig. 4.4 Fabricated Zoflex Layer on PDMS*

The 4PM of the Zoflex sample showed a resistance of 2-5 Ω compared to a few kΩ resistance in the Wacker samples. On comparison with all the materials, Zoflex had the highest conductivity ~$1\times10^4$ S/m with superior flexibly. Table 4.1 shows the comparison of all the materials that were tested based on conductivity and flexibility.

*Table 4.1 Comparison of Materials Based on Conductivity and Flexibility*

| **Material** | **Conductivity(S/m)** | **Flexibility** |
|---|---|---|
| Carbon paste | ~2 | Low |
| Silver paint | ~3 | Low |
| Silver paste | $2.86x10^3$ | Low |
| Silver grease | $1x10^3$ | It is a semi-liquid substance |
| Wacker LR3162 | ~6.25 | Excellent |
| Wacker LR3163 | ~0.444 | Excellent |
| Zoflex FL45 | $1\times10^4$ | Very good |

From Table 1, it can be inferred that Wacker LR3162 and Zoflex are the suitable materials for the conductive layer based on their conductivity and flexibility. Though Wacker had a higher flexibility than Zoflex, poor conductivity was the main disadvantage in LR3162. Therefore, Zoflex with high conductivity and high flexibility was chosen as the material for the conductive rubber layer.

### 4.2.4 Metal Layer

High conductivity metal such as gold, copper etc. have used widely for forming the metallization layer. In the previous work performed by Takshi and Madden, [72] a thin layer of gold on Wacker LR3162 was used. In their work, good adhesion between gold and the Wacker layer was demonstrated. In this research, gold as well as copper films were studied for their adhesion properties. For thin film deposition, the E-beam evaporator was utilized because of the high quality of the deposited layer. (See appendix B). A two-layer structure of metal film on Zoflex was fabricated on PDMS. The dimensions of the layers are discussed in section 4.3.

Both the gold and copper deposited Zoflex samples were subjected to several cycles of strain (up to100 stretches) to study the adhesion properties. From Fig.4.5, it can be seen that copper has better adhesion compared to gold on Zoflex after 100 cycles. Moreover, the multi-layer stretchable conductor approach was planned to be used for making RF and antenna devices in this research. The RF and antenna applications require several microns thick films based skin depth to produce low loss devices. (See section 5.3.1) So it was decided to use copper, as it had better adhesion, as well as, it is inexpensive for producing thick films. The thick copper layers were fabricated using sputtering technique which is explained in appendix C.

(i) (ii)

*Fig. 4.5 Comparison of Crack Formation in Metal Deposited on Zoflex Samples of Thickness 500 nm Stretched Over 100 Cycles. (i) Gold and (ii) Copper*

**4.3 Multi-Layer Structures**

From the section 4.2, the materials for the substrate, conductive rubber layer and metal layer were chosen as PDMS, Zoflex and copper. In chapter 3, one layer, two-layer and three-layer structures using metal and conductive rubber were discussed. In the section, the different structures will be fabricated and tested to study their performance.

Different Zoflex-Copper metal layer combinations can produce different performance when stretched based on the overlap of the layers. The different structures, namely, a) Zoflex, b) Zoflex-copper, c) copper-zoflex, d) Copper-zoflex-copper were fabricated to analyze their performance. The layers used copper of thickness 4 μm and Zoflex of 100 μm. The thickness was chosen based on the skin depth which is explained in section 5.3.1.To fabricate a multilayer structure, the samples were pre-strained to 10% prior to the copper deposition. The pre-strains gives rise to buckle stress which allows the metal layers to be stretched to the pre-strained value. In this case, metal layers were pre-

strained to 10%. So in this case, up to 10% the metal layers may help in conduction. Beyond that, Zoflex forms over-lapping islands and helps to maintain the electrical contact at high strains. The different layer combinations are shown in Fig. 4.6.

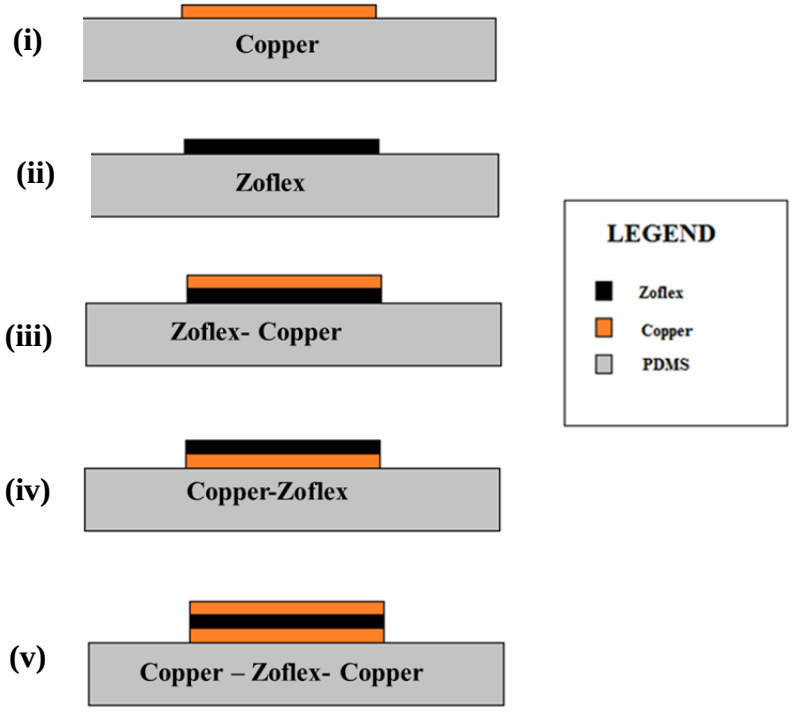


*Fig. 4.6 Multi-Layer Combinations. (i) Single layer of copper on PDMS, (ii) Single layer of zoflex on PDMS, (iii) Two-layer structure of copper on top zoflex which is on top of PDMS, (iv) Two-layer structure of zoflex on top copper which is on top of PDMS, (v) Three layer structure of copper on top of zoflex on top of copper which is on PDMS.*

The fabrication process of the multi-layer structures involved curing of PDMS, zoflex and sputtering of copper. The fabrication of a multi-layer sample of copper-zoflex-copper is shown in Fig. 4.7. For clarity of understanding, the material mentioned first is taken as the bottom layer. For instance, Copper-Zoflex means copper is the bottom layer. Depending on the layer combination, the particular step can be skipped.

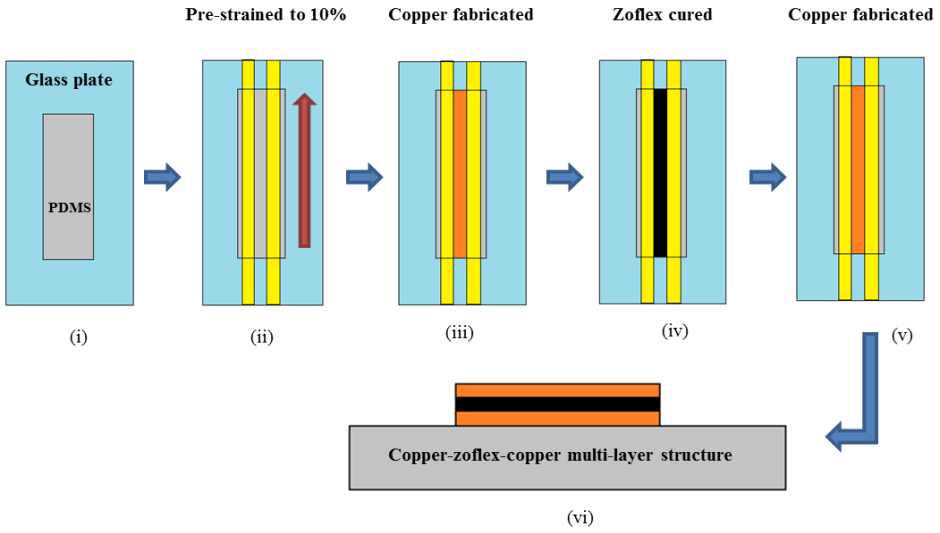


*Fig. 4.7 Fabrication Process of Copper-Zoflex-Copper Multi-Layer Structure. i) PDMS substrate is cut to dimensions, ii) PDMS is pre-strained to 10% and masked using Kapton tapes, iii) Bottom copper layer is sputtered, iv) Zoflex layer is cured, v) Top copper layer is sputtered , vi) Side view of multi-layer sample.*

### 4.4 Strain-Conductivity Analysis

The multi-layer samples were subjected to strains from 0 to 25% and resistance was measured using 4-probe measurement technique discussed in section 3.5. This was repeated over cycles to verify if the performance was repeatable. The measurement set up is discussed in section 4.4.1.

#### 4.4.1 Measurement Set-up

The measurement set up consists of a Keithley 2602A SYSTEM Source-meter® which has the capability to do 4-probe resistance measurements. A custom made stretch setup was used to stretch the sample in a controlled manner. The stretch testing set-up, placement of 4-probes on the sample and the measurement set-up are shown Fig. 4.8.

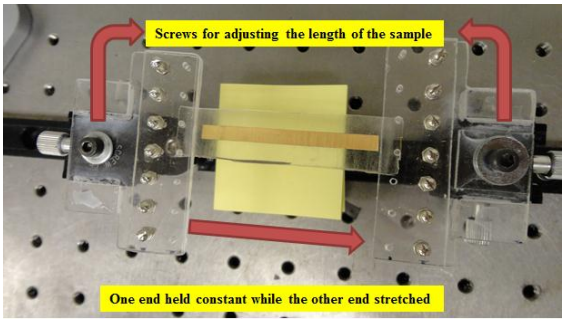


(i)

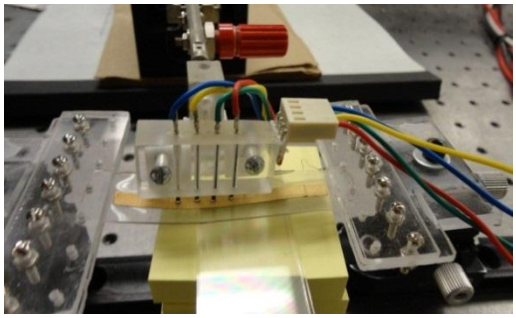

(ii)

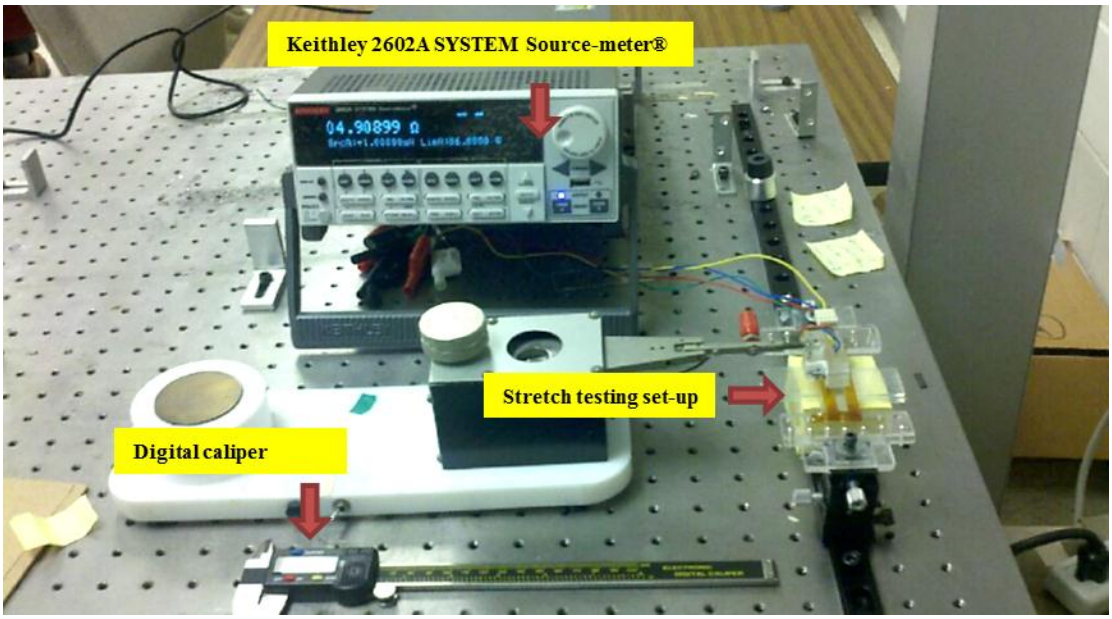


(iii)

*Fig. 4.8 4-Probe Measurement Set-Up. i) Stretch testing set-up, ii) Placement of 4-probes on the sample for measurement, iii) Complete set-up*

The mechanical strain can be varied by adjusting the length of the sample. This was done by holding one end constant while the screws at the other end were adjusted to stretch the sample. A digital caliper was used to measure the length of the sample. The probes were placed on the sample once the amount of strain was fixed and resistance measurements were taken by the source-meter.

### 4.4.2 Measurement of Single-Layer Structure of Zoflex on PDMS

The Zoflex on PDMS structure shown in Fig 4.6 (ii) was fabricated as discussed in section 4.2.3.7. The sample had a length of 53.73 mm, thickness of 100 um and center conductor width was 2.49 mm. Measurements at 0% strain showed a resistance less than 5 ohms. The sample was stretched over 3 cycles to completely study the variation of resistance with strain. This is shown in Fig 4.9. It was observed that the Zoflex material does not crack and lose electrical connectivity when stretched. The resistance increases when stretched which may be due to separation of conductive particles in the Zoflex layer. Accordingly, the conductivity of the material decreases over strain. It can also be observed that the Zoflex sample also has a repeatable performance over several cycles of strain.

Furthermore, it can be observed from Fig. 4.9 that the first cycle the forward has lowest conductivity and the conductivity increases after the first stretch. This can be explained based on the re-arrangement of particles due to stretching effect discussed in section 2.2.4. When Zoflex is exposed to current for the first time, conducting particles try to form a conducting path through the sample. So initially, there is a higher resistance offered to the passage of current and hence the conductivity is lower in the first cycle. This period for the Zoflex to form conductive paths when exposed to the current for the first time can be called as the settling time of Zoflex. Once, the conducting paths are formed, the Zoflex layer becomes stable and offers a stable resistance. Thus, repeatable conductivity measurements are observed from the second and third cycle as seen from Fig. 4.9.

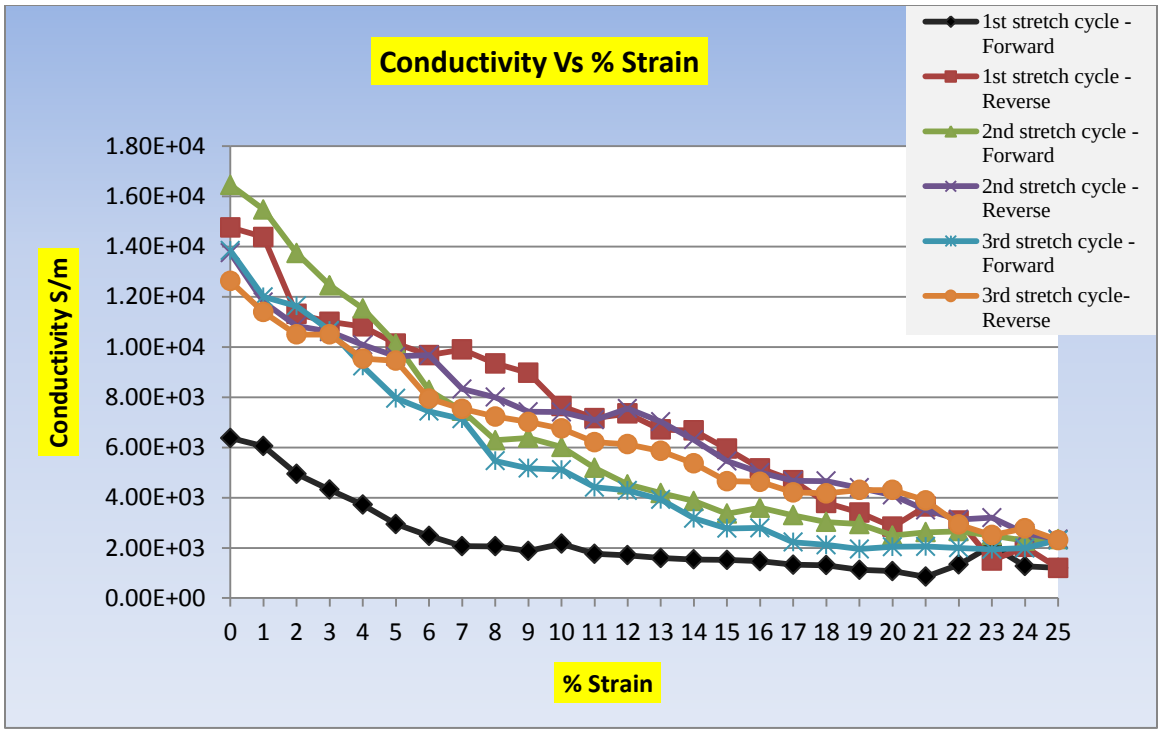


*Fig. 4.9 Change of Conductivity of Zoflex Structure with Strain*

### 4.4.3 Measurement of Two-Layer Structure of Copper-Zoflex on PDMS

The two-layer structure consisting of copper as the bottom layer and Zoflex on top of it shown in Fig 4.6 (iv) was fabricated using the procedure shown in Fig 4.7. The step (v) was skipped as it was a two-layer structure. The center conductor had a length of 50 mm, thickness of 104 μm which includes 100 μm zoflex and 4 μm of copper beneath and a width 2.52mm. This structure has approximately 2 times improvement in conductivity compared to the Zoflex structure at 0% strain. The Copper- Zoflex structure was also subjected to strain from 0 to 25 % and the resistance was measured for every percent of strain. Fig. 4.10 shows the performance of Copper-Zoflex structure with strains.

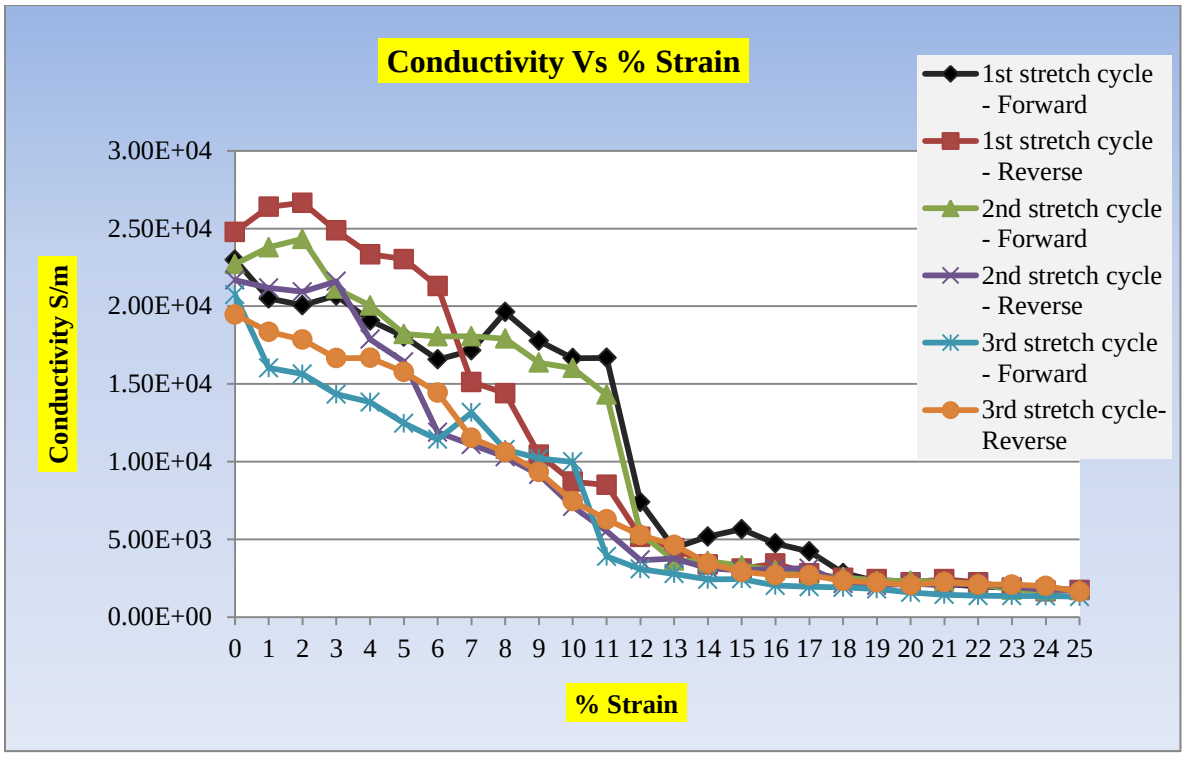


*Fig. 4.10 Change of Conductivity of Copper-Zoflex Structure with Strain*

It can be seen from Fig. 4.10, the first cycle (forward and reverse) and second (forward) cycle have a high conductivity. This may be due to the fresh copper layer beneath which may have not developed many micro-cracks. From the second (reverse cycle), it can be seen the structure had a repeatable performance from 0 to 25%. The conductivity decreased with increase in strain but it almost restored to the same value at 0% strain. The variation in resistance in all the three cycles when it reached 0% strain was +/- 0.1 ohms. Also, the other two-layer structure with Zoflex on the bottom and copper (Fig. 4.6 (iii)) was tested and it was observed that the performance of this structure is similar to the Zoflex on top of copper structure discussed here.

### 4.4.4 Measurement of Three-Layer Structure of Copper-Zoflex-Copper on PDMS

The Copper-Zoflex-Copper multi-layer structure (Fig 4.6(v)) had a Zoflex layer of thickness 100 μm sandwiched between two layers of copper of thickness 4 μm. The center conductor had a length of 54 mm and a width of 2.52 mm. It was observed that this structure has ~20 times higher conductivity compared to the Zoflex and Copper-Zoflex structures at 0% strain. Fig. 4.11 shows the performance of Copper-Zoflex-Copper multi-layer structure with strain.

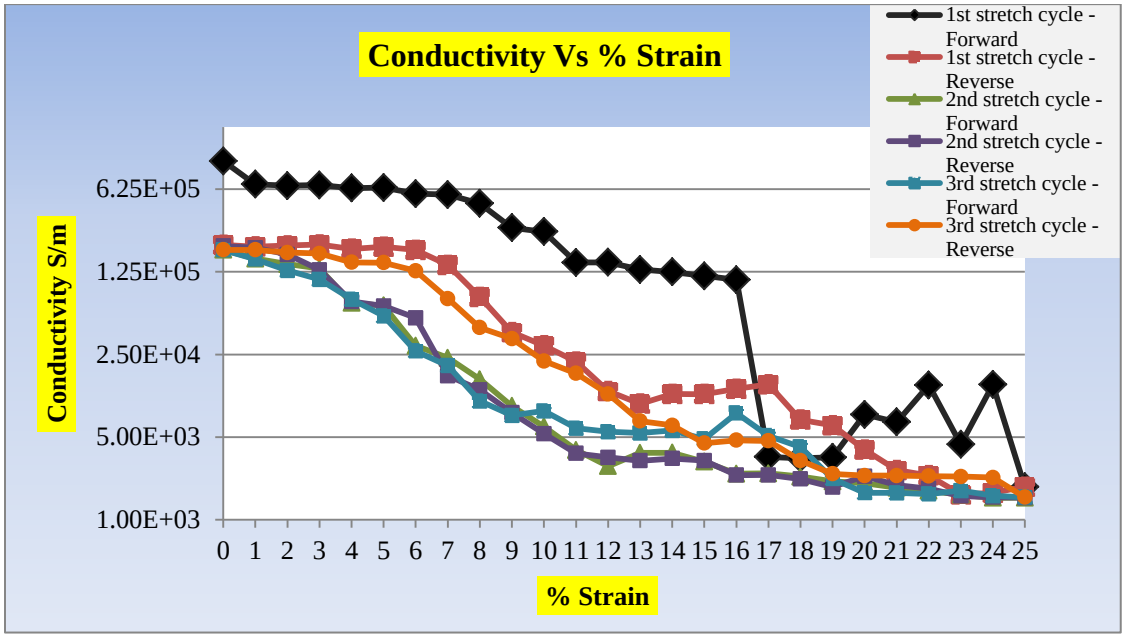


*Fig. 4.11 Change of Conductivity of Copper-Zoflex-Copper Structure with Strain*

It can be observed that from Fig 4.11 that the first forward cycle had a very high conductivity of ~$1\times10^6$ S/m which may be due to fresh copper layers with few cracks. The conductivity dropped when it was further stretched which was likely due to the formation of micro-cracks in the copper films both in the top and bottom layers. From the second cycle, a stable structure with over-lap of copper islands on the Zoflex layer was

formed and hence a repeatable performance with a conductivity of ~$2\times10^5$ S/m at 0% strain was observed. The low conductivity at high strains may be because of non-overlap of copper islands and hence the conductivity was closer to the conductivity of a single Zoflex layer.

### 4.4.5 Comparison of Multi-Layer Structures

To get a better idea as to how the conductivity increases due to the multi-layer approach, a single cycle of strain of all the structures discussed in section 4.4.2, 4.4.3 and 4.4.4 are compared. (See Fig. 4.12). It can be seen from the Fig. 4.12 that, addition of copper layer improves the effective conductivity. The Copper-Zoflex structure has ~2 times higher conductivity and Copper-Zoflex-Copper had ~20 times higher conductivity compared to the Zoflex structure. This is evident in strains up to 10%. Beyond that, the performance becomes similar to the Zoflex structure. In terms of the resistance, addition of each layer of copper helps to decrease the resistance by approximately 7-10 times. The change of resistance due to stretching can be seen in Fig. 4.13.

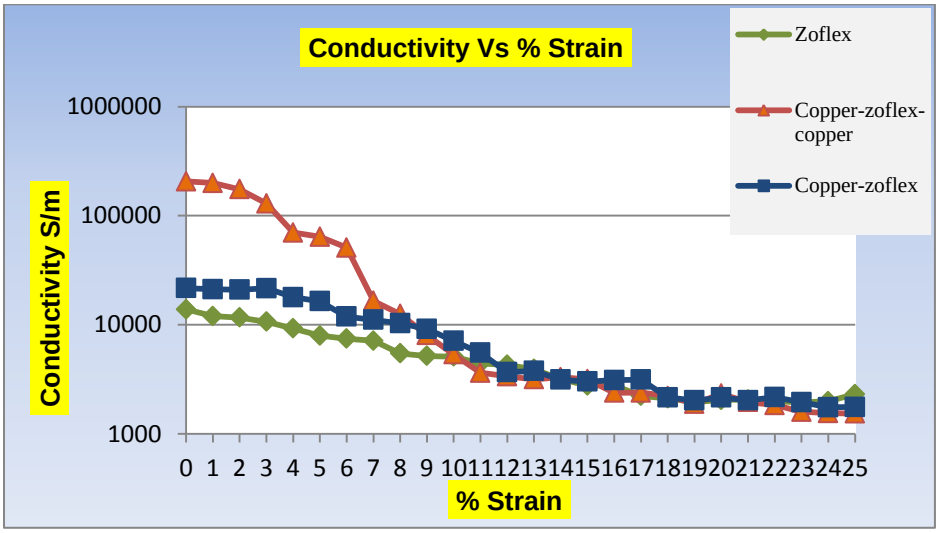


*Fig. 4.12 Comparison of Conductivity of Multi-Layer Structures*

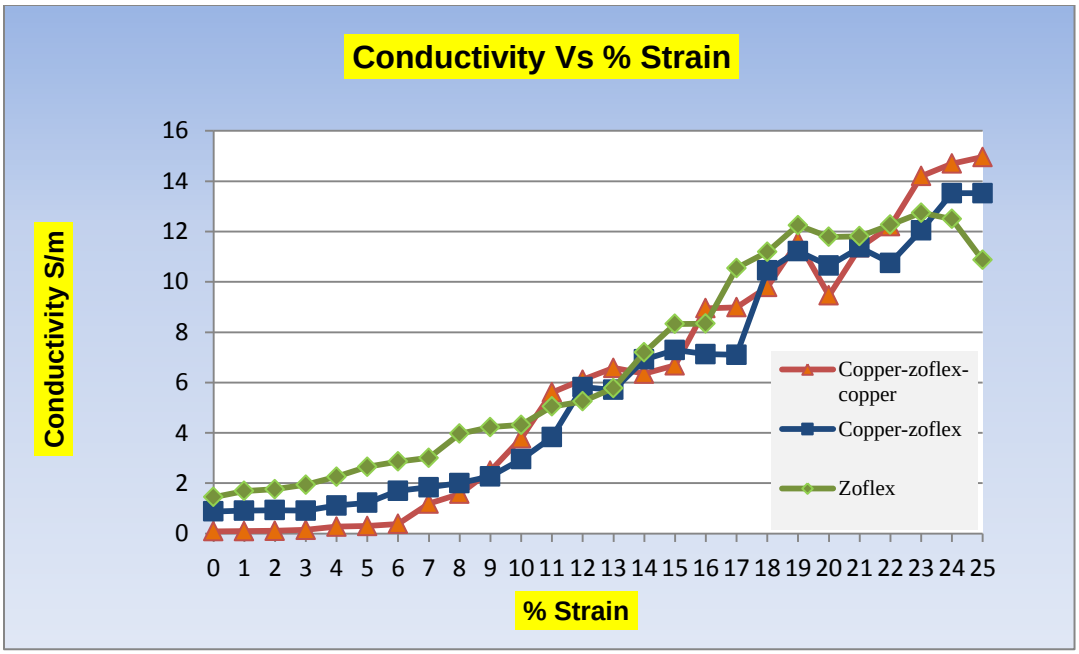


*Fig. 4.13 Comparison of DC Resistance of Multi-Layer Structures*

### 4.5 Conclusion

In this chapter, various materials for the fabrication of a stretchable conductor were investigated. PDMS was chosen as the substrate layer. For the conductive rubber layer, materials like Carbon paste, Silver paint, Silver paste, Silver grease, Wickers-ELASTOSIL® LR3162 A/B and ZOFLEX®FL45 were studied. It was seen that among all the materials Wacker and Zoflex had a high flexibility. On comparison, it was found that Zoflex was much better in terms of conductivity. For the metal layer, two metals with high conductivity – gold and copper were tested. The gold and copper deposited samples were stretched up to100 times to study permanent damages and material delamination. It was found that copper had much better adhesion whereas the gold films started to delaminate after several cycles of strain.

The different combinations of metal and conductive rubber layers discussed theoretically in chapter 3 were fabricated and tested. From the measurements, it was seen that Copper-Zoflex-Copper structure had the highest conductivity of ~$2\times10^5$ S/m and the performance was repeatable over several cycles of strain. Also, it was observed that addition of copper layers helps to increase the effective conductivity of the multi-layer structures. Further, the results of the fabricated multi-layer structures agree with the performance of the different structures predicted using equivalent circuit models in chapter 3.

# CHAPTER 5- FLEXIBLE MICRO-STRIP TRANSMISSION LINES

## 5.1 Introduction

Flexible/stretchable RF circuits have many applications like inexpensive RFID tags, wearable devices, conformal antennas etc. as discussed in section 2.2. However, the main of challenge for making RF devices using flexible electronics technology has been the low conductivity which leads to poor performance as well as the complexity of the approach. So, the conductivity has to be high enough to achieve low loss and also the fabrication approaches have to be relatively simple and versatile to design all kinds of circuits. The relatively high conductivity of the multi-layer samples (~$2\times10^5$ S/m) demonstrated in chapter 4 is promising for RF and antenna devices.

In this chapter, design and testing of flexible micro-strip line using the multi-layer approach is discussed. The micro-stripline topology can be used to study the RF performance of the multi-layer structures. The main focus in this chapter is study the loss due to the different multi-layer structures discussed in section 4.3.

In the first part of the chapter, the micro-strip line geometry and the loss mechanism is explained. The dielectric characterization of PDMS using open-ended coaxial probe measurement to measure the permittivity and loss tangent is discussed. The theoretical equations to calculate the dimensions of a 50-ohms transmission line are discussed. The multi-layer stretchable conductor approach is used to fabricate 50-ohms

micro stripline and two-port measurements are performed to study the transmission and reflection properties. In the last section, the effect of bending on the flexible micro-strip lines is also discussed.

## 5.2 Micro-Stripline Geometry

Micro-strip lines are the widely used transmission lines because it can be easily fabricated and integrated with other passive and active devices [79]. The micro-strip lines consist of two conductors – a top (signal) conductor and a ground plane. These are present at the top and bottom surface of a dielectric material as shown in Fig. 5.1. The important parameters for designing a micro-strip include width (W) of the top conductor, thickness of the substrate (h), permittivity and loss tangent of the dielectric substrate and conductivity of the top conductor. Due to fringing fields, the mode of wave propagation is quasi-Transverse Electro-Magnetic (TEM). Also, when width of the center conductor becomes electrically large non-TEM propagation occurs which leads to higher modes, radiation [80].

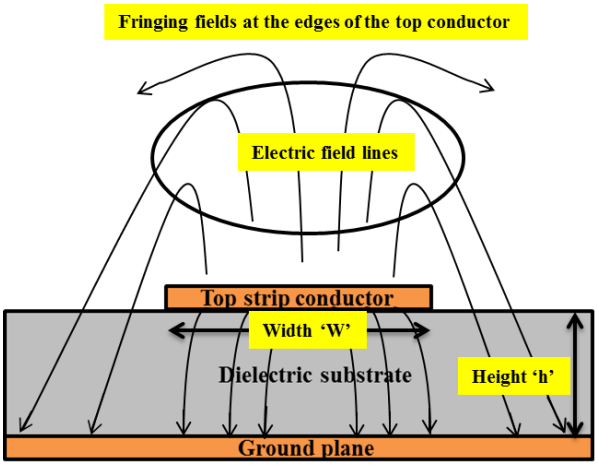


*Fig. 5.1 Side View of Micro-Stripline*

### 5.3 Loss Mechanism

An infinitely small section of a transmission can be assumed to be composed of four components- resistance R, inductance L′, capacitance C′ and conductance G′ shown in Fig. 5.2. These four components represent the behavior of the transmission line. The resistance R′ is due to the finite conductivity of the conductors, the conductance G′ represents the dielectric loss of the substrate, the inductance L′ is due to the self-inductance of the conductors and the capacitance C′ is due to the close proximity of the conductors [81]. Also, it is important to note that the primed values indicate that the parameters are normalized with respect to length.

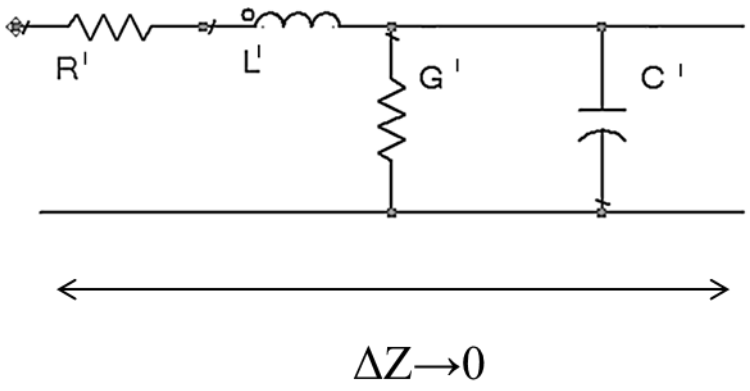


*Fig. 5.2 Lumped Element Circuit Model of a Transmission Line*

If the transmission line is considered to be lossy, then propagation of the wave through it causes an attenuation and delay which is represented by the propagation constant ($\gamma$). The propagation constant is given by,

$$\gamma = \alpha + j\beta \tag{5.1}$$

where $\alpha$ represents the attenuation constant and $\beta$ represents the phase constant. The attenuation constant $\alpha$ is composed of four components which add up to produce to the total attenuation.

$$\alpha = \alpha C + \alpha D + +\alpha R \tag{5.2}$$

where,

$\alpha C$ represents the attenuation due to metal conductivity

$\alpha D$ represents the attenuation due to loss tangent of the dielectric substrate

$\alpha G$ represents the attenuation due to conductivity of the dielectric

$\alpha R$ represents the attenuation due to radiation

### 5.3.1 Attenuation Due to Conductor

The conductor loss in a micro-strip line is due to the top conductor and the bottom ground plane. The total resistance offered by both the conductors contributes the term R´ in Fig. 5.2. The surface resistivity $R_S$ of the conductor and the attenuation due to the conductor $\alpha C$ are given by,

$$R_S = \sqrt{\frac{\omega \mu o}{2\sigma}} \tag{5.3}$$

$$\alpha c = \frac{R_S}{Z_O \times W} \text{ Np/m} \tag{5.4}$$

where $\omega = 2\pi f$ and f is the frequency, $\mu o$ - Permeability of free space, $\sigma$ - Bulk conductivity of the conductor, $Z_O$ is the characteristic impedance and W is the width of the conductor. It can be seen from equation (5.4), that surface resistivity of the conductor increases with frequency. Hence, at high frequencies high attenuation will be observed

due to conductors. Also, from equation (5.3) and (5.4), it can be observed that for high conductivity materials, the attenuation due to conductors will be low. Further, unlike DC frequency, where the whole the conductor is used for conduction, at high frequencies the amount of penetration of the EM waves into the material depends on the frequency. This frequency dependent penetration of EM waves into the material is known as skin depth. It is given by the equation (5.5) [79].

$$\delta s = \sqrt{\frac{1}{\pi f \mu \sigma}} \tag{5.5}$$

where $\delta s$ - Skin depth. By comparing equations (5.3) and (5.5),

$$R_S = \frac{1}{\sigma \times \delta s} \tag{5.6}$$

From equation (5.6), it can be understood that to reduce the loss due to metal conductors, thickness of the metal layer must be higher than the skin depth. Generally, 5 times the skin depth helps to reduce the bulk resistivity of the conductor to 0.7% of its full value [82].

In this research, two materials used for the conductive layer were Zoflex and copper. The extracted DC conductivity of zoflex from chapter 4 (~$1\times10^4$S/m) and copper with a well-known bulk conductivity ($5.8\times10^7$S/m) were plotted using equation (5.5) to study variation of skin depth in the desired frequency range of 1 to 5 GHz. This shown in Fig. 5.3. From Fig. 5.3, it can be observed that, copper due its high conductivity, has a low skin depth. Zoflex, being the material with a low conductivity, has a large skin depth which means that a thick material is needed to achieve low loss at high frequencies. In the multi-layer approach, where copper and zoflex layer combination are used, theoretically the effective conductivity is expected to be closer to copper at low strains

and closer to zoflex at high strains. So, a comparatively thicker layer of copper (few times the skin depth) has to be used to reduce the attenuation due to copper at low strains. Hence, copper of thickness 4µm was used in this research. The Zoflex layer has to be several times thicker than the skin depth (~100µm) to reduce loss at high strains. But using a thick zoflex layer reduces the stretchability of the device. Also from equation (3.10), it is better to have a thin layer of Zoflex to obtain high effective conductivity of the multi-layer structure. Taking this into account, the thickness of the zoflex layer was chosen as 100µm (~one time skin depth).

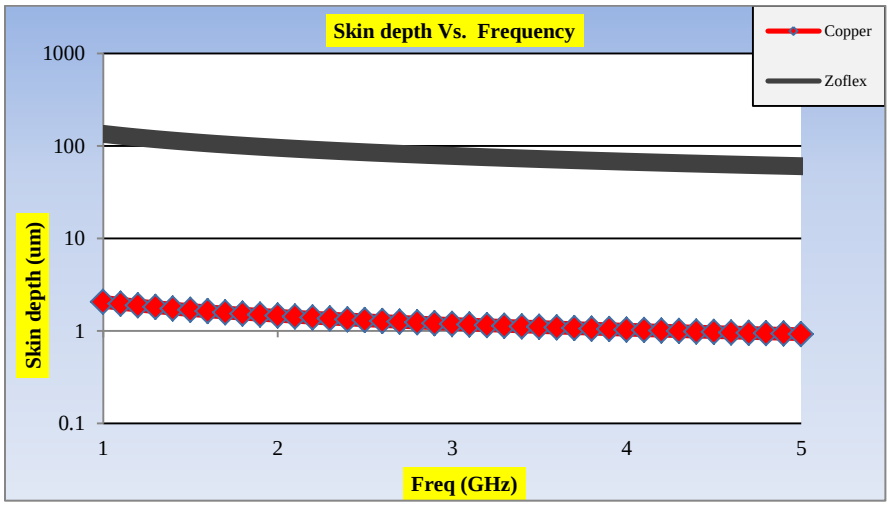


*Fig. 5.3 Variation of Skin Depth of Copper and Zoflex with Frequency*

### 5.3.2 Attenuation Due to Loss Tangent of the Dielectric

The attenuation due to loss tangent ($\tan(\delta)$ ) of the dielectric can be significant if the material used is lossy as well as when it is used at high frequencies. The attenuation due to dielectric loss can be given by,

$$\alpha D = \frac{k_O \times \varepsilon r(\varepsilon eff - 1) \times \tan(\delta)}{2\sqrt{\varepsilon eff}(\varepsilon r - 1)} \text{ Np/m} \qquad (5.7)$$

$$k_o = \omega\sqrt{\mu\varepsilon} \tag{5.8}$$

where $\varepsilon eff$ is the effective permittivity. Thus, it can be seen that the loss tangent is directly proportional to the frequency and hence increases with frequency.

### 5.3.3 Attenuation Due to Conduction of the Dielectric

If the dielectric substrate does not have good insulating properties, then it can produce a loss due to current leakage to the current ground plane. This is accounted by the term G´ in the lumped element model. Generally, this value is very low because most of the substrates have a high resistivity. The loss due to substrate conductivity is given by equation (5.9) [83].

$$\alpha G = \frac{G\prime Zo}{2} \text{ Np/m} \tag{5.9}$$

### 5.3.4 Attenuation Due to Radiation

When the micro-striplines start to radiate, the radiation causes attenuation to the energy of the input signal. This creates a loss known as the radiation loss. Generally, the radiation loss is due to impedance mismatch caused by poor connection. Also, using thick substrates for the micro-strip lines may give rise to radiating waves.

## 5.4 Dielectric Characterization of PDMS

The PDMS was fabricated using Dow corning Sylgard®184. The permittivity and loss tangent specified by the vendor was 2.68 and 0.001 at a frequency of 100 KHz. Since the multi-layer approach was planned to be used for RF applications, it was decided to characterize PDMS in the microwave frequency range up to 3 GHz. The method chosen for the characterization of PDMS was open-ended co-axial probe measurement. This was

done with the help of the HP dielectric kit 85070B. The test bench consisted of VNA 8719D, HP dielectric kit and computer running HP 85070 software program as shown in Fig. 5.4. The software controlled the VNA to measure the complex reflection co-efficient of the Material Under Test (MUT) and then it was converted to complex permittivity of the MUT.

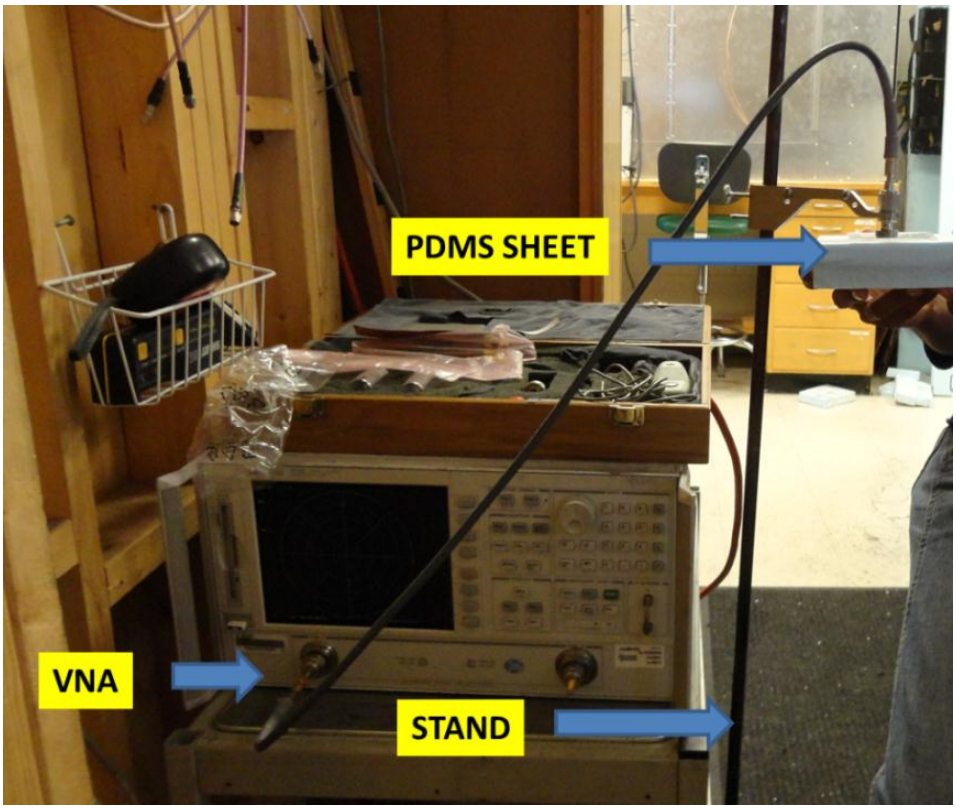


*Fig. 5.4 Test Set-Up Used for Dielectric Characterization of PDMS*

The VNA was interfaced to the computer using GPIB and Lab view 2010. The open-ended coaxial probe and test stand were set up. The test frequency range was set to 50 MHz – 3 GHz. The calibration was performed using the standards - Short (S), open (O) and water (W). Distilled water was used as it is free from contamination. The

software displayed the complex permittivity in terms of ε', ε'' and loss tangent of the material. The calibration standards are shown in Fig. 5.5.

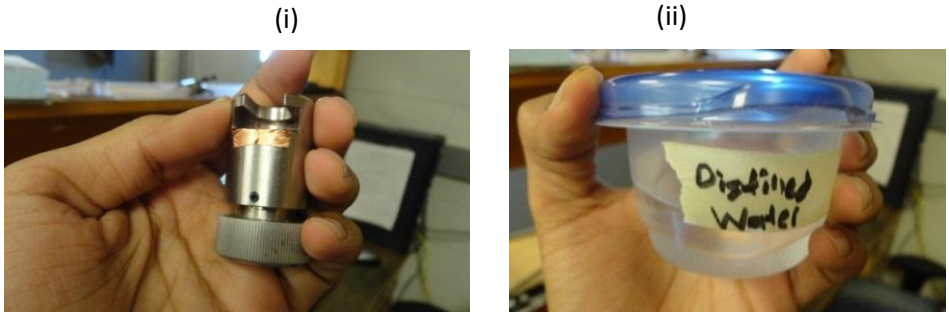


*Fig. 5.5 Calibration Standards Used for Dielectric Characterization of PDMS. i) Short and ii) Water*

The PDMS sheet of thickness 1mm was placed on a rigid material and held close to the probes. Care was taken to ensure that the inner and outer conductors of the co-axial probe touched the material completely. The measured permittivity and loss tangent are shown in Fig. 5.6. The permittivity and loss tangent were measured as 3.1 and ~0.02 up to 3 GHz.

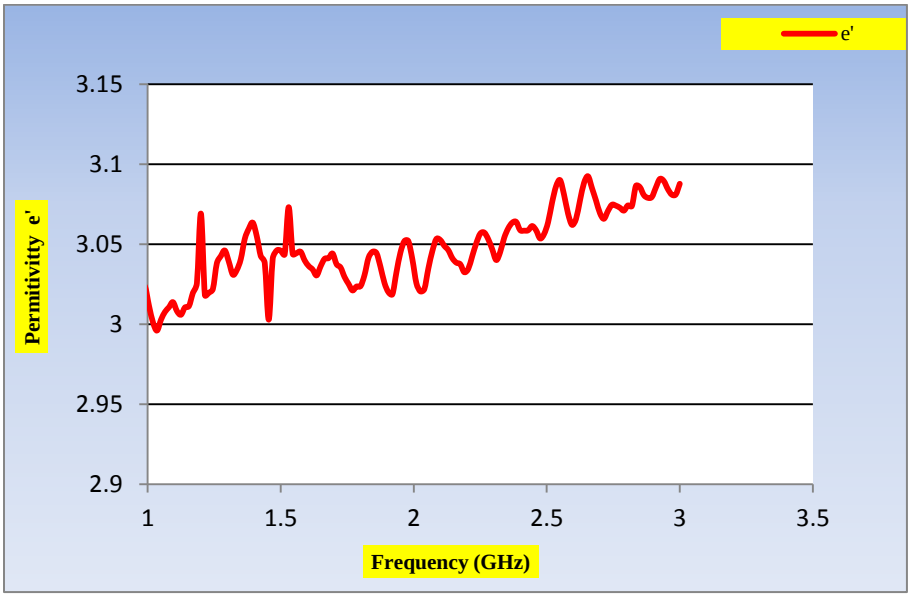


*Fig. 5.6 (i) Permittivity of PDMS*

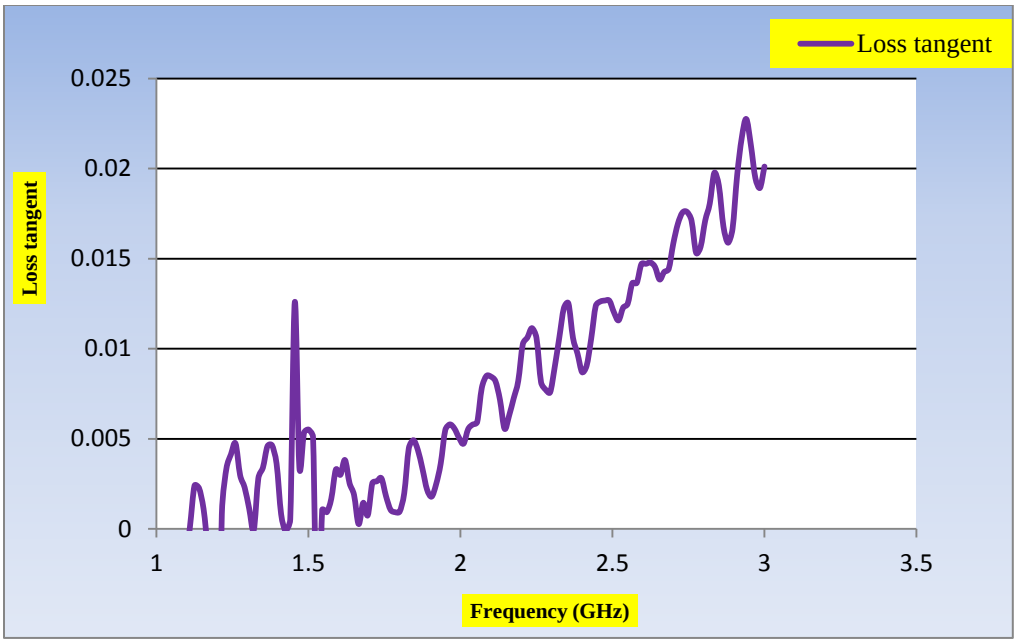


*Fig. 5.6 ii) Loss Tangent of PDMS*

### 5.5 Design of 50-Ohms Micro-Stripline

The geometry of micro-strip lines and the important parameters needed for the calculation of dimensions of a micro-strip line has been discussed in section 5.2. Generally, micro-strip lines of impedance 50 ohms are widely used in various RF circuits. The width of the top conductor and height of the substrate determines the characteristic impedance. The length accounts for the delay of the signal through the transmission line. The theoretical formulas for the calculation of the dimensions for the 50 ohms micro-strip lines are given below.

#### 5.5.1 Theoretical Equations for the Calculation of Dimensions of 50-Ohms Micro-Striplines

Since the electric field extends in the air in addition to the dielectric substrate an effective dialectic constant is found. This is given by equation (5.10) [79].

$$\varepsilon eff = \frac{\varepsilon r + 1}{2} + \frac{\varepsilon r + 1}{2}\left[1 + \frac{12 \times h}{W}\right]^{-1/2} \tag{5.10}$$

For a given characteristic impedance $Z_O$ and an effective dielectric constant $\varepsilon eff$, the W/h ratio can be found using,

$$\frac{W}{h} = \begin{cases} \dfrac{8e^{A}}{e^{A} - 2} & \text{for W/h} \le 1 \\ \dfrac{2}{\pi}\left[B - 1 - \ln(2B-1) + \dfrac{\varepsilon eff - 1}{2\varepsilon eff}\left\{\ln(B-1) + 0.39 - \dfrac{0.61}{\varepsilon eff}\right\}\right] & \text{for W/h} \ge 1 \end{cases} \tag{5.11}$$

where,
$$A = \frac{Z_O}{60}\sqrt{\frac{\varepsilon eff + 1}{2}} + \frac{\varepsilon eff - 1}{\varepsilon eff + 1}\left[0.23 + \frac{0.11}{\varepsilon eff}\right] \tag{5.12}$$

$$B = \frac{377\pi}{2Z_O\sqrt{\varepsilon eff}} \tag{5.13}$$

Using (5.10)-(5.13) the width of the 50-ohms micro-strip can be found.

### 5.5.2 Use of Agilent ADS Linecalc Tool for the Calculation of Dimensions of 50-Ohms Micro-Striplines

Instead of the theoretical equations discussed in section 5.5.1, the Linecalc tool of Agilent ADS can also be used to accurately calculate the dimensions of the 50-ohms micro-strip lines. The parameters used for calculating the dimensions are listed in Table 5.1.

*Table 5.1 Parameters Used for the Calculation of Dimensions of 50-Ohms Micro-Striplines*

| **Substrate Parameters** | **Description** | **Value** |
|---|---|---|
| **εr** | Relative dielectric constant | **3.1** |
| **TanD** | Dielectric loss tangent | **0.02** |
| **Mur** | Relative permeability | **1** |
| **H** | Substrate thickness | **1 mm** |
| **Cond** | Top conductor conductivity | **5.8e+7 S/m** |
| **T** | Copper thickness | **4µm** |
| **F** | Frequency | **2.4 GHz** |
| **$Z_O$** | Characteristic impedance | **50 ohms** |

The line width was calculated as 2.5 mm at a frequency of 2.4 GHz.

## 5.6 Fabrication and 2-Port Measurements of Multi-Layer Structures

### 5.6.1 Fabrication

The different multi-layer structures – Zoflex, Copper-Zoflex. Zoflex- Copper and Copper-Zoflex-Copper – were fabricated using the technique discussed in section 4.3. In order to study the loss due to the top conductor layer, a copper ground plane was used. The fabricated flexible transmission line is shown in Fig. 5.7.

*Fig. 5.7 Fabricated Flexible Micro-Stripline with Copper Ground Plane*

### 5.6.2 2–Port Measurements

The 2-port measurements of the micro-strip lines were done to verify the loss and match in the desired frequency range of 1-5 GHz. The measurement test bench is shown in Fig. 5.8. A SOLT (Short, open, load, thru) calibration was performed before the measurement. The cables were taped to the bench to avoid mismatch caused near the connectors. The SMA was soldered to copper tape at the back and silver paste was used near the pin of the connector to improve contact to the center conductor.

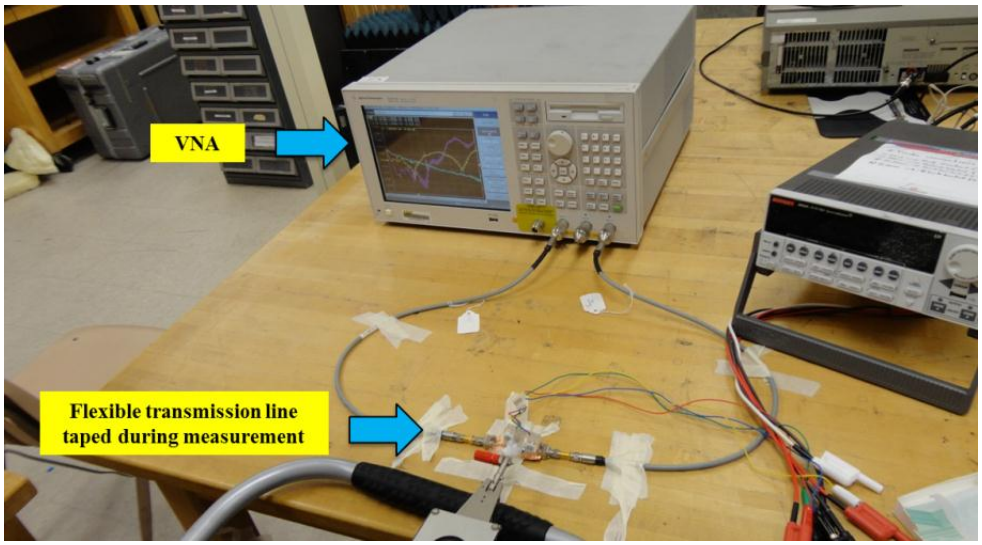


*Fig. 5.8 Test Bench for 2-Port Measurements*

### 5.6.3 Measurement Results

The 2-port measurements of the flexible transmission lines were done. The plots of measured S11 and S21 are shown in Fig. 5.9 (i) and (ii). From Fig. 5.9 (i), it is observed that all the structures except the direct copper on PDMS are matched with S11 close to -10dB. The direct copper on PDMS behaved like an open circuit due to the complete cracking of copper layer beyond 1% strain. Hence, it had a high reflection as observed in Fig. 5.9(i). The reason that Copper-Zoflex structure has a slight mismatch may due to variation in the width of the conductor layer during fabrication. From Fig 5.9 (ii), it can be seen that the copper tape had a low loss of 0.53 dB. This value is low because of the high conductivity of copper tapes with no deformities in the structure. Of the fabricated samples, the Zoflex structure had a high loss sample had a loss of 3.76 dB. This was expected due to the low conductivity of Zoflex structure and hence produces attenuation as discussed in section 5.3.1.

The multi-layer structures – Zoflex-Copper had a loss of 2.25dB, Copper-Zoflex had a loss of 4.3dB and the Copper-Zoflex-Copper layer had a loss of 1.54dB. The multi-layer structures, due to a higher effective conductivity than Zoflex, were expected to demonstrate lesser loss. Also, it can be observed that Copper-Zoflex had a very high loss, even higher than Zoflex. On investigation of the sample, it was found that center conductor width was closer do 2.7 mm which could have caused an impedance mismatch. Another reason could have been due to formation of large micro-cracks in the bottom copper layer. Hence, the effect of copper layer is reduced and the conductivity is closer to that of Zoflex. Thus, the impedance mismatch along with a cracked copper layer formation may be the reason for a high loss.

On comparison of the Zoflex, Zoflex-Copper and Copper-Zoflex-Copper structures, it can be observed that by adding copper layer the effective conductivity is improved and hence the loss can be reduced up to 58%.

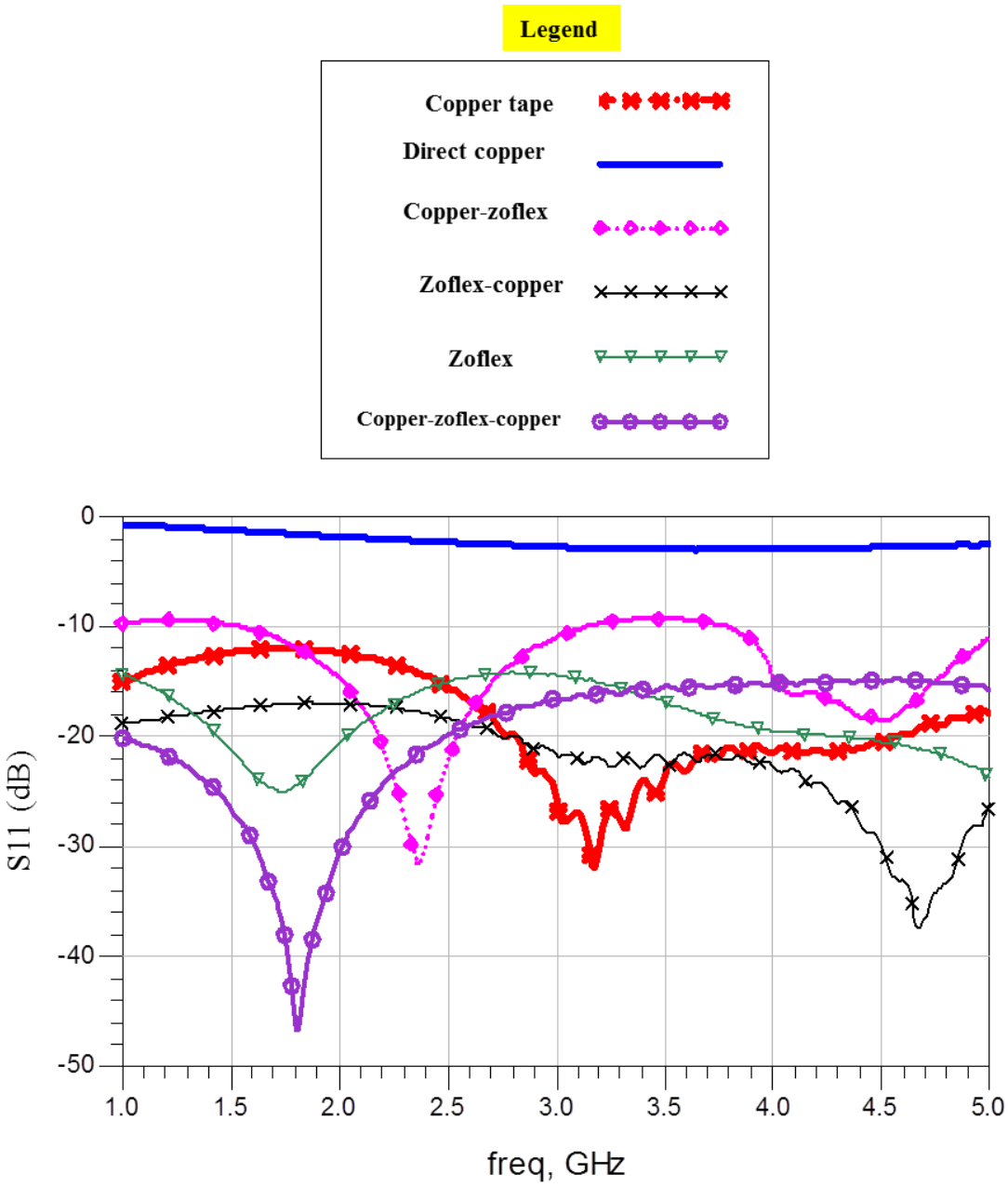


*Fig. 5.9 i) Measured S11 (dB) of the Multi-Layer Structures*

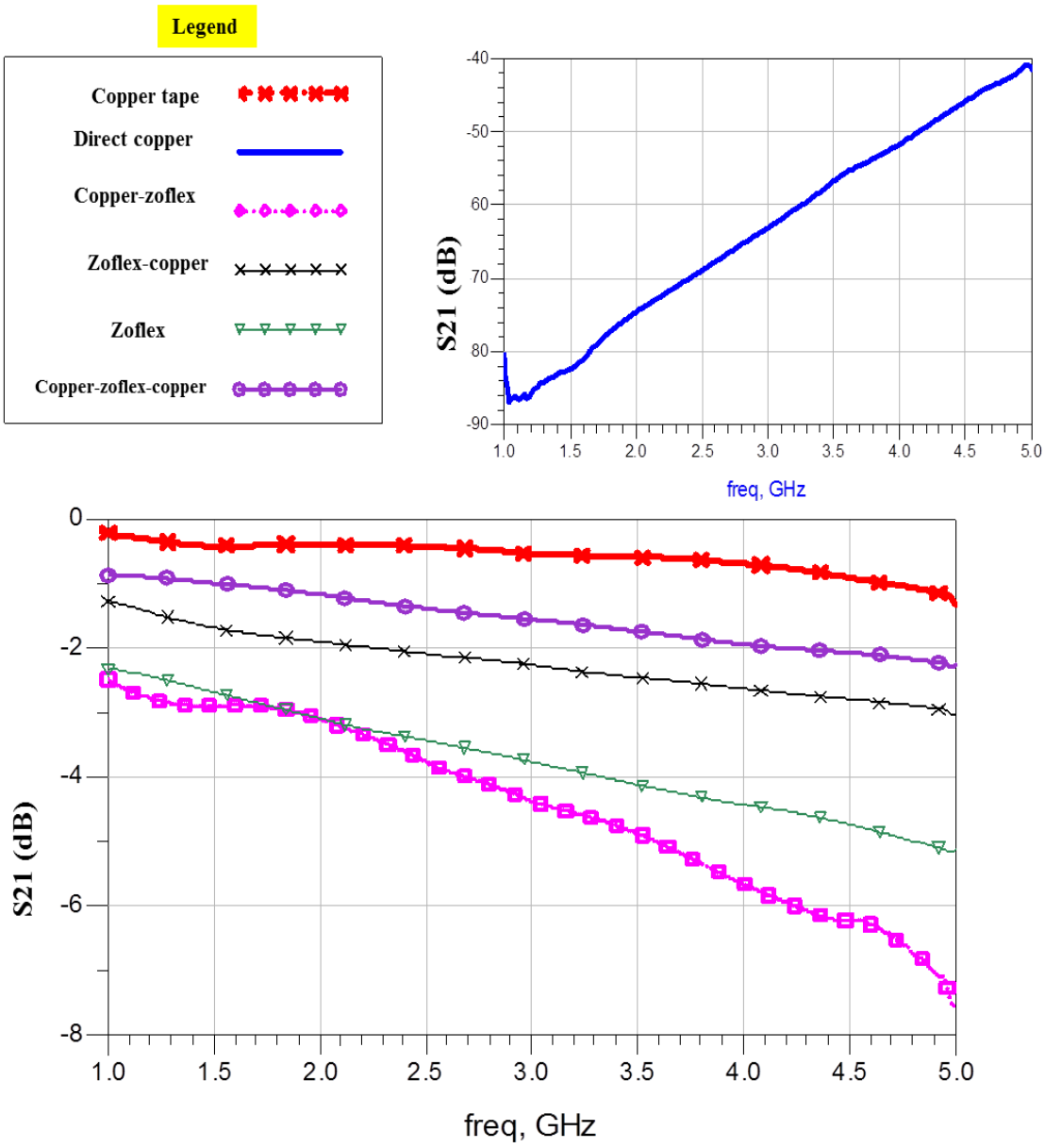


*Fig. 5.9 ii) Measured S21 (dB) of the Multi-Layer Structures*

### 5.7 Performance Analysis Due to Bending of the Micro-Striplines

The Copper-Zoflex-Copper micro-strip line was bent on surfaces with different radius of curvature as shown in Fig. 5.10. The sample was taped to avoid movement which can cause errors in the measurement.

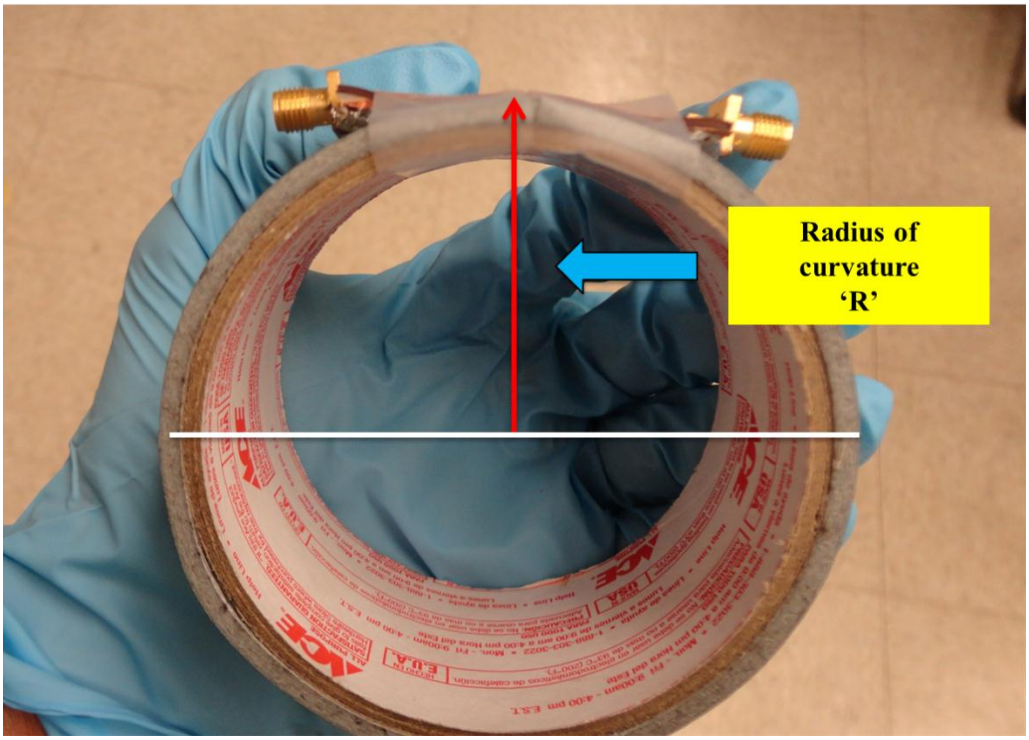


*Fig. 5.10 Bending of Flexible Micro-Stripline on Curved Surfaces with Different Radius of Curvature 'R'*

The flexible transmission line was placed on three different objects with radius of curvature – 15mm, 42.25mm and 43.75mm. It was observed that the loss increases with decrease in radius of curvature. The sample on the curved surface with 15 mm radius showed a high loss. This because, when the sample was bent on surfaces with low radius of curvature, the pressure exerted on the connectors increases which may cause a mismatch near the connectors and increase the loss of the structure. Also, the bending can

damage the over-lapped metal islands of the multi-layer structure which may also be the reason for a higher loss observed due to bending. The loss measurement in the other two curved surfaces (42.25mm and 43.75mm) which had nearly the same dimensions, showed almost the same loss. Finally, the sample was placed on a planar surface and loss was measured to be close to the original value before bending the sample. This demonstrated that the multi-layer sample was not irreversibly damaged due to bending. The loss measurement due to bending is shown in Fig. 5.11.

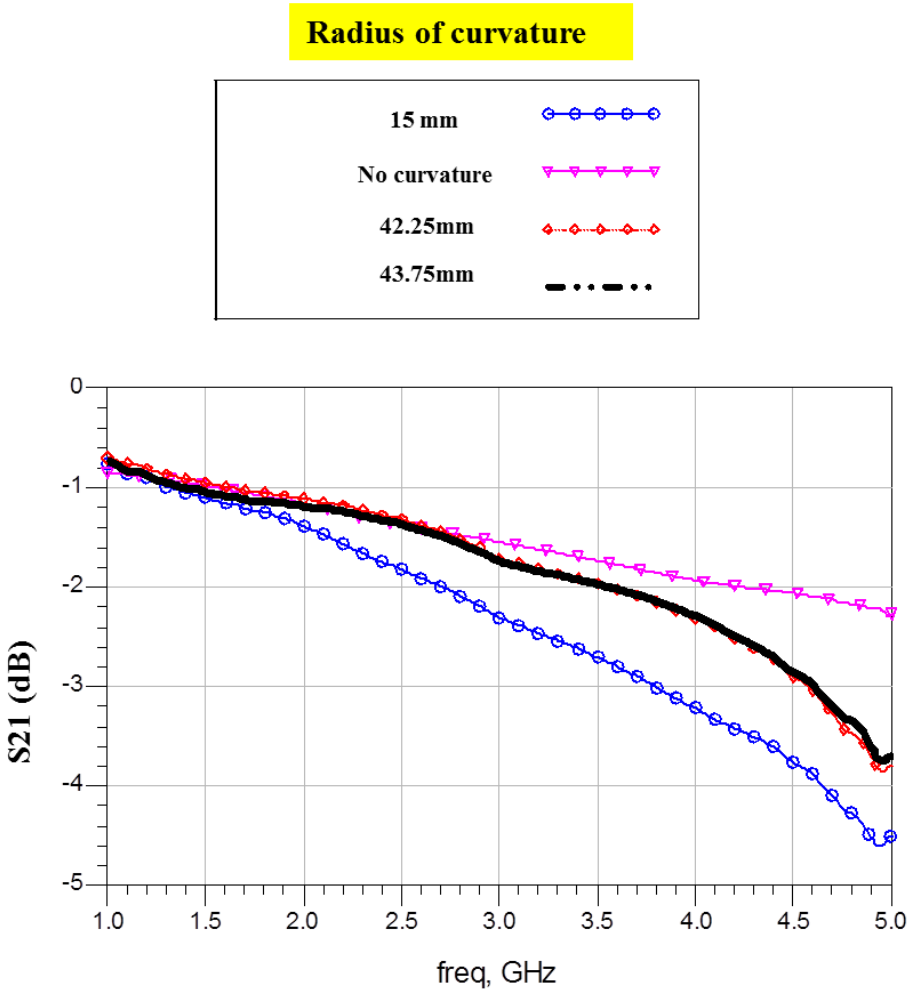


*Fig. 5.11 Loss Measurement Due to Bending*

## 5.8 Conclusion

In this chapter, an approach to fabricate flexible transmission lines was demonstrated. The dielectric characterization of PDMS was done using open-ended co-axial probe measurement to study the permittivity and loss tangent. The different multi-layer structures were fabricated based on the multi-layer stretchable conductor approach and tested. From the measurements, it was seen that the multi-layer approach can be used to reduce the loss of the Zoflex by 58% at high frequencies. The flexible micro-striplines were also bent and loss due to bending was investigated. It was observed that multi-layer structure based micro-striplines are not permanently damaged due to bending. Thus from this chapter, it can be inferred that the multi-layer stretchable conductors approach can be used for making planar RF circuits and antennas.

# CHAPTER 6

# RECONFIGURABLE PATCH ANTENNA

## 6.1 Introduction

A flexible micro-stripline using the multi-layer stretchable conductors which allows the device to bend without getting damaged was demonstrated in chapter 5. It was demonstrated that using a ideal combination of Copper and Zoflex the loss can be reduced up to 58% and hence the approach can be used for making planar RF circuits and antennas. In this chapter, the multi-layer approach will be used to design a reconfigurable antenna to study the efficiency of the approach for antenna applications. Previous works on making flexible/stretchable antennas using various techniques such pre-straining, micro-fluidics, electrically conductive composite and conductive textiles have been discussed in section 2.2.3.

Since the antenna fabricated using the multi-layer approach can be stretched, its performance can be tuned mechanically. A patch antenna design was chosen to demonstrate the mechanical tuning of the multi-layer stretchable conductor antenna. The advantages of a patch antenna are that it has a low profile, conformable to non-planar surfaces, simple and inexpensive [84]. In this chapter, different feeding techniques of the patch antenna are discussed to choose the best technique to feed antenna. The theory and working of the patch antenna are also explained. Antenna model is designed using 3D

EM simulation software HFSS to study the effects of stretching on the antenna performance. In the last section, the fabrication and measurements of the multi-layer patch antennas are discussed.

### 6.2 Design Considerations

Generally, polymers used as substrates for stretchable antennas withstand high strains (140% for PDMS and up to 700% for silicone) [42]. But the measurement of antenna to demonstrate stretchability using mechanical straining has been limited due to rigid feed and connectors [40, 41]. A stretchability only up to 40% was demonstrated though theoretically up to 100% was possible due to rigid feed of antenna [41]. A hybrid structure consisting of stiff silicone rubber near the connectors and soft silicone for stretching the antenna was used to achieve strains up to 120% [85]. But the process of fabrication is complicated. To overcome this, a feeding structure which is not affect by stretching was designed in [42]. A similar kind of design has been used for our approach.

The popular techniques for feeding a patch antenna are : inset feed, co-axial probe, proximity coupling and aperture coupled feed [84]. The inset feed and co-axial probe are simple to fabricate but the feed can be disturbed while stretching the patch and is not suitable for the multi-layer approach. The aperture coupled feed and proximity-coupled feed can be used as the feed does not physically touch the radiating patch. The aperture-coupled feed design was chosen since ground plane between the substrates isolates the feed and reduces interference [84].

### 6.3 Theory of Aperture-Coupled Patch Antenna

#### 6.3.1 Introduction

The aperture-coupled feed patch antenna contains two substrates namely, feed and the patch substrate separated by a ground plane. A micro-stripline feeds the radiating patch through a slot in the ground plane. The antenna design is shown in Fig. 6.1.

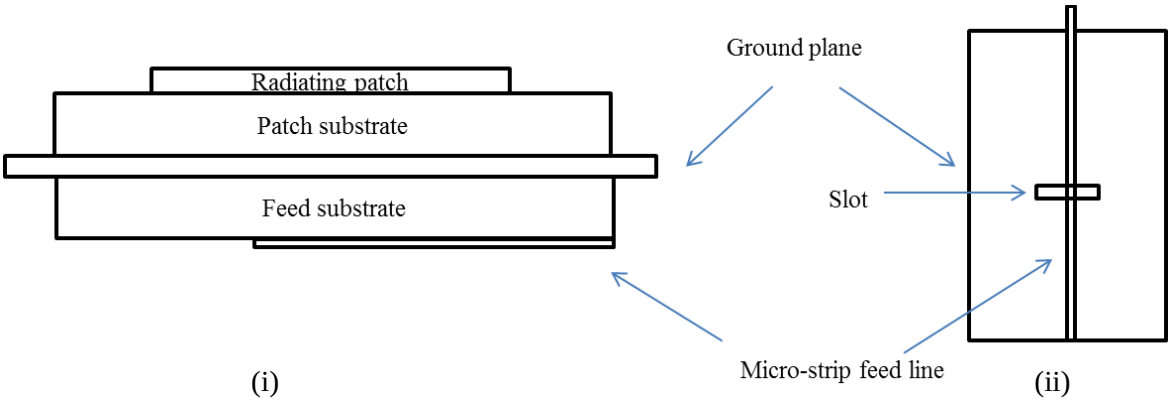


*Fig. 6.1 Aperture-Coupled Patch Antenna. (i) Side view, (ii) Ground plane with slot*

The feed substrate is designed to support guided waves between the feed line and the ground plane. The guides waves are dominant if the substrate is electrically thin ($h<\lambda/50$) and has a large permittivity ($\varepsilon r>5$) [86]. In contrast, the radiating patch is designed to increase radiating waves at the edges and reduce guided waves under the patch. So this requires thick dielectric substrate ($h>\lambda/10$) with a low permittivity ($\varepsilon r<3$). Compromising the requirements for patch and feed substrates leads to low radiation efficiency and increased spurious radiation from the feed line [86].

#### 6.3.2 Principle of Operation

The micro-strip feed line shown in Fig. 6.2 is an open-ended transmission line with minimum current and maximum voltage at the edge of the line. Generally, the

distance between the open-end and the center of the slot is chosen as λ/4. This is a quarter-wave transformer transforms the open-circuit to a short-circuit at the center of the slot. So, the current is maximum and voltage is minimum at the center of the slot. With the slot as the center, λ/4 patch is designed on either side making the total length of the patch as λ/2. Thus, voltage is maximum at the radiating ends of the patch and current is maximum at the center of the patch.

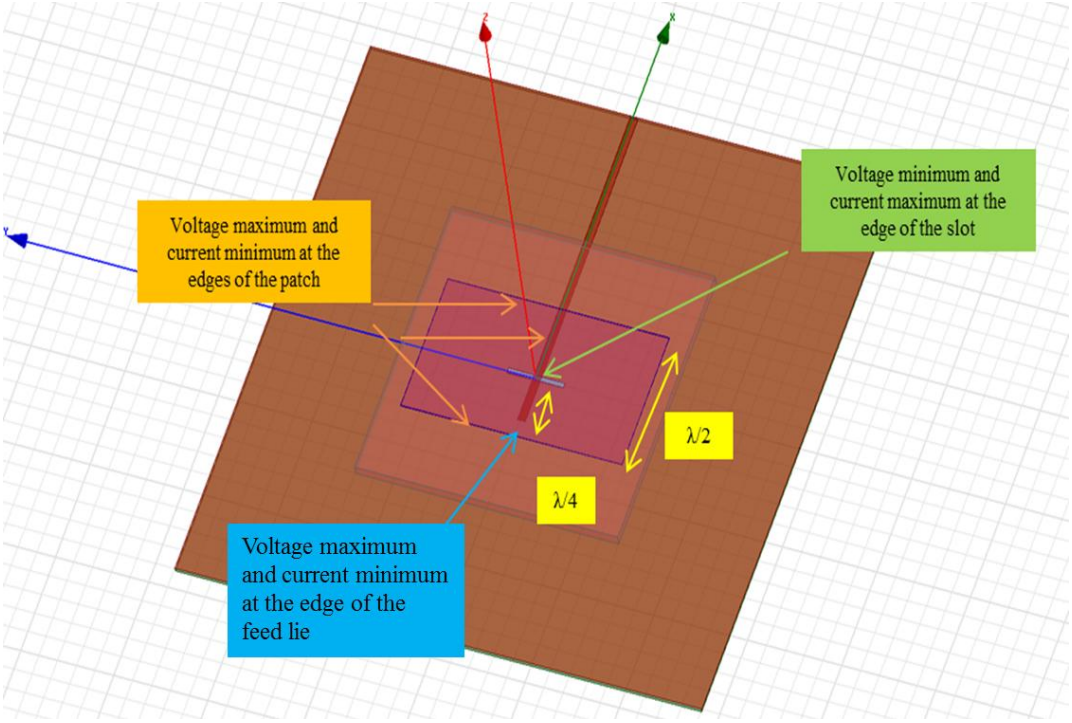


*Fig. 6.2 Principle of Operation of Aperture-Coupled Patch Antenna*

The distance between the center of the slot and the edge of the open-ended transmission line may be less than λ/4 in actual design. But even the smaller length acts like a quarter wave transformer due to ground slot and patch loading effects [87]. In Fig. 6.2, the direction of current in feed line is along x-axis. This generates an electric field at

the slot that excites the patch antenna fields and currents as shown in Fig. 6.3. The far field radiation from this distribution is x-polarized along z-axis.

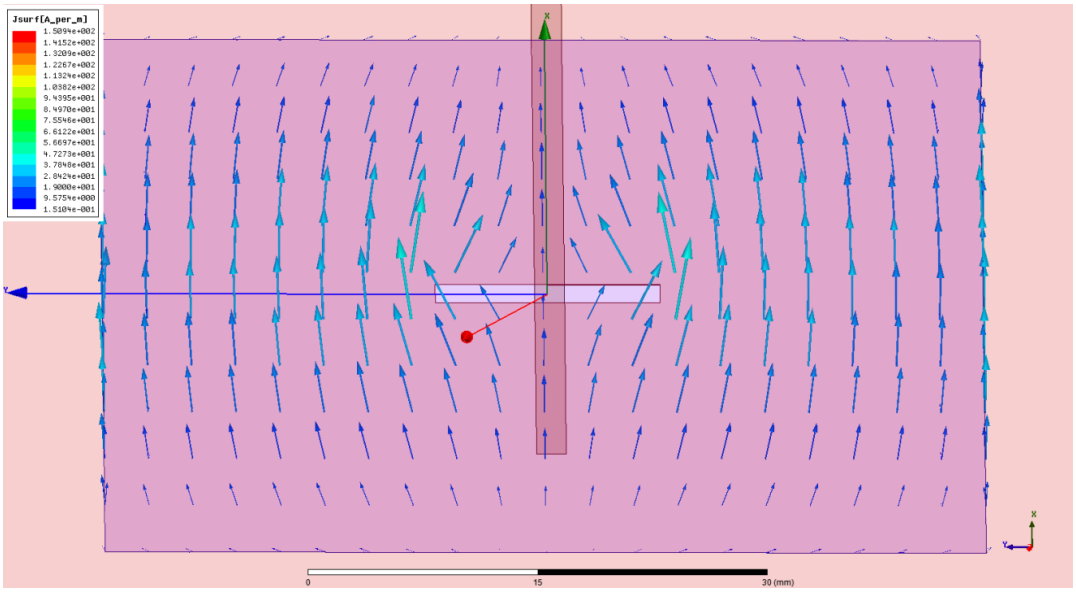


*Fig. 6.3 Current Distribution on the Surface of the Patch*

### 6.4 Theoretical Equations for Calculating Antenna Dimensions

The radiating length and width of the patch can be found if the substrate height, dielectric permittivity and loss tangent of the substrates are known. The width of the patch is given by equation (6.1).

$$W = \frac{vo}{2\,fr \times \sqrt{\mu o \times \varepsilon o}} \left[ \frac{2}{\varepsilon r + 1} \right]^{1/2} \tag{6.1}$$

where,

$vo$ - Velocity of light in free-space

$fr$ - Resonance frequency

$\mu o$ - Permeability of free space

$\varepsilon o$ Permittivity of free space

$\varepsilon r$ - Relative permittivity of the material.

Since the waves inside the patch substrate spread into air as well an effective dielectric constant is found using equation (6.2) [84].

$$\varepsilon eff = \frac{\varepsilon r + 1}{2} + \frac{\varepsilon r + 1}{2}\left[1 + \frac{12 \times h}{W}\right]^{-1/2} \tag{6.2}$$

Due to fringing, the length of the patch becomes electrically larger by ΔL on each side of the radiating patch. Hence the actual length of the patch is calculated by subtracting the extra length due to fringing. The length of the patch is given by,

$$L = \lambda / 2 - 2\Delta L$$

$$L = \lambda / 2 - (2 \times h \times 0.412) \times \left[\frac{\left[\varepsilon eff + 0.3\right]\left[\frac{W}{h} + 0.264\right]}{\left[\varepsilon eff - 0.258\right]\left[\frac{W}{h} + 0.8\right]}\right] \tag{6.3}$$

Using (6.1), (6.2) and (6.3) the length and width for a patch antenna on the PDMS substrate (εr=3.1 loss tangent =0.02) of thickness 2 mm was calculated as 26.70 mm and 33.79 mm respectively. The theoretical values of the length and width of the patch were used as the starting point for the design of the antenna discussed in section 6.5.

## 6.5 Antenna Design Using HFSS

### 6.5.1 Antenna Design

The 3D EM simulator Ansoft HFSS was used to design the antenna model. It uses finite element method (FEM) to find the solution. The aperture-coupled patch antenna was designed with Rogers RO3003 (εr=3, loss tangent =0.0013, thickness=0.75mm) as

the feed substrate and PDMS (εr=3.1, loss tangent =0.02, thickness= 2 mm) as the patch substrate with a ground plane in between them. The dimensions of the micro-strip feed line on the bottom of the feed substrate were calculated using ADS Linecalc. The parameters used for calculation are tabulated in Table 6.1.

*Table 6.1 Parameters Used for the Calculation of Width of the 50-Ohms Micro-Strip Feed Line*

| Substrate Parameters | Description | Value |
|---|---|---|
| **Er** | Relative dielectric constant | **3** |
| **TanD** | Dielectric loss tangent | **0.0013** |
| **Mur** | Relative permeability | **1** |
| **H** | Substrate thickness | **0.75 mm** |
| **Cond** | Conductor conductivity | **5.8e+7 S/m** |
| **f** | Frequency | **3.1 GHz** |

The width of the feed line was calculated as 1.88 mm. The calculated feed dimensions were used to design the bottom feed layer in HFSS. The feed substrate of dimensions of 90×90×0.75 mm was designed above the feed line. A ground plane with a slot was designed over the feed substrate. The slot was initially designed to be λ/4 from the open-end of the feed line. To make the currents x-polarized on the patch, the length and width of the slot were initially chosen in the ratio 10:1. The patch substrate with the radiating patch on top was placed over the slotted ground plane. The step-wise design of the aperture coupled patch antenna is shown in Fig. 6.4.

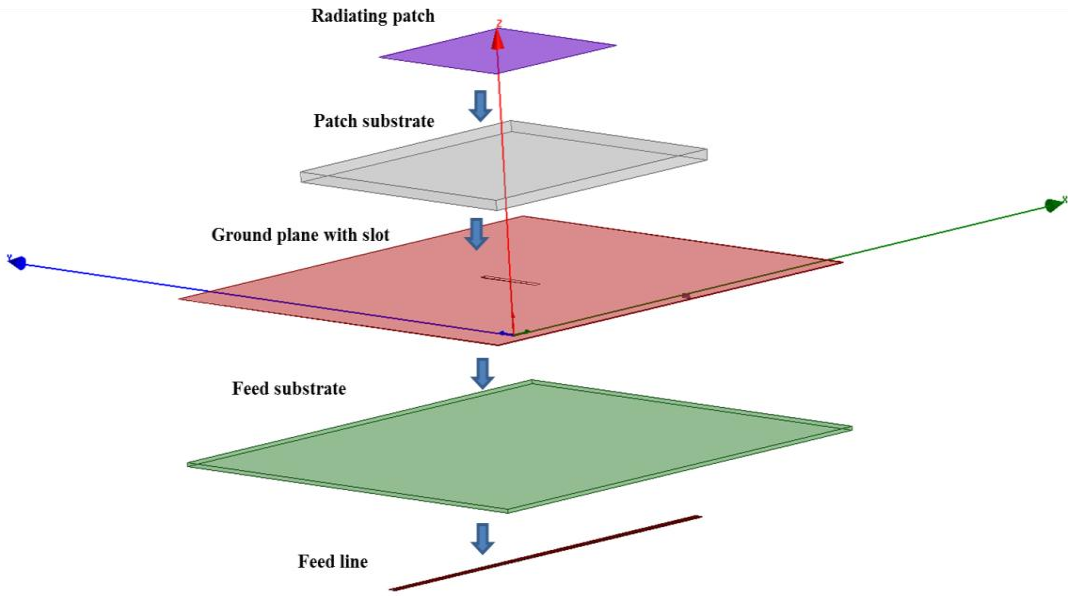


*Fig. 6.4 Stacked Layers of Aperture-Coupled Patch Antenna*

To avoid disturbance to the feed while stretching the radiating patch, a surface mount connector was fed from the bottom of the patch. In this way, except the stretchable substrate and the radiating patch, dimensions of all the other components remain fixed during measurements. The vertical fed aperture-coupled patch antenna is shown in Fig. 6.5.

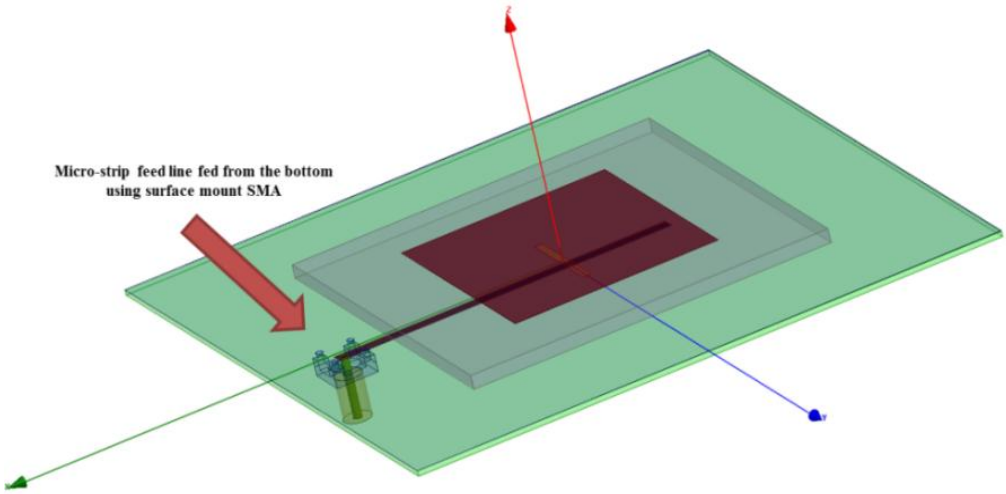


*Fig. 6.5 Aperture-Coupled Patch Antenna with Vertical Feed*

The surface mount connector Johnson 819D was accurately modeled in HFSS based on the dimensions specified by the manufacturer. Via-holes of dimensions 0.5 mm were made in the feed substrate to make contact to the ground plane. The modeled connector with via-holes and pads is shown in Fig. 6.6.

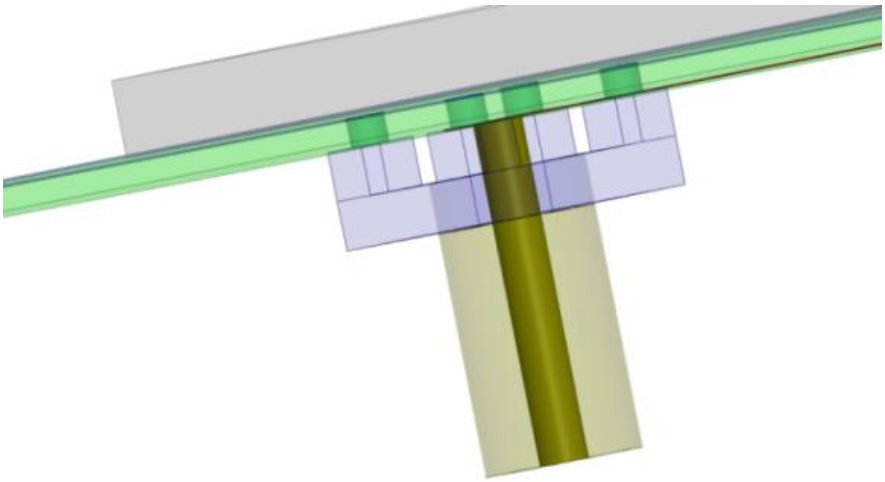

*Fig. 6.6 Surface Mount Connector with Via-Holes in the Feed Substrate*

### 6.5.2 Design Parameters for Antenna Impedance Matching

The aperture-coupled patch antenna was tuned in order to make the antenna resonate at 3.1 GHz with input impedance close to 50 ohms. The return loss was also decreased well below -20 dB so that even when the antenna is stretched to 25% the antenna's return loss will be below -10dB. The various parameters which can be used to tune the antenna are the length and width of the resonating patch, the distance between the open-end of the feed line and center of the slot and the width and length of the slot. Fig. 6.7 shows the various parameters used for tuning the antenna.

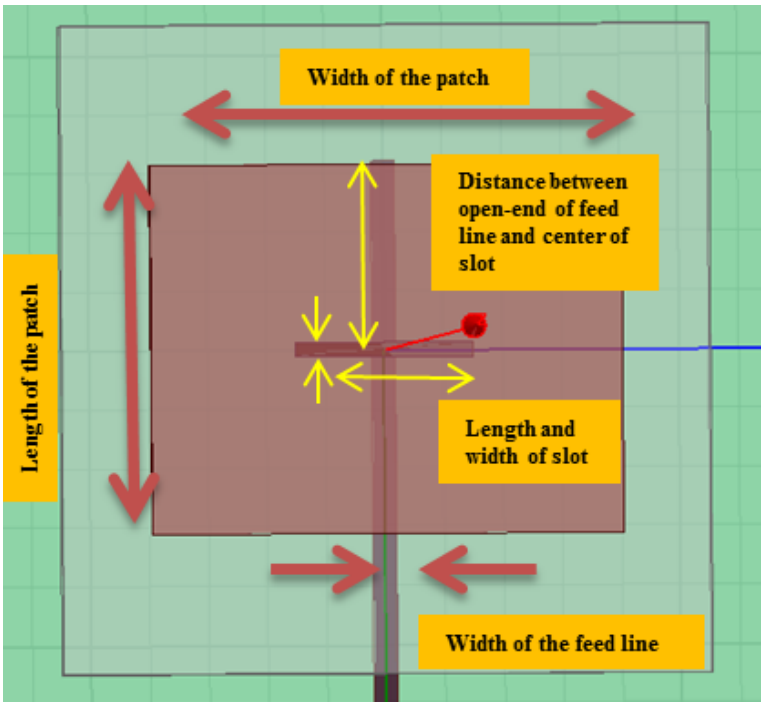


*Fig. 6.7 Patch Antenna Tuning Parameters*

The antenna was tuned by using the parameters shown in Fig. 6.7. The finalized patch antenna dimensions for resonance at 3.1 GHz are shown in Table 6.2.

*Table 6.2 Finalized Dimensions of Patch Antenna*

| Parameters | Dimensions (mm) |
|---|---|
| Length of patch conductor | 26 |
| Width of patch conductor | 35 |
| Length of patch substrate | 55 |
| Width of patch substrate | 55 |
| Thickness of patch substrate | 2 |
| Length of feed substrate | 90 |
| Width of feed substrate | 90 |
| Thickness of feed substrate | 0.75 |
| Length of feed line | 53.5 |

*Table 6.2: (continued)*

| | |
|---|---|
| **Width of feed line** | **2** |
| **Radius of outer conductor of connector** | **2.032** |
| **Radius of inner conductor of connector** | **0.635** |
| **Via radius** | **0.5** |

## 6.6 Antenna Fabrication

The different multi-layer patches: Zoflex, Copper- Zoflex and Copper-Zoflex-Copper were pre-strained to 10% and fabricated according to the desired dimensions using the same technique used for the fabrication of multi-layer stretchable conductors discussed in chapter 4. The feed substrate, with the feed line on the bottom surface and ground plane with slot on the top surface, was fabricated using LPKF milling machine. The surface mount connector was soldered to the feed line. The fabricated multi-layer patch and the patch taped on the ground plane are shown in Fig. 6.8 and Fig. 6.9.

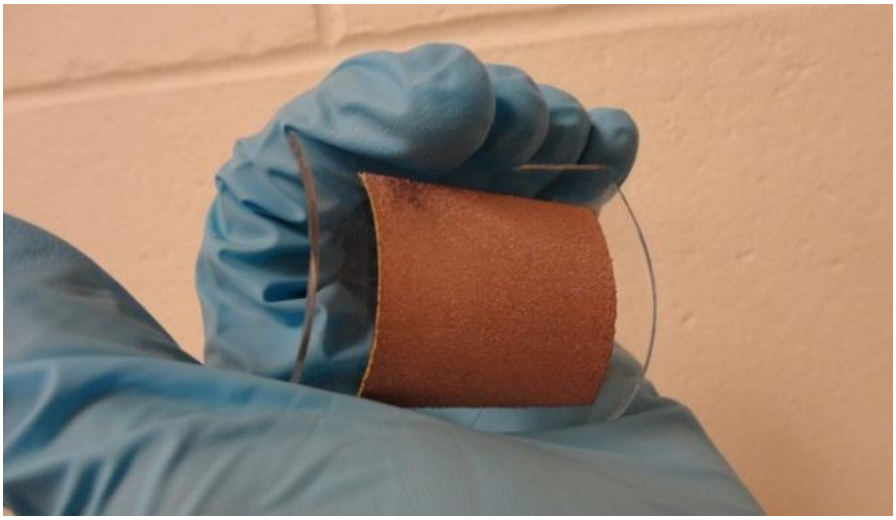

*Fig. 6.8 Fabricated Multi-Layer Patch*

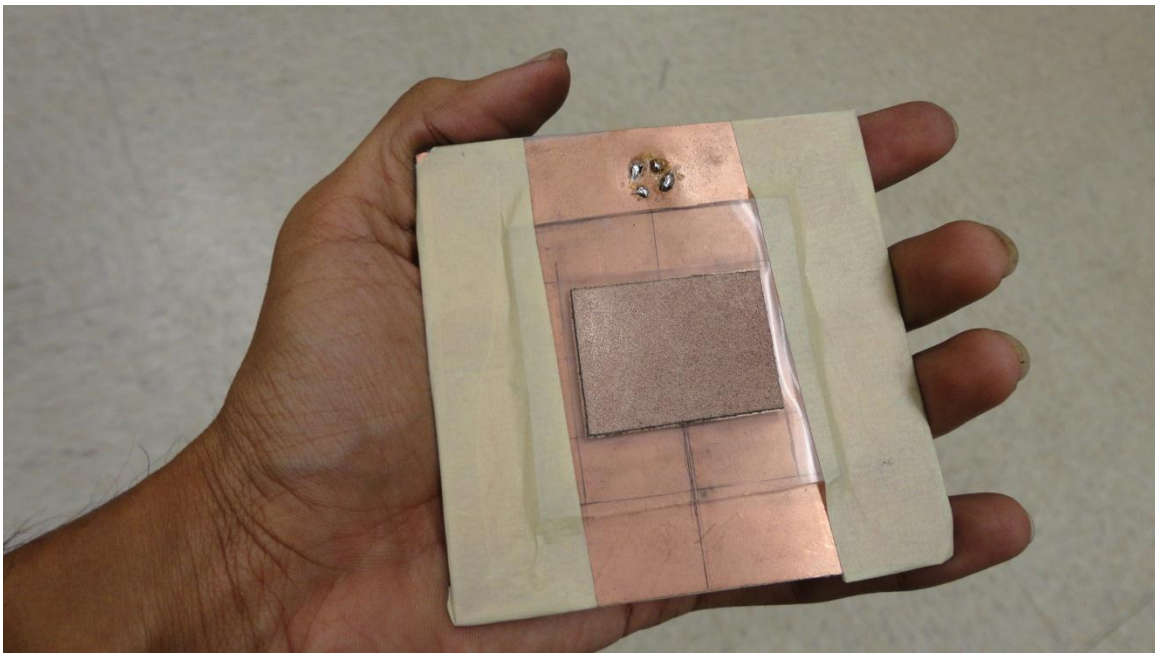

*Fig. 6.9 Multi-Layer Patch Taped on the Ground Plane*

### 6.7 Performance Analysis of Antenna

#### 6.7.1 Study of Copper Patch Antenna

The patch antenna model designed in section 6.5.1 was studied with copper as the conductor for the radiating patch. The antenna was tuned close to 50 ohms at 3.1 GHz. The antenna was designed to resonate with S11 less than -20dB. For the measurement, a copper tape on PDMS substrate was used design the copper patch antenna. The antenna was measured in an anechoic chamber to measure the resonance frequency and the radiation properties. The measured and simulated results of the copper patch antenna are shown in Fig. 6.10.

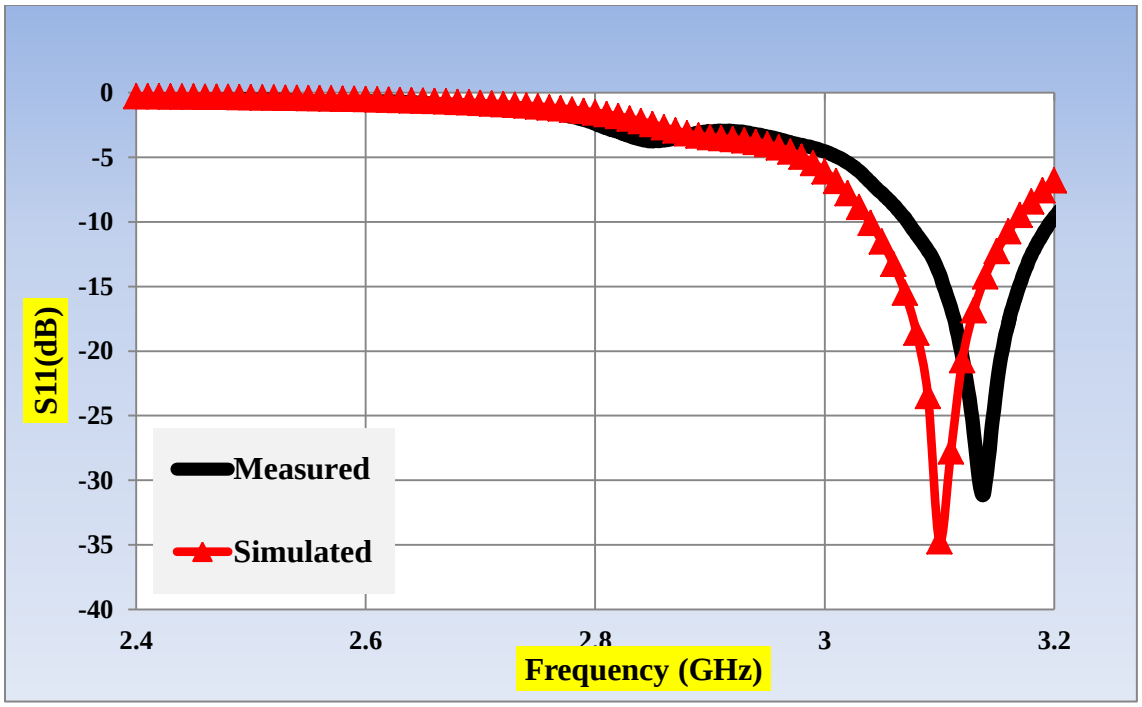


*Fig. 6.10 Simulated and Measured Results of Copper Patch Antenna*

Also, the radiation pattern was studied to see if the antenna resonated symmetrically in the broadside direction. The simulated E-plane (Co and cross) radiation pattern is shown in Fig. 6.11. The antenna had a simulated efficiency of 65% at 3.1 GHz. The low radiation efficiency is due to relatively thin patch substrate. Increasing the thickness of the patch can improve the radiation efficiency. But, it limits the stretching of the antenna. The antenna had a simulated realized gain of 7.33 dBi.

The copper tape patch antenna was measured to have a peak gain 6.24 dBi of at 3.1 GHz. The PDMS was measured using open-ended coaxial probe measurements which require infinitely thick substrates for accurate measurements. In this case, a thin substrate was used. So, PDMS may be lossier than the actual measurements which could contribute to a lower measured gain. The antenna had a bandwidth of ~4%. This was due to the low

substrate thickness and also the aperture-coupled feed patch antennas generally have low bandwidth (1-4%) [84].

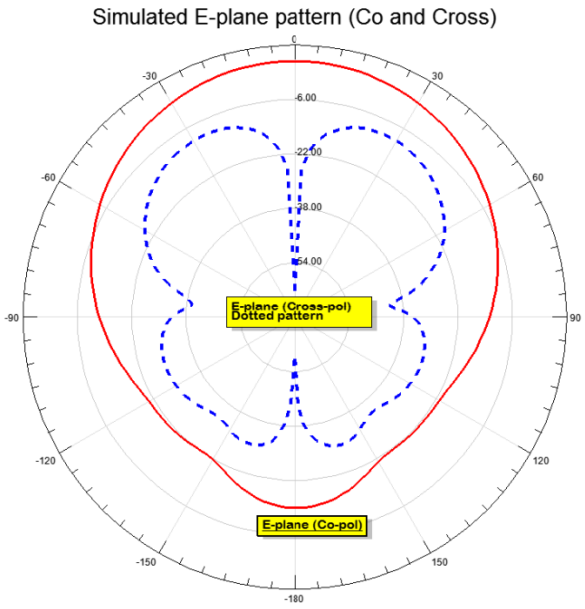


*Fig. 6.11 E-Plane Radiation Pattern of Copper Patch Antenna*

### 6.7.2 Antenna Stretching

The main advantage of using a stretchable substrate for the patch is that it can be used to tune the antenna by varying the patch length which shifts the resonance frequency. The antenna was held constant at one side and stretched along the other side in the x-direction. Since the surface currents in this model are x-polarized the resonance length is also along the x-direction. The patch antenna stretching is shown in Fig. 6.12. Ideally, the antenna can be stretched from 0% up to 25%. In the actual measurements, due to limitations of a stretch set-up, the antenna had to be stretched manually and only up to ~10% strains was possible.

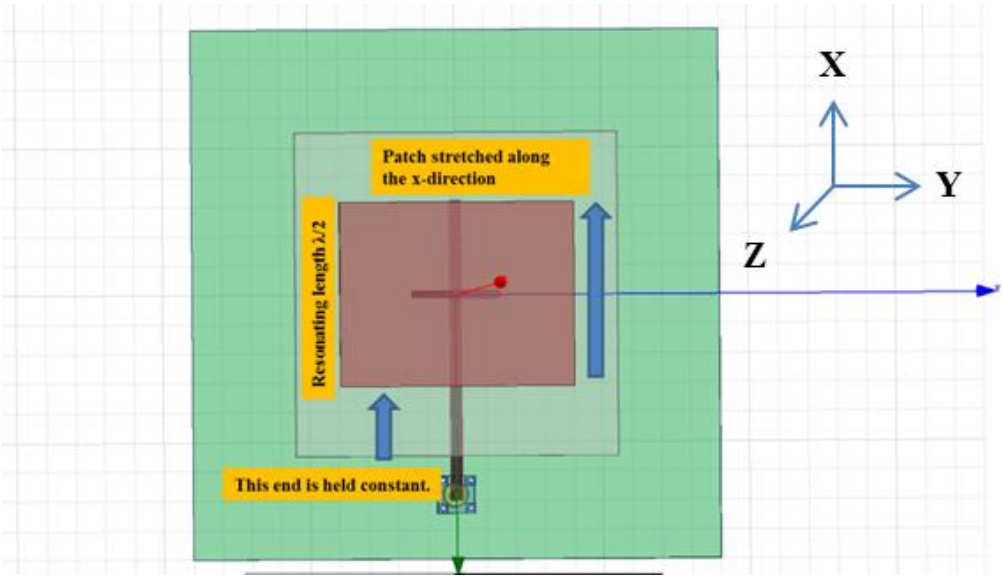


*Fig. 6.12 Mechanical Tuning of Patch Antenna by Holding One End Constant and Stretching Along the Resonating Length*

### 6.7.3 Study of Multi-Layer Patch Antennas

#### 6.7.3.1 Zoflex Patch Antenna

The Zoflex patch of thickness 100 µm and conductivity $1\times10^4$ S/m (extracted from chapter 4) was used for the simulation. The antenna was stretched up to 25% in the simulations and was observed that it can be tuned from 3.1 to 2.51 GHz. The variation of peak gain, peak realized gain, peak directivity and bandwidth with strain was studied using HFSS and are given in appendix D. The fabricated Zoflex patch was taped on the ground plane and tested. The antenna was stretched as discussed in section 6.7.2. The antenna resonated at 3.2 GHz. The reason the antenna resonated at slightly higher frequency may be due to errors in permittivity measurements. The permittivity of PDMS may be lower than the actual measurement. The fabricated antenna was stretched and the frequency shifting was observed. Due to limitations in antenna stretching, it was stretched

only up to 6%. It was observed the antenna was able to be tuned mechanically from 3.2 GHz to 2.95 GHz. The antenna was measured to have a peak gain 0.96 dBi at 3.2 GHz. The simulated and measured results of the Zoflex patch antenna are shown in Fig. 6.13.

#### 6.7.3.2 Copper-Zoflex Patch Antenna

The Copper-Zoflex patch of thickness 104 µm and conductivity of $2\times10^4$ S/m (extracted from chapter 4) was used for the simulation. The simulations were performed in the same way as the Zoflex patch antenna. The fabricated Copper-Zoflex patch was tested. The Copper-Zoflex patch antenna resonated at 3.2 GHz and it was stretched up to ~10% which tuned the antenna from 3.2 GHz to 2.87 GHz. The antenna was measured to have a peak gain 1.7 dBi at 3.2 GHz. It was seen that the peak gain was improved due to the addition of copper layer which increased the effective conductivity. The simulated and measured results of the Zoflex patch antenna are shown in Fig. 6.14. It can also be seen that the Copper- Zoflex antenna radiates better with the addition of copper layer.

#### 6.7.3.3 Copper-Zoflex-Copper Patch Antenna

The Copper-Zoflex patch of thickness 108 µm and conductivity of $2\times10^5$S/m (extracted from chapter 4) was used for the simulation. The fabricated Copper-Zoflex-Copper patch antenna resonated at 3.03 GHz and was stretched up to ~7% which shifted the antenna's resonance frequency from 3.03 GHz to 2.91 GHz. The antenna was measured to have a peak gain 4.36 dBi at 3.03 GHz. The simulated and measured results of the Zoflex patch antenna are shown in Fig. 6.15. It can be observed that this antenna radiates better than Zoflex and Copper-Zoflex antenna. The important observation is the improvement in peak gain due to the increase in effective conductivity of the Copper-Zoflex-Copper patch.

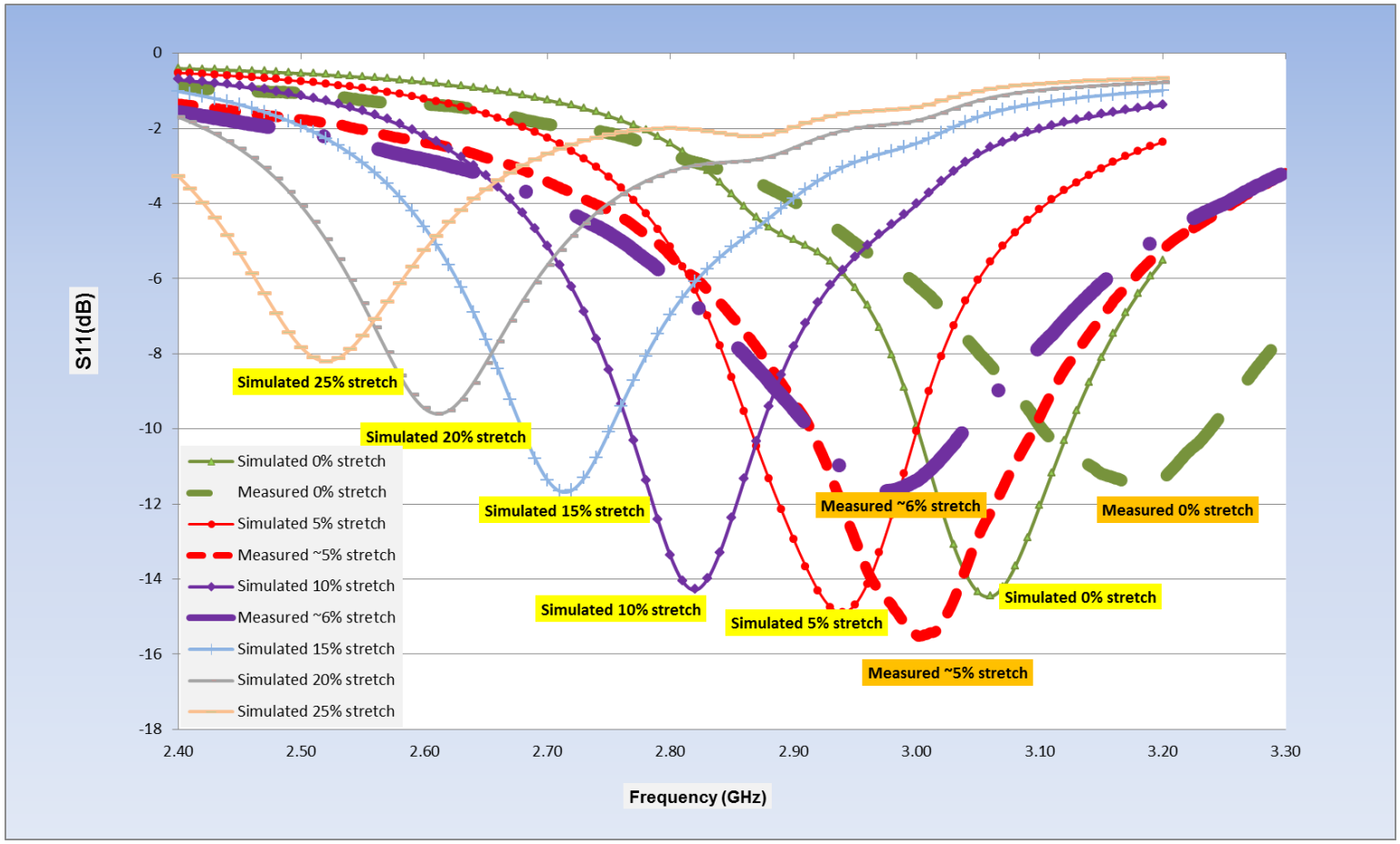


*Fig. 6.13 Simulated and Measured Results of Zoflex Patch Antenna*

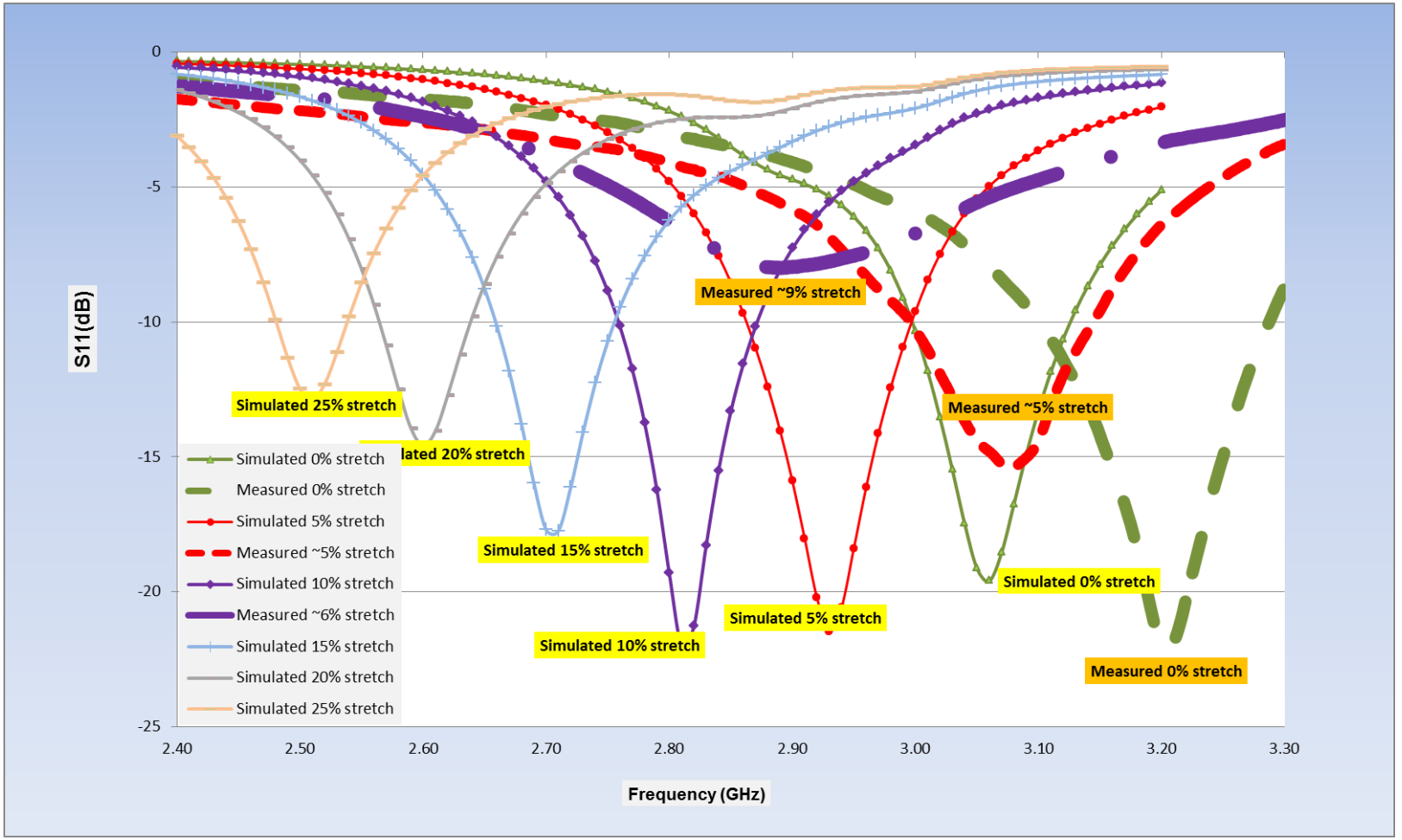


*Fig. 6.14 Simulated and Measured Results of Copper-Zoflex Patch Antenna*

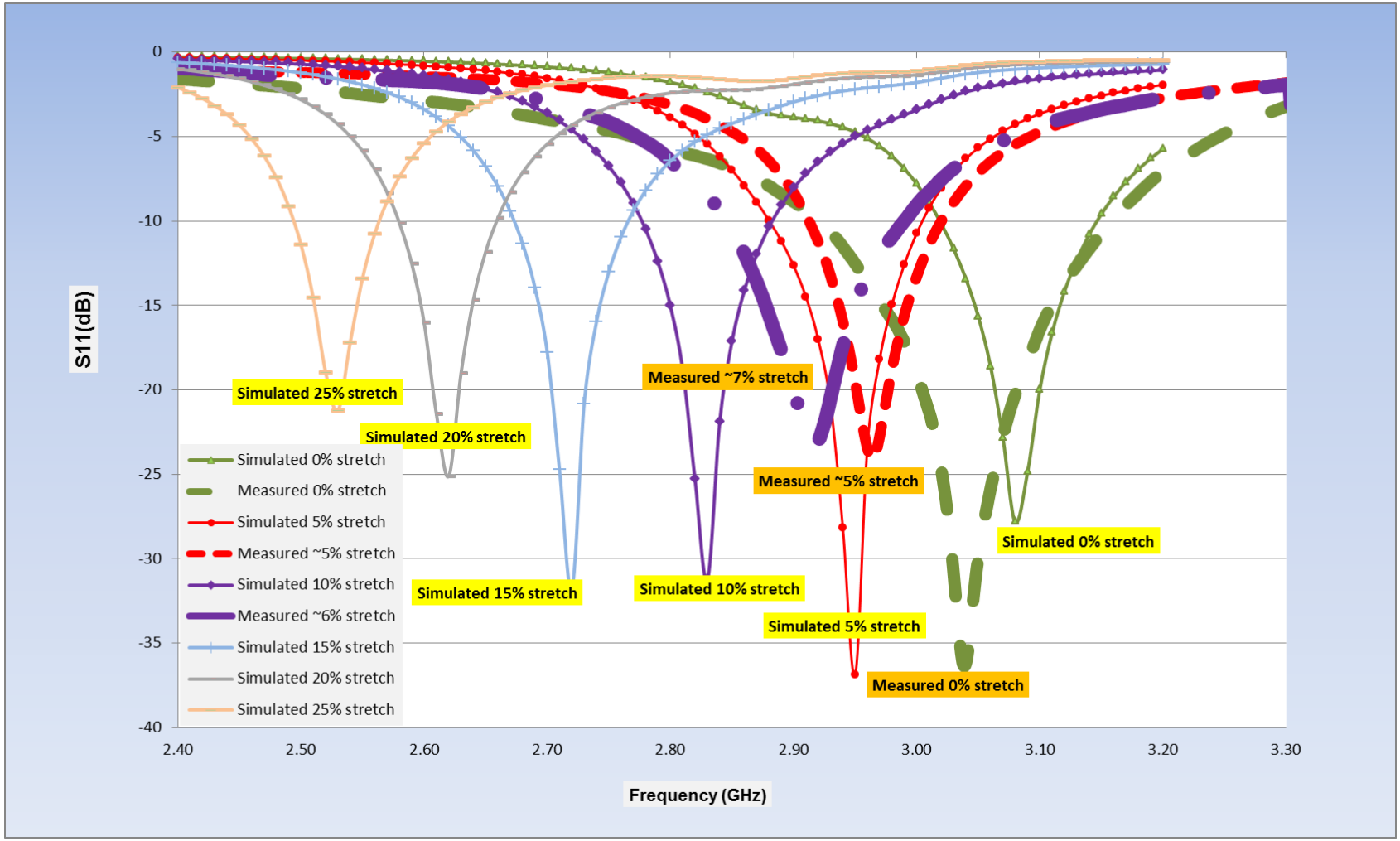


*Fig. 6.15 Simulated and Measured Results of Copper-Zoflex-Copper Patch Antenna*

### 6.7.4 Comparison of Peak Gain Patch Antennas

Though, it can be seen that the all the multi-layer patches demonstrated reconfigurability, the main difference is seen in the peak gain. Due to improvement in effective conductivity, the peak of gain of the antenna increases with the addition of copper layer. The peak gain was improved up to 3.3 dBi compared to the Zoflex patch antenna using the multi-layer approach. The measured peak gains of the different antennas are listed in Table 6.3.

*Table 6.3 Comparison of Measured Peak Gain of Copper and Multi-Layer Patch Antennas*

| Patch conductor | Peak gain (dBi) |
|---|---|
| Copper tape | 6.24 |
| Zoflex | 0.96 |
| Copper-Zoflex | 1.7 |
| Copper-Zoflex-Copper | 4.36 |

## 6.8 Conclusion

In this chapter, a reconfigurable patch antenna was designed using aperture-coupled feeding technique. This feeding technique helped to avoid disturbances caused to the feed when the antenna was stretched. The 3D EM simulator software HFSS model was used to design the aperture-coupled patch antenna at 3.1 GHz and study the effect on antenna performance due to stretching. The extracted DC conductivity of the multi-layer structures from chapter 4 was used to develop antenna models to predict the performance of the different multi-layer patches. The multi-layer patches were fabricated and tested. It was demonstrated that the antenna can be tuned mechanically by stretching along the

resonating length. Also, the peak gain was improved by 3.3 dBi using the multi-layer approach.

One of the limitations has been the non-availability of a set-up to stretch the antenna up to 25%. The stretch set-up used in chapter 4 was not useful for stretching the patch antenna. So the antenna had to be mechanically tuned. Thus, only stretching up to ~10% was possible.

Also, it was observed that the fabricated multi-layer patches resonated at slightly different frequencies than 3.1 GHz. The reason for the different multi-layer patches to resonate at higher frequency than expected could be due to errors in permittivity measurements. The permittivity of PDMS was characterized using open-end co-axial probe measurements in chapter 5. This method assumes infinitely thick substrates and hence the results can be inaccurate for thin patches. The actual permittivity might have been lower than the measured permittivity of PDMS.

In addition to this, differences in the peak gains of simulation and measured results were observed. Simulation in HFSS uses extracted conductivity from chapter 4 and hence the values used might not represent the exact conductivity of the multi-layer patches. This disparity in the conductivity used for simulation might be the reason for differences in the simulated and measured results. Also, pre-straining caused reduction in the thickness of patches at the pre-strained edge from 2mm to less than 1.5 mm. Since reduction in thickness reduces the gain of the antenna, the measured peak gain values may have been further reduced compared to the simulated results. Future work would be to develop a set-up to stretch the antenna up to 25%, study a better technique to characterize PDMS and also study the pre-strained fabrication of the multi-layer patches.

# CHAPTER 7

# CONCLUSION

## 7.1 Summary

In this thesis, a detailed work on flexible electronics has been done. The work done can be divided into three sections: Study and development of stretchable conductors, design and testing of flexible micro-striplines, and design and testing of a reconfigurable patch antenna.

In the first part of the work, a review of the work done in field of flexible electronics was performed. The key advantages and the scope of flexible electronics were provided. The important techniques used for the fabrication of flexible electronics like pre-strained thin metal deposition, horse-shaped metal patterning, micro-fluidics, conductive rubbers/ Electrically conductive composites (ECC), E-fibers/conductive textiles and ion implantation were discussed. The merits and de-merits of these techniques were also listed.

A multi-layer approach for the fabrication of stretchable conductors was proposed. The multi-layer approach uses a combination of metal films and conductive rubber on a flexible substrate. Equivalent circuit models were proposed to explain the theory of stretchable conductors. The different structures of stretchable conductors- single layer, two-layer and three structures were discussed in detail under stretched and

unstretched conditions. The models provided a good insight as to the function of each layer in the multi-layer structures. It also helped to understand that the conductive rubbers need to have a high conductivity in order to have low resistance under stretched conditions. Also, it was observed that the surface roughness of the conductive rubber layers was critical to the performance of the multi-layer structure under stretched conditions.

The fabrication of stretchable conductors was done in a step-wise manner. Various materials were investigated and studied to find best materials for the substrate, conductive rubber layer and metal layer of the stretchable conductor. The different materials considered for the substrate layer include- PDMS and Silicone. On comparison, PDMS was chosen because of better adhesion of metal layer on the substrate surface [72]. The various materials studied for the conductive rubber layer include- Carbon paste, Silver paint, Silver paste, Silver grease, Wackers and Zoflex. The materials were classified based on the important characteristics of a conductive rubber namely, conductivity and flexibility. From the study, it was found that Zoflex had the highest conductivity and flexibility among all the materials. For choosing the metal layer, the two widely used metals – gold and copper were studied. It was observed that copper had better adhesion and so copper was chosen as the metal layer.

Different multi-layer structures shown in Fig.4.6 were fabricated and tested. From the measurements, it was observed that the multi-layer structure of Copper-Zoflex-Copper on PDMS had the highest conductivity of ~$2\times10^5$ S/m. The samples were subjected to strains up to 25% using a custom made stretch testing set-up. The results showed that the multi-layer structures do not lose conductivity even when strained up to

25% and also the multi-layer structures demonstrated repeatable performance over several cycles of strain. The measurement results also showed good agreement with the performance predicted by the equivalent circuit models.

One of the applications of flexible electronics is for making conformal RF devices and antennas. This was the work in the second part of the thesis, which was about the design and testing of flexible micro-striplines using the multi-layer approach. The dielectric characterization of PDMS was performed using HP dielectric kit. The permittivity and loss tangent of PDMS was found to 3.1 and ~0.02 respectively up to 3 GHz. The dimensions of the micro-striplines were calculated theoretically as well as using Agilent ADS tool Linecalc.

The micro-striplines were fabricated and S-parameters characterization was done using VNA. It was found that the multi-layer structures– Zoflex, Copper-Zoflex and Copper-Zoflex-Copper were matched in the frequency range from 1 GHz to 5 GHz. Among the multi-layer structures, Copper-Zoflex-Copper had the lowest loss. It was demonstrated that by addition of copper layer the effective conductivity increases and hence the loss was reduced more than 50%. The micro-striplines were also bent using different radius of curvature and the loss was measured. It was observed that the device was not damaged due to bending. Also, the loss reduced to the original value when the device was placed on flat surfaces and demonstrated repeatable performance.

In the third part of the thesis, a reconfigurable patch antenna at 3.1 GHz was fabricated and tested. Different types of feeding techniques of patch antenna were studied and aperture-coupled feeding technique was chosen since ground plane isolated the feed and the patch substrate. Hence, the feed would not be disturbed due to stretching of the

patch substrate. Ansoft HFSS was used to design the aperture-coupled patch antenna at 3.1 GHz. The model was used to study the effect of stretching on the antenna performance as well as predict the performance of different multi-layer structures.

The different multi-layer patches were fabricated using the same technique used for the fabrication of stretchable conductors. The slotted ground plane as well as the micro-strip feed line was fabricated on the feed substrate using LPKF milling machine. The different multi-layer patch antennas were tested and it was demonstrated that the multi-layer approach can be used to make reconfigurable antennas. Also, the multi-layer approach improved the peak gain up by 3.3dBi compared to a conductive rubber based patch antenna.

### 7.2 Current Research and Recommendation for Future Work

The issues in the antenna fabrication and measurements were discussed. The current research is focused on studying the effect of pre-straining on PDMS substrate. The pre-strained thick PDMS substrates suffer from hysteresis and hence this causes dimensional mismatch and affects the antenna performance as discussed earlier. In the ongoing research, the optimum level up to which the PDMS substrate can be pre-strained for fabrication is being studied. Also, the other issue about inaccurate permittivity measurements is being looked into. Better techniques to characterize PDMS films are being studied. A set-up to stretch the antenna and test to strains up to 25% is also being worked on.

This work using multi-layer stretchable conductors for RF and antenna applications has demonstrated the feasibility of the approach. The work performed and

the results achieved in this thesis provide valuable information as to the design and fabrication of conformal, light-weight devices for RF and antenna applications. In this thesis, a flexible micro-stripline and a reconfigurable patch antenna were demonstrated using the multi-layer approach. The multi-layer technology is simple, inexpensive and has the scope to develop many kinds of planar RF devices like reconfigurable filters, switches, matching circuits for active devices, couplers as well as various planar antenna geometries for beam-steering, beam-forming and wideband applications. In addition to this, as discussed in section 2.2, RF and antennas devices is just one of the many applications that is possible using this technology. The multi-approach can also be used to develop sensors for body-health monitoring, structural health monitoring, detecting changes in pressure, temperature etc.

Based on the experience of working with the multi-layer stretchable conductors approach, the following are the recommendations of the author:

1) The conductivity of the multi-layer stretchable conductors can be improved if more number of Copper and Zoflex layers is used. This can increase the effective conductivity of the multi-layer structure and will be studied in future.
2) Also, the conductivity of the multi-layer stretchable conductors can be significantly improved if the surface roughness of Zoflex is reduced in the current research. The surface roughness of Zoflex affects the performance of multi-layer structures at high strains as it reduces over-lapping metal island formation, which makes the performance of the multi-layer structures similar to the Zoflex structure.

3) Moreover, due to limitations in improvement of the surface roughness of commercial Zoflex, one of the approaches in future is to develop our own conductive rubber layer.
4) Furthermore, the improvements in the surface roughness of Zoflex layer can improve the conductivity of the multi-layer structures and hence improve the performance of RF and antenna devices.
5) In the measurement of flexible micro-striplines, it was observed that bad connectors causes mismatch and increases the overall loss. So, a better technique to reduce the effect of connector loss can help to get more accurate measurements of the loss of the multi-layer structures.

## REFERENCES


1. Rogers, J.A. and Y. Huang, *A curvy, stretchy future for electronics,* Proceedings of the National Academy of Sciences, 2009. Volume 106, Issue 27, p. 10875-10876.

2. Reuss, R.H., et al., *Macroelectronics: Perspectives on technology and applications,* Proceedings of the IEEE, 2005. Volume 93, Issue 7, p. 1239-1256.

3. Lumelsky, V.J., M.S. Shur, and S. Wagner, *Sensitive skin.* Sensors Journal, IEEE, 2001. Voulme 1, Issue 1, p. 41-51.

4. Mehdipour, A., et al., *Conductive carbon fiber composite materials for antenna and microwave applications,* NRSC 2012.

5. Hosokawa, K., K. Hanada, and R. Maeda, *A polydimethylsiloxane (PDMS) deformable diffraction grating for monitoring of local pressure in microfluidic devices,* Journal of Micromechanics and Microengineering, 2002, Volume 12, p. 1.

6. Lee, D.W. and Y.S. Choi, *A novel pressure sensor with a PDMS diaphragm,* Microelectronic Engineering, 2008. Voume 85, Issue 5, p. 1054-1058.

7. Lee, C.Y., W.J. Hsieh, and G.W. Wu, *Embedded flexible micro-sensors in MEA for measuring temperature and humidity in a micro-fuel cell,* Journal of Power Sources, 2008, Volume 181, Issue 2, p. 237-243.

8. Yang, Y.J., et al., *An integrated flexible temperature and tactile sensing array using PI-copper films,* Sensors and Actuators A: Physical, 2008, Volume 143, Issue 1, p. 143-153.

9. Lee, C.Y., G.W. Wu, and W.J. Hsieh, *Fabrication of micro sensors on a flexible substrate,* Sensors and Actuators A: Physical, 2008. Voume 147, Issue 1, p. 173-176.

10. Sibinski, M., M. Jakubowska, and M. Sloma, *Flexible temperature sensors on fibers,* Sensors, 2010. Volume 10, Issue 9, p. 7934-7946.

11. Cheng, M., et al., *A flexible capacitive tactile sensing array with floating electrodes*, Journal of Micromechanics and Microengineering, 2009. Volume19, p. 115001.

12. Hasegawa, Y., et al., *Fabrication of a wearable fabric tactile sensor produced by artificial hollow fiber*, Journal of Micromechanics and Microengineering, 2008, Volume 18, p. 085014.

13. Zaytseva, N.V., et al., *Development of a microfluidic biosensor module for pathogen detection*, Lab Chip, 2005, Volume 5, Issue 8, p. 805-811.

14. Wang, Y., et al., *Super Elastic Graphene Ripples for Flexible Strain Sensors*, ACS nano, 2011.

15. Lim, M.A., et al., *A New Route towards Ultra-Sensitive, Flexible Chemical Sensors: Metal Nanotubes by Wet-Chemical Synthesis along Sacrificial Nanowire Templates*, ACS nano, 2012.

16. Yin, J., et al., *Molecularly Mediated Thin Film Assembly of Nanoparticles on Flexible Devices: Electrical Conductivity versus Device Strains in Different Gas/Vapor Environment*, ACS nano, 2011.

17. Yi, J., J.M. Lee, and W.I. Park, *Vertically aligned ZnO nanorods and graphene hybrid architectures for high-sensitive flexible gas sensors*, Sensors and Actuators B: Chemical, 2011, Volume 155, Issue 1, p. 264-269.

18. Someya, T., et al., *Conformable, flexible, large-area networks of pressure and thermal sensors with organic transistor active matrixes*, Proceedings of the National Academy of Sciences of the United States of America, 2005. Volume 102, Issue 35, p. 12321.

19. Huang, Y., et al., *Design and experiment of flexible multi-functional tactile sensors for robot skin.* Jiqiren(Robot), Huang, Y., et al., Design and experiment of flexible multi-functional tactile sensors for robot skin. Jiqiren(Robot), Vol. 33, no. 3, pp. 347-353, 359. May 2011.

20. Akagi, T., et al., *Development of Flexible Sensors for Measuring Human Motion and Displacement of Novel Flexible Pneumatic Actuator.* Journal ref: International Journal of Automation Technology, 2011. Volume 5, Issue 5, p. 621-628.

21. Crawford, G.P., *Flexible flat panel display technology*. John Wiley & Sons, Ltd., p. 1-9

22. Chuang, T.K., et al., *Top-emitting 230 dots/ in. active-matrix polymer light-emitting diode displays on flexible metal foil substrates*, Applied Physics Letters, 2007. Volume 90, p. 151114.

23. Gelinck, G.H., et al., *Flexible active-matrix displays and shift registers based on solution-processed organic transistors.* Nature Materials, 2004. Volume 3, Issue 2, p. 106-110.

24. D'Andrade, B. and A.Z. Kattamis, *Flexible Active-Matrix Organic Light Emitting Displays.* Silicon Valley Engineering Council, 2009: p. 18.

25. Steudel, S., et al., *Design and realization of a flexible QQVGA AMOLED display with organic TFT,*. Organic Electronics, Volume 13, Issue 9, September 2012, p. 1729–1735, 2012.

26. Allen, K.J., *Reel to real: prospects for flexible displays.* Proceedings of the IEEE, 2005, Volume 93, Issue 8, p. 1394-1399.

27. Choo, H., J. Ryoo, and H. Choo, *Design of a Flexible Planar RFID Tag Antenna with Low Performance Degradation from Nearby Target Objects*, Journal of The Korea Electromagnetic Engineering Society, 2011, Volume 11, Issue 1, p. 1-4.

28. Potyrailo, R.A., *Multivariable passive RFID vapor sensors: roll-to-roll fabrication on a flexible substate,* Analyst issue 12, 2012.

29. Leung, S.Y.Y. and D.C.C. Lam, *Performance of Printed Polymer-Based RFID Antenna on Curvilinear Surface,* Electronics Packaging Manufacturing, IEEE Transactions on, 2007. Volume 30, Issue 3, p. 200-205.

30. Wang, S. and G. Wang, *Passive UHF RFID Tag for Cigarette Pack Identification,* Advances in Electrical Engineering and Electrical Machines, 2011, p. 405-411.

31. Ngai, E., et al., *RFID research: An academic literature review (1995–2005) and future research directions,* International Journal of Production Economics, 2008. Volume 112, Issue 2, p. 510-520.

32. Lu, J.C., et al. *Study and Implementation of RFID Eseals for Power Meters,* Innovations in Bio-inspired Computing and Applications (IBICA), 2011,IEEE Second International Conference, p. 352-355.

33. Zhou, Y., et al. *Conformal load-bearing polymer-carbon nanotube antennas and RF front-ends, APSURSI* 2009, IEEE, p. 1-4.

34. Salonen, P., et al. *Dual-band wearable textile antenna,*Antennas and Propagation Society International Symposium, 2004. IEEE 2004, p. 463-466, Volume 1.

35. Rahmat-Samii, Y. *Wearable and implantable antennas in body-centric communication, Antennas and Propagation, 2007. EuCAP 2007, p. 1-5.*

36. Ukkonen, L., L. Sydanheimo, and Y. Rahmat-Samii. *Sewed textile RFID tag and sensor antennas for on-body use, Antennas and Propagation (EUCAP), 2012, p. 3450-3454.*

37. Zhang, L., et al. *E-fiber electronics for body-worn devices, Antennas and Propagation (EUCAP), 2012, p.760-761.*

38. Rahmat-Samii, Y. and J. Kim, *Implanted antennas in medical wireless communications,* Synthesis Lectures on Antennas, 2005. Voume 1, Issue 1, p. 1-82.

39. *Frequency-tunable soft composite antennas for wireless sensing.* Sensors and Actuators A: Physical, 2012.

40. Cheng, S., et al., *Liquid metal stretchable unbalanced loop antenna.* Applied Physics Letters, 2009, Voume 94, p. 144103.

41. Cheng, S., et al., *Foldable and stretchable liquid metal planar inverted cone antenna.* Antennas and Propagation, IEEE Transactions on, 2009. Volume 57, Issue 12, p. 3765-3771.

42. Mazlouman, S.J., et al., *A Reconfigurable Patch Antenna Using Liquid Metal Embedded in a Silicone Substrate.* Antennas and Propagation, IEEE Transactions on, 2011. Voume 59, Issue 12, : p. 4406-4412.

43. Liu, Q., et al. *A stretchable PIFA antenna, Antennas and Propagation Conference (LAPC), 2011 Loughborough*. 2011, p. 1-4.

44. So, J.H., et al., *Reversibly deformable and mechanically tunable fluidic antennas,* Advanced Functional Materials, 2009. Volume 19, Issue 22, p. 3632-3637.

45. Lee, S., et al., *Reversibly Stretchable and Tunable Terahertz Metamaterials with Wrinkled Layouts,* Advanced Materials, 2012, Volume 24, Issue 26, p. 3491-3497.

46. Shah, C., et al., *Elastomeric silicone substrates for terahertz fishnet metamaterials,* Applied Physics Letters, 2012. Volume 100 , Issue 6, p. 1-3.

47. Khodasevych, I., et al., *Elastomeric silicone substrates for terahertz fishnet metamaterials,* Applied Physics Letters, 2012. Volume 100 , Issue 6, p. 061101-061101-3.

48. Ou, J.Y., et al., *Reconfigurable photonic metamaterials,* ACS Nano letters, 2011.

49. Tavassolian, N., S. Nikolaou, and M.M. Tentzeris. *A Flexible UWB Elliptical Slot Antenna with a Tuning Uneven U-shape Stub on LCP for Microwave Tumor Detection,* Microwave Conference, 2007. APMC 2007. Asia-Pacific, p. 1-4.

50. Iguchi, S., et al., *A flexible and wearable biosensor for tear glucose measurement.* Biomedical microdevices, 2007, Voume 9, Issue 4, p. 603-609.

51. *Sylgard®184 silicone elastomer kit datsheet from Dow corning.*

52. Holy, C., et al., *Use of a biomimetic strategy to engineer bone,*Journal of Biomedical Materials Research Part A, 2003, Volume 65, Issue 4, p. 447-453.

53. Ma, P.X. and R. Zhang, *Microtubular architecture of biodegradable polymer scaffolds,*Journal of biomedical materials research, 2001. 56(4): p. 469-477.

54. Ko, H.C., et al., *A hemispherical electronic eye camera based on compressible silicon optoelectronics,*nature, 2008, Voume 454, Issue 7205, p. 748-753.

55. Rowell, M.W., et al., *Organic solar cells with carbon nanotube network electrodes,*Applied Physics Letters, 2006. Volume 88, Issue 23, p. 233506-233506-3.

56. Lacour, S.P., et al., *Stretchable gold conductors on elastomeric substrates,* Applied Physics Letters, 2003. Volume 82, p. 2404.

57. Brosteaux, D., et al., *Design and fabrication of elastic interconnections for stretchable electronic circuits.* Electron Device Letters, IEEE, 2007. Volume 28, Issue 7, p. 552-554.

58. Carta, R., et al., *Design and implementation of advanced systems in a flexible-stretchable technology for biomedical applications.* Sensors and Actuators A: Physical, 2009.Volume 156, Issue 1, p. 79-87.

59. Kim, D.-H., et al., *Epidermal Electronics* ,Science, 2011 Voume 333, Issue 6044, p. 838-843.

60. Lacour, S.P., et al., *Design and performance of thin metal film interconnects for skin-like electronic circuits,* Electron Device Letters, IEEE, 2004, Volume25, Issue 4, p. 179-181.

61. Lacour, S.P., et al., *Mechanisms of reversible stretchability of thin metal films on elastomeric substrates,* Applied Physics Letters, 2006, Voume 88, p. 204103.

62. Graz, I.M., D.P.J. Cotton, and S.P. Lacour, *Extended cyclic uniaxial loading of stretchable gold thin-films on elastomeric substrates,* Applied Physics Letters, 2009, Volume 94, p. 071902.

63. Li, T., et al., *Stretchability of thin metal films on elastomer substrates,* Applied Physics Letters, 2004, Volume 85,Issue 16, p. 3435-3437.

64. Zhigang, W. and S. Cheng, *Microfluidic electronics*,. Lab Chip, 2012.

65. Agar, J., et al. *Electrically conductive silicone nano-composites for stretchable RF devices, Microwave Symposium Digest (MTT), 2011, p. 1-4.*

66. Tronquo, A., et al., *Robust planar textile antenna for wireless body LANs operating in 2.45 GHz ISM band.* Electronics Letters, 2006 Voume 42, Issue 3, p. 142-143.

67. Wang, Z., et al. *Multilayer printing of embroidered RF circuits on polymer composites, APSURSI* 2011 IEEE, p. 278-281.

68. Zhang, W., A.A. Dehghani-Sanij, and R.S. Blackburn, *Carbon based conductive polymer composites,* Journal of materials science, 2007. Volume 42, Issue 10, p. 3408-3418.

69. Van Beek, L. and B. Van Pul, *Internal field emission in carbon black-loaded natural rubber vulcanizates,* Journal of Applied Polymer Science, 1962, Volume 6, Issue 24, p. 651-655.

70. Rosset, S., et al., *Ion-implanted compliant and patternable electrodes for miniaturized dielectric elastomer actuators,* Electroactive Polymer Actuators and Devices (EAPAD), 2008, 6927, p. 69270W-10.

71. Rosset, S., et al., *Metal ion implantation for the fabrication of stretchable electrodes on elastomers,* Advanced Functional Materials, 2009. Volume 19, Issue 3, p. 470-478.

72. Takshi, A. and J.D. Madden, *Multilayer Stretchable Conductors with a Large Tensile Strength,* Journal of Elastomers and Plastics, 2010, Volume 42, Issue 4, p. 365-373.

73. McDonald, J.C., et al., *Fabrication of microfluidic systems in poly(dimethylsiloxane),* Electrophoresis, 2000, Volume 21, Issue1, p. 27-40.

74. Oliveira, G.N.d., L.C.S. Nunes, and P.A.M.d. Santos, *Shear strain determination of the polymer polydimethysiloxane (PMDS) using digital image correlation in different temperatures,* Journal of Physics: Conference Series, 2011, Volume 274, Issue 1, p. 012073.

75. Armani, D., C. Liu, and N. Aluru. *Re-configurable fluid circuits by PDMS elastomer micromachining,* Micro Electro Mechanical Systems, 1999. MEMS '99. p. 222-227.

76. *SPI supplies website, www.spi.com.*

77. Wacker webiste, *www. wacker.com.*

78. *Zoflex, website http://www.rfmicrolink.com/products.html.*

79. Pozar, D.M., *Microwave Engineering* (Third edition ).

80. Mumcu, G., *Lecture notes on Microstrip Matching Networks,* RF & Microwave Circuits II.

81. Pozar, D.M., *Microwave and RF wireless systems,* Third edition, John Wiley & sons.

82. *RF sheet resisitance topic in microwave101 website, (http://www.microwaves101.com/encyclopedia/RF_sheet_resistance.cfm).*

83. Microwave 101 website, *www.microwave101.com.*

84. Balanis, C.A., *Antenna theory analysis and design,* Third edition, Wiley India edition

85. *Stretchable Microfluidic Radiofrequency Antennas,* Advanced Materials, 2010, Volume 22, p. 2749-2752.

86. Kuchar, A., *Aperture-coupled microstrip patch antenna array,* Technische Universität Wien, Master Thesis, 1996.

87. Civerolo, M.P., *Aperture Coupled Microstrip Antenna Design and Analysis,* Masters thesis, 2010.

88. *E-beam evaporator manual , Nanontechnology research and education center (NREC).*

89. *CRC sputtering tool manual.*

**APPENDICES**

**Appendix A: Masking on PDMS**

A Kapton® tape was used to mask the PDMS for patterning of conductive layer on top of PDMS. This approach helps to control the thickness as well as the shape of the conductive layer. In this process, Kapton® tapes of length 50 mm, width 5 mm and thickness 100 um was taped on the PDMS substrate. After applying the conductive layer the tapes can be removed to just leave the conductive layer on top of the PDMS substrate. The Fig. A1 shows the process of masking on PDMS.

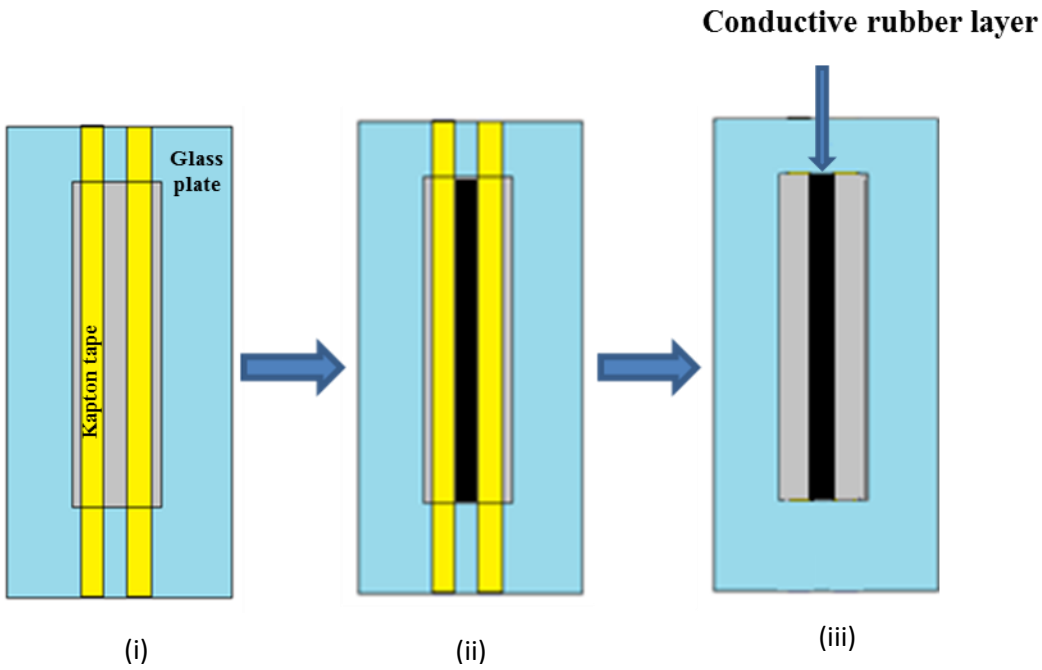


*Fig. A1 Masking on PDMS. i) Kapton tape is used for masking , ii) the conductive layer is formed on top of PDMS and cured , iii) Kapton tape removed after curing*

## Appendix B: E-Beam Evaporation

The E-beam evaporator at Nanotechnology research and education center (NREC) was used for the fabrication. [88] The E-beam evaporator used at NREC is shown in Fig. B1. It consists of chamber which is pumped to high vacuum (~$10^6$ TORR) for the metal deposition. It also has the capability to hold several metal targets for multi-layer deposition. The metal that needs to be deposited is chosen and the high voltage power supply of ~7.25kV is switched on. The electron beam is adjusted so that it falls on the crucible that holds the target. Once the metal has been melted, the shutter is opened which exposes the surface to be coated. The rate of deposition is monitored using SQM-160 thickness monitor and the rate of deposition is controlled by adjusting the current. Once the deposition is done, the E-beam is tuned off and the chamber is pumped down to atmospheric pressure. In this research, gold and copper films of thickness 500nm were deposited. Since both the metal had poor adhesion to PDMS, thin layers of chromium (20 nm) for gold deposition and titanium (20nm) for copper deposition were used. The conditions used for deposition is shown in Table B1.

*Table B1 Deposition Rates of Metals Used in E-Beam Evaporation.*

| Metal | Current (mA) | Deposition rate(A°/s) |
|---|---|---|
| **Gold** | **60** | **3** |
| **Chromium** | **40** | **2** |
| **Copper** | **60** | **3** |
| **Titanium** | **40** | **2** |

**Appendix B (Continued)**


*Fig. B1 E-Beam Evaporator at NREC*

## Appendix C: Sputtering

The E-beam evaporator is a very useful tool for making thin films (<1µm). But for thicker films in the range of a few microns, the sputtering technique is a better choice. In this technique, the target is loaded and the samples are placed in a small chamber which to pumped to vacuum in the range of 4-6 milliTORR. Once the vacuum was reached, the power supply was switched on and the current was adjusted to control the rate of deposition. The CRC sputtering used is NREC [89] is shown in Fig.C1.

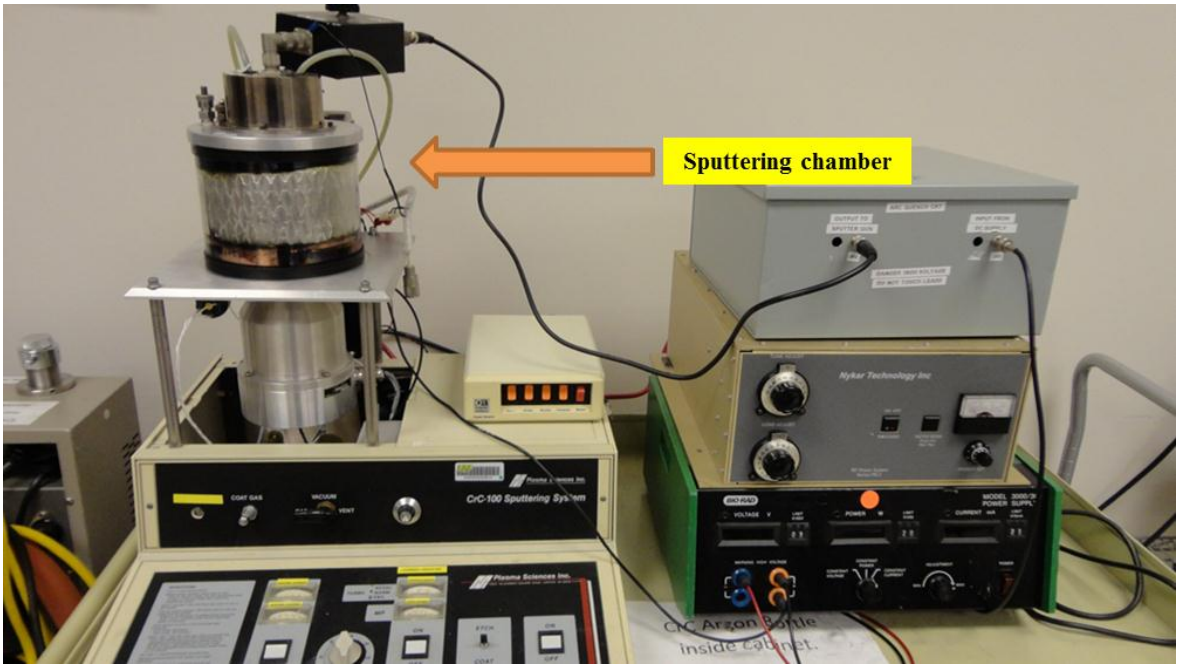


*Fig. C1 CRC Sputtering Tool at NREC*

**Appendix C (Continued)**

In this research, sputtering was mainly used for copper deposition. Since copper had poor adhesion to PDMS, a thin layer of titanium was deposited first. The titanium deposition was carried out first and then the copper film was deposited. Titanium was deposited at 360 V, 150 mA current at a pressure of 5 milliTORR for 10 minutes. Using this method, a thin titanium film of thickness 100 nm was fabricated. Since the CRC tool was able to hold only one target, it was pumped down after the titanium deposition and target was changed to copper. The copper film was deposited at 100 mA current, 440 V at pressure of 5 milliTORR for 2 hours. Using this method, copper film of thickness 4µm was fabricated.

## Appendix D: Study of Variation of Antenna Parameters Due to Stretching Using HFSS

The 3D EM simulator software Ansoft HFSS was used to design the aperture-coupled feed patch antenna discussed in section 6.5. The multi-layer patches were designed using extracted conductivities from chapter 4. The conductivities used for Zoflex, Copper-Zoflex and Copper-Zoflex-Copper were $1\times10^{4}$S/m, $2\times10^{4}$S/m and $2\times10^{5}$S/m. The patches were stretched from 0 to 25% and the antenna parameters variation was studied. The variation of antenna parameters due to stretching is given in Table D1. It can be seen that the conductivity affects the gain and efficiency of the antenna. Higher conductivity leads to higher gain and efficiency.

## Appendix D (Continued)

*Table D1 Study of Variation of Multi-Layer Patch Antenna Parameters Due to Stretching Using HFSS*

| % Strain | Patch Conductor | Frequency (GHz) | Peak Directivity (dBi) | Peak Gain (dBi) | Peak realized gain (dBi) | Efficiency % | %BW |
|---|---|---|---|---|---|---|---|
| 0 | Zoflex | 3.06 | 9.85 | 6.36 | 6.15 | 44.76 | 4.09 |
| | Copper-Zoflex | 3.06 | 9.63 | 6.84 | 6.76 | 52.51 | 4.204 |
| | Copper-Zoflex-Copper | 3.08 | 9.63 | 7.23 | 7.216 | 61.23 | 4.127 |
| | | | | | | | |
| 5 | Zoflex | 2.94 | 9.05 | 5.41 | 5.21 | 43.17 | 4.19 |
| | Copper-Zoflex | 2.93 | 9.085 | 6.11 | 6.049 | 50.325 | 4.64 |
| | Copper-Zoflex-Copper | 2.95 | 8.69 | 6.37 | 6.37 | 58.662 | 4.24 |
| | | | | | | | |
| | | | | | | | |
| 10 | Zoflex | 2.82 | 8.67 | 4.56 | 4.36 | 38.84 | 3.77 |
| | Copper-Zoflex | 2.81 | 8.29 | 4.92 | 4.87 | 45.93 | 4.007 |
| | Copper-Zoflex-Copper | 2.83 | 7.97 | 5.465 | 5.465 | 56.021 | 3.73 |
| | | | | | | | |
| 15 | Zoflex | 2.71 | 8.71 | 3.65 | 3.32 | 31.18 | 2.68 |
| | Copper-Zoflex | 2.71 | 8.54 | 4.57 | 4.52 | 40.54 | 3.54 |
| | Copper-Zoflex-Copper | 2.72 | 8.34 | 5.419 | 5.416 | 50.96 | 3.42 |
| | | | | | | | |
| 20 | Zoflex | 2.61 | 8.55 | 2.85 | 2.35 | 26.62 | NIL |
| | Copper-Zoflex | 2.6 | 8.33 | 4.04 | 3.87 | 37.04 | 2.89 |
| | Copper-Zoflex-Copper | 2.62 | 8.29 | 5.105 | 5.09 | 47.95 | 3.05 |
| | | | | | | | |
| 25 | Zoflex | 2.52 | 8.46 | 2.15 | 1.488 | 23.33 | NIL |
| | Copper-Zoflex | 2.51 | 8.31 | 3.56 | 3.64 | 33.58 | 2.29 |
| | Copper-Zoflex-Copper | 2.53 | 8.29 | 4.767 | 4.74 | 44.44 | 2.74 |